Epithelial morphogenesis of the *Caenorhabditis elegans* pharnyx

Jeffrey Philip Rasmussen

A dissertation

submitted in partial fulfillment of the

requirements for the degree of

Doctor of Philosophy

University of Washington

2011

James R. Priess, Chair

Thomas A. Reh

Valeri Vasioukhin

Program Authorized to Offer Degree:

Molecular and Cellular Biology

University of Washington

Abstract

Epithelial morphogenesis of the *Caenorhabditis elegans* pharnyx

Jeffrey Philip Rasmussen

Chair of the Supervisory Committee:
Affiliate Professor James R. Priess
Department of Biology

The assembly of cells into functional organs requires the coordination of cell shape
and polarity with organ architecture. Although defects in cell shape and polarity can
lead to human disease, the in vivo regulation of these processes during organ forma-
tion is poorly understood. In this thesis, I used the *Caenorhabditis elegans* pharynx
as an in vivo model to study organogenesis. Similar to many human organs, the phar-
ynx is a tube formed from a monolayer of polarized epithelial cells that surround a
central lumen. The pharyngeal lumen develops midway through embryogenesis when
cells polarize along a central axis to form an epithelial cyst. Using live cell imaging,
I found that cyst development is preceded by the grouping of pharyngeal precursors
into a bilaterally symmetric intermediate. The organization of cells into this bilateral
intermediate requires the POP-1/TCF cell fate pathway and the pharyngeal organ
identity factor PHA-4/FoxA. Cyst formation begins when cells within the bilateral
structure undergo a mesenchymal to epithelial transition and localize apical polarity
determinants along their inner surfaces. These inner surfaces then constrict, creating
the central lumen. I found that laminin, an integral basement membrane component,
is required to define the axis of pharyngeal polarity. In laminin mutants, cells develop
inverted polarity and constrict their outer surfaces, resulting in multiple pharyngeal

lumens. After cyst formation, pharyngeal cells adopt highly reproducible morphologies. A previous ultrastructural study found that two cells, called pm8 and vpi1, develop into toroidally shaped single-cell tubes. By combining live cell microscopy with genetic analysis, I showed that pm8 and vpi1 form toroids via a novel mechanism: They wrap around the midline and then self-fuse, thereby creating an intracellular lumen. The self-fusion of pm8 and vpi1 into toroids requires fusogens and activation of the Notch signaling pathway in pm8. Thus, organogenesis of the pharynx requires sequential action of global, tissue-level signals, such as laminin, and local, cell-specific signals, such as Notch.

TABLE OF CONTENTS

LIST OF FIGURES

LIST OF TABLES

ACKNOWLEDGMENTS

DEDICATION

to my friends,

Jay Kaplan

David Mansbach

and, to my grandparents,

Colonel Philip and Muriel Maher

Lieutenant Colonel James and Martha Rasmussen

Chapter 1

INTRODUCTION

Many human organs contain epithelial cells, which serve essential absorptive and secretory functions and are our primary barriers to the environment. Epithelial cells are connected by strong adhesive contacts, known as adherens junctions, and have distinct apicobasal polarity. Epithelial cells localize components of the PAR complex (in mammals, Par3/Par6/aPKC) to their apical surface and receptors, such as integrins, that bind to a specialized extracellular matrix (ECM), the basement membrane, to their basal surface. Loss of epithelial cell adhesion and polarity can lead to carcinoma, the most prevalent type of cancer (reviewed by Lee and Vasioukhin, 2008; Bryant and Mostov, 2008).

During development, epithelial organs can change shape through a number of morphogenetic processes. Sheets of epithelial cells can bend by constricting one surface, lengthen by convergence-extension, or develop branches by sprouting. These processes can have profound effects on tissue and embryonic shape (e.g., Priess and Hirsh, 1986) and can be reiteratively combined to create highly elaborate organs, such as the lung (Metzger et al., 2008). Epithelial organs can be organized as monolayers of cells, as multi-layered stratified tissues, or a combination. Individual epithelial cells can adopt columnar, cuboidal or wedge shapes; certain epithelial cells develop complex shapes, such as kidney podocytes.

One common type of epithelial organizaiton is the epithelial tube. Many mam-

malian organs, including the vasculature, lung, pancreas, kidney, and intestine, are tubular structures. Biological tubes serve to transport fluids, nutrients, and gases between tissues. Tubular organs exhibit a remarkable diversity of size and architecture, ranging in size from microns to meters. Most tubes are organized as a monolayer of epithelial cells that have a specialized apical membrane facing the internal lumenal space and a basal surface in contact with basement membrane surrounding the tube (Figure 1.1A). In many tubes, the individual epithelial cells are wedge-shaped with a narrow apical surface and a broad basal surface. Malformations in tubular organs lead to a number of human maladies, such as polycystic kidney disease, aneurysms, neural tube closer defects and hydrocephalus. Thus, understanding the basic developmental mechanisms leading to tube formation and maintenance will guide tissue-engineering therapeutic approaches, which have already begun to show promise (Raya-Rivera et al., 2011).

This chapter summarizes several current models for tubulogenesis and serves as an introduction to the model system for this thesis, the *Caenorhabditis elegans* pharynx.

1.1 Mechanisms of multi-cellular tube formation

Most tubular organs contain multiple cells in cross section. Multi-cellular tubes can form via a variety of mechanisms, for example by rolling up a sheet of cells to surround an internal, lumenal space, or by creating a lumenal space inside a cylinder of cells through cavitation/apoptosis or cord hollowing/exocytosis (Figures 1.2A–C). Several excellent reviews summarize these morphogenetic behaviors (Lubarsky and Krasnow, 2003; Baer et al., 2009; Uv et al., 2003; Xu and Cleaver, 2011; O'Brien et al., 2002; Datta et al., 2011; Bryant and Mostov, 2008), therefore this section is not meant to be exhaustive, but will rather highlight recent examples of interest.

Tubes can form by reshaping epithelia. During vertebrate neurulation, signals

from the notochord cause a portion of the ectoderm to form the neural plate, a flat sheet of epithelial cells. To form the neural tube, cells of the neural plate constrict their apical surfaces causing the tissue to bend, eventually folding back onto itself (Figure 1.2A). Apical constriction of several vertebrate epithelia requires the actomyosin cytoskeleton and Rho kinases (ROCKs) (Hildebrand, 2005). In chick embryos, apical localization of ROCKs requires direct binding by Shroom3, an actin-binding protein (Nishimura and Takeichi, 2008). Inhibition of Shroom3 caused a failure in neural tube closure. Similarly, mice mutant for Shroom have defects in neural tube morphogenesis, suggesting a conserved requirement for these proteins (Hildebrand and Soriano, 1999). Following apical constriction, cells from either end of the neural plate must precisely align with each other to seal the tube. Although further analysis of cellular behaviors is needed to fully understand tube closure, complex patterns of cell are observed during this time, and require ROCK (Nishimura and Takeichi, 2008).

Tubes can form by *de novo* polarization of mesenchymal cells. The mesenchymal-to-epithelial transition underlies several types of tubulogenesis and can take several different forms depending on the context. The zebrafish intestine begins as a solid cylinder of non-polarized endodermal cells. Polarization of the endoderm begins at discrete foci of PAR protein localization within the developing tube. These foci are thought to form small lumens, which subsequently expand and coalesce to form a single lumen that runs the length of the intestine. Mutations in aPKCλ or knockdown of Claudin15 or an Na+/K+ ATPase pump cause a failure of lumen coalescence, resulting in multiple intestinal lumens (Horne-Badovinac et al., 2001; Bagnat et al., 2007). These results suggest a model whereby PAR-mediated polarity directs fluid transport to create a single lumen. Consistent with this model, mutants that increase fluid secretion result in an expansion of the intestinal tube (Bagnat et al., 2010). Cell rearrangements may also play a role in the process, however, this has not been

analyzed in detail.

A mesenchymal-to-endothelial transition was recently shown to underlie tubulogenesis of the mouse dorsal aorta (Strilić et al., 2009). The aorta begins as a solid cord of endothelial cells, containing two or three closely apposed cells in cross-section. At this stage, VE-cadherin localizes along the cell-cell interface and the lumenal marker CD34/Sialomucin is diffusely localized within the cells. The cells then polarize, localizing VE-cadherin to cell junctions, CD34 to the lumenal-facing membrane and create a small, slit-like lumen (Strilić et al., 2009). Proper polarization of CD34 required VE-cadherin. Since the aorta is discontinuous as this stage, directed fluid transport is unlikely to play a role in lumen formation. Rather, the negatively charged sialic acids that decorate CD34 and other sialomucins were shown to be required, suggesting that cell-cell repulsion is responsible (Strilić et al., 2010). Action of the actomyosin cytoskeleton at the apical surface then bends the apical membrane to enlarge the lumen (Strilić et al., 2009). Future work will be required to determine if cell-cell repulsion is required in other developing tubes; intriguingly, several other tubular organs contain apically localized mucins and glycoproteins.

An essential step during de novo tubulogenesis is defining the apical surface, site of the future lumen. Recent work in an in vitro model of tubulogenesis has led to a molecular model of lumen formation in Madin-Darby canine kidney (MDCK) cells (Bryant et al., 2010). In this system, contacts with the ECM appear orient cyst polarity as cells cultured in the absence of matrix (Wang et al., 1990) or in the presence of a β-integrin blocking antibody reverse their polarity (Yu et al., 2005). Addition of exogenous laminin to cysts with inverted polarity can reorient the apical surface to the interior (O'Brien et al., 2001). The sialomucin podocalyxin is initially localized to the outer, ECM-contacting surfaces of MDCK cells. Podocalyxin then localizes to the apical surface by transcytosis, which requires Rab8a and Rab11a. Rab8a and

Rab11a are also required for apical targeting of the polarity regulator Par3 and apical activation of the GTPase Cdc42 (Bryant et al., 2010).

ECM-mediated regulation of Par3 is also crucial for endothelial development in mouse. Targeted deletion of β-integrin in endothelial tissue resulted in a failure to form lumens. Loss of $\beta1$-integrin resulted in a loss of Par3 mRNA expression, and ectopic expression of Par3 was sufficient to rescue the $\beta1$-integrin lumenless phenotype. These results suggest that polarity of endothelial cells is initiated by β-integrin contacts with the ECM, which regulate Par3 expression and apical polarity (Zovein et al., 2010). In MDCK cells, the ECM-mediated polarization requires Rac1 (O'Brien et al., 2001), which activates a RhoA-ROCK I-myosin II pathway (Yu et al., 2008), and it will be exciting to understand if similar events occur in endothelial cells.

In addition to having ECM outside (basement membrane), many developing tubes have ECM inside (apical matrix). Although in many tubular systems the nature of the apical matrix remains nebulous, studies from the *Drosophila* trachea have found that apical matrix is critical for lumen size control. During tracheal development, a transient filament of chitin fills the lumen. Chitin is not required for tubular polarity or integrity; rather, it regulates uniform expansion and elongation of the tube (Tonning et al., 2005). Deposition of functional chitin requires components of the septate junction and chitin-modifying enzymes (Tonning et al., 2005; Luschnig et al., 2006; Wang et al., 2006; Moussian et al., 2006). Chitin is not the only component of the tracheal apical matrix important for morphogenesis (see below). A similar model for tubular size control has been proposed in the glial-like cells of *C. elegans* that surround sensory neurons (Perens and Shaham, 2005; Oikonomou et al., 2011), however, the apical matrix is not known to contain chitin and is likely complex (Bacaj et al., 2008).

1.2 Tiny tubes: Mechanisms of single-cell tube formation

Although most tubes are multi-cellular in cross-section, several organ systems, including the human vasculature (Bär et al., 1984), contain examples of tubes composed of a single-cell in cross-section. These single-cell, or unicellular, tubes can take on several distinct shapes, which can be distinguished by examining their pattern of apical junctions. For example, "seamed" unicellular tubes consist of a single cell rolled up into "C"-shape, and sealed by an autocellular junction (Figures 1.1A,C). "Seamless" unicellular tubes lack an autocellular junction and can be either "donut-shaped" or "ramified." The donut-shaped tubes are single cells penetrated by a lumen, with ring junctions on either side (Figures 1.1A–C). Ramified tubes contain a lumen that terminates within the cell; accordingly, ramified cells form a ring junction only at the side of the cell with an open lumen (Figures 1.1A–C). Interestingly, from a topological perspective, donut-shaped tubes are toroids, while seamed and ramified cells are spheres; thus, these different types of unicellular tubes might be formed by very different mechanisms. All three types of unicellular tubes have been documented in the model organisms *C. elegans* and *Drosophila* and likely exist in other organisms with less well-described anatomy.

The simplest model to explain the formation of a seamed tube is that a cell somehow wraps back on itself and self-seals with an autocellular junction. The stalk cells of the *Drosophila* trachea are seamed tubes and form a stack of connected cells during 2° branching (Samakovlis et al., 1996a). Live-imaging of stalk cell morphogenesis found that they form by intercalation (Ribeiro et al., 2004). The secondary branches are initially formed by pairs of cells arranged around the lumen; during branch extension, the pairs of cells intercalate with each other by wrapping around the lumen before zipping up to form autocellular junctions. Cell intercalation involves extensive remodeling of adherens junctions. Stalk cell morphogenesis requires the apical matrix

proteins Piopio and Dumpy (Jazwinska et al., 2003) and is inhibited by the transcription factor Spalt (Ribeiro et al., 2004). The *C. elegans* renal system is formed by three interconnected unicellular tubes: the pore, duct and excretory cells. The pore cell is a seamed cell and is also thought to form by self-wrapping (Stone et al., 2009). Intriguingly, the pore cell is replaced during post-embryonic development without disrupting tube function (Sulston et al., 1983). Pore cell replacement may share features with stalk cell intercalation as morphological intermediates of the two processes appear similar.

Two models have been proposed for the morphogenesis of ramified cells. In *C. elegans*, the excretory cell is a ramified cell required for osmoregulation. The excretory cell lumens run the entire length of the animal—a remarkable feat of bioengineering (Buechner, 2002). Genetic screens have identified a number of genes required for formation of the excretory cell lumen; these mutants have a characteristic cystic phenotype (Buechner et al., 1999). Mutant analysis suggests that the initial lumen is formed by pinocytosis of a large vacuole that then is extended by vesicle fusion at the sites of lumen outgrowth, a process known as cell hollowing (Figure 1.2D). Lumen outgrowth and maintenance requires a chloride intracellular channel, suggesting anion balance is critical (Berry et al., 2003). An alternative model has been recently proposed for development of the ramified terminal cells of the *Drosophila* trachea. Live imaging of terminal cell morphogenesis revealed that the lumen appears to initiate as an invagination of the apical surface, initially at the site of contact with the neighboring stalk cell. Lumen extension occurs by addition of vesicles along the length of the lumen. Both the lumen initiation and extension requires microtubules (Gervais and Casanova, 2010).

Cell hollowing may also play a role in the morphogenesis of donut-shaped cells. Cultured human endothelial cells can form tubular structures in vitro, a process that

appears to involve large intracellular vacuoles (Folkman and Haudenschild, 1980). Similar vacuoles were described during development of the zebrafish intersegmental blood vessels (ISVs), which may be formed by a series of connected donut-shaped cells (Kamei et al., 2006). However, this is controversial as other studies have found that the ISVs contain multiple cells in cross-section and that lumen formation occurs not intracellularly, but intercellularly (Wang et al., 2010; Blum et al., 2008). Branches of the *Drosophila* trachea are connected by two donut-shaped cells, called fusion cells, which align to ensure lumenal connectivity between adjacent branches (Samakovlis et al., 1996b). Similar to the terminal cells, lumen formation appears to initiate at the site of contact between the fusion cell and neighboring stalk cell. Invagination from this surface creates a ramified cell that must align with, and fuse lumens to, the other fusion cell. Contact of the fusion cells creates a focus of E-cadherin that aligns the fusion cell cytoskeleton (Lee et al., 2003). Lumen fusion requires trafficking of intracellular vesicles along the cytoskeleton to the invaginating lumen (Jiang et al., 2007). Alternatively, as I show in this thesis, donut-shaped cells in *C. elegans* can form via wrapping and self-fusion (see Chapter 2; Rasmussen et al., 2008; Stone et al., 2009).

1.3 The *C. elegans* pharynx: a model epithelial tube

The *C. elegans* embryo is an excellent system to study epithelial morphogenesis. The *C. elegans* system has several beneficial features, including facile forward and reverse genetics, a small, well-described genome, epithelial cells and orthologs of most human epithelial genes (Labouesse, 2006), an invariant cell lineage, the ability to manipulate cells within the animal, and hermaphrodite adults that produce embryos that develop ex utero. All stages of development are transparent facilitating observation of cellular behaviors. The *C. elegans* anatomy is relatively simple; the worm is built

from two epithelial structures: an outer layer of hypodermis (epidermis) and an inner digestive system. The digestive system is a series of connected tubular organs: the pharynx (foregut), intestine (midgut), and rectum (hindgut). Morphogenesis of these structures begins midway through embryogenesis, when most cells are post-mitotic and prior to embryonic movement (Sulston et al., 1983).

1.3.1 Pharyngeal form and function

The pharynx is a simple epithelial tube used for feeding and provides an attractive system for studying tubulogenesis at single-cell resolution. The adult pharynx contains 95 cells and its anatomy has been described in ultrastructural detail (Albertson and Thomson, 1976). The pharynx contains several different types of cells: neurons, glands, myoepithelial cells, and marginal cells (supporting epithelial cells). The epithelial cells of the pharynx are organized as a monolayer surrounding a central lumen and are encased by a basement membrane. The pharynx has a bilobed shape that can be divided into functional compartments. Bacteria enter the anterior pharynx, the procorpus, before being trapped in the first bulb, the metacorpus. The isthmus moves food between the metacorpus and the terminal bulb where it is crushed by the grinder before being passed through the valve into the intestine (Figure 1.3A). The general form and function of the *C. elegans* pharynx are conserved in diverse clades of nematodes (Khatoon and Erasmus, 1971; Yuen, 1968; Doncaster, 1962; Mapes, 1965b,a; Chitwood and Chitwood, 1950; Bird, 1971; Lee, 1968).

The epithelial cells of the pharynx are organized into cell groups along the anterior-posterior axis, with region-specific anatomy (Albertson and Thomson, 1976). The myoepithelial cells form cell groups pm1 (pm for pharyngeal muscle) through pm8. The nine marginal cells form groups mc1 (mc for marginal cell) through mc3. The valve epithelial cells from groups vpi1 (vpi for valve pharynx/intestine) through vpi3.

Most cell groups contain multiple cells and are organized with triradiate symmetry around the lumen, which itself is triradiate, or Y-shaped. Individual cells are named for their cell group and position within the cell group; for example, mc3DL is the dorsal, left cell in the mc3 group. In cross-section, most of the pharynx is a multicellular tube, with marginal cells interleaved between the myoepithelial cells (Figure 1.3B). There is one notable exception, the terminal muscle cell, pm8, which forms a donut-shaped single-cell tube. pm8 is connected to vpi1, which is the anterior cell of the valve and is also donut-shaped. The other valve cell groups vpi2 and vpi3 form rings of three and two cells, respectively.

1.3.2   Pharyngeal morphogenesis

Development of the pharynx begins in the early embryo when maternally provided factors induce expression of the forkhead transcription factor PHA-4, the master regulator of pharyngeal development. PHA-4 is expressed in the descendants of two early embryonic cells, called ABa and MS (see below; reviewed by Mango, 2009). Following induction of PHA-4, pharyngeal cells gastrulate; MS descendants gastrulate first, followed by ABa descendants (Sulston et al., 1983; Nance and Priess, 2002; Harrell and Goldstein, 2011). Midway through embryogenesis the pharyngeal cells aggregate together into a cyst that adopts a radially symmetric, rosette-like structure (Leung et al., 1999). Cells in the cyst develop apicobasal polarity and are wedge-shaped, with a small apical surface facing the lumen and a broad basal surface contacting basement membrane (see Chapter 3). The pharyngeal basement membrane contains type IV collagen, laminin, perlecan, and nidogen (Kramer, 2005). Subsequently, the pharynx develops triradiate symmetry as evidenced by the formation and expansion of the Y-shaped lumen (Leung et al., 1999).

Surprisingly little is known about morphogenesis of the pharynx, in part because

mutations that affect major components of the cytoskeleton including HMR-1/E-cadherin, PAT-3/β-integrin, INA-1/α-integrin, and DLG-1/discs large, do not yield obvious pharyngeal defects (Costa et al., 1998; Williams and Waterston, 1994; Baum and Garriga, 1997; Bossinger et al., 2001). Two studies examined how the anterior cells of the cyst attach to the anterior of the animal (Portereiko and Mango, 2001; Portereiko et al., 2004). Pharyngeal attachment requires the anterior cells to reorient their polarity, epithelialize, and contract (Portereiko and Mango, 2001). Epithelialization of the anterior cells requires the kinesin-like protein ZEN-4/MKLP and its partner CYK-4/RhoGAP (Portereiko et al., 2004), although how they function in the anterior cells is unknown.

1.3.3   Commitment to pharyngeal cell fate

Although our understanding of pharyngeal morphogenesis remains rudimentary, quite a bit has been learned about the molecular events that recruit cells to become pharyngeal tissue (Mango, 2009). PHA-4 expression requires maternal factors in both the AB and MS lineages, although the details are quite different.

In the AB cell lineage, two sister blastomeres ABa and ABp have equal potential express PHA-4 and acquire pharyngeal cell fate (Priess and Thomson, 1987). However, pharyngeal fate is inhibited in ABp and then induced in ABa by sequential Notch interactions at the 4- and 12-cell stages of embryogenesis, respectively (Priess, 2005). The first Notch interaction induces expression of the bHLH transcription factor REF-1. REF-1 is thought to inhibit expression of two T-box transcription factors, *tbx-37* and *tbx-38*, which are critical for AB pharyngeal development (Neves and Priess, 2005; Good et al., 2004). *tbx-37* and *tbx-38* are expressed in ABa prior to the second Notch signal and, together with Notch, induce PHA-4 expression in ABa descendants.

In the MS cell lineage, asymmetric segregation localizes the maternal protein SKN-

1, a cap and collar transcription factor, to the EMS blastomere. EMS-derived cell fates require SKN-1 (Bowerman et al., 1992). EMS will divide to give rise to the E and MS blastomeres that produce intestine and mesoderm (pharynx and muscle), respectively. The asymmetric division of EMS requires POP-1, a TCF/LEF-1 homolog; loss of *pop-1* results in EMS producing two E-like daughters, suggesting it is required for MS development (Lin et al., 1995). In the MS cell, POP-1 is thought to inhibit E cell fate (Calvo et al., 2001), allowing SKN-1 to activate expression of *med-1* and *med-2*, which in turn activate *ceh-51* and *tbx-35*; *med-1/2* or *ceh-51/tbx-35* mutants lack MS-derived cell fates (Maduro et al., 2007, 2001; Broitman-Maduro et al., 2006, 2009). *ceh-51/tbx-35* mutants fail to express PHA-4 in MS descendants (Broitman-Maduro et al., 2009), although the molecular connection between CEH-51/TBX-35 and PHA-4 has not been elucidated.

In addition to PHA-4 being necessary and sufficient for pharyngeal cell fate (Horner et al., 1998; Kalb et al., 1998; Mango et al., 1994), it is required throughout life for pharyngeal function (Kaltenbach et al., 2005). Similarly, foregut development in several systems also requires foxA transcription factors (Carlsson and Mahlapuu, 2002). To understand how PHA-4 functions, several approaches have been taken to identify PHA-4 targets. Microarray analysis of mutants that produce more or less pharynx than wild-type embryos identified a set of PHA-4 target genes. Analysis of these targets and their PHA-4 binding sites revealed that genes expressed earlier in development had higher affinity binding sites than those expressed later. This suggests a model that early in development, when levels of PHA-4 are limiting, only high-affinity targets are expressed, whereas later, when levels of PHA-4 increase, both high- and low-affinity targets are expressed (Gaudet and Mango, 2002). A bioinformatic study identified combinatorial binding sites that can also influence timing of PHA-4 dependent gene expression (Gaudet et al., 2004). Recently, ChIP-Seq (chro-

matin immunoprecipitation followed by sequencing) was used to identify a global set PHA-4 targets (>4,000 genes, ~20% of the genome) at different stages of wild type development (Zhong et al., 2010).

Interestingly, PHA-4 is required to specify all of the pharyngeal cell types, yet these cell types are quite different. For example, the myoepithelial cells are contractile and pump food through the pharynx (Avery and Thomas, 1997), whereas the gland cells secrete mucins into the lumen (Smit et al., 2008). These functional differences have corresponding molecular differences: the myoepithelial cells express the muscle-specific myosin *myo-2*; the gland cells express the gland-specific *phat* genes. How PHA-4 coordinates with cell-type specific factors to generate the diverse pharyngeal cell types is not fully understood. The myoepithelial cells partially require the PHA-4 target CEH-22 for *myo-2* expression (Okkema and Fire, 1994; Okkema et al., 1997; Gaudet and Mango, 2002). In the gland cells, HLH-6 activates *phat* gene expression (Smit et al., 2008) and *hlh-6* is likely a target of PHA-4 (Raharjo and Gaudet, 2007). However, *hlh-6* mutants do not completely lack gland cells, suggesting other factors are involved. The full story is likely quite complex as individual cell groups (within a cell type) have unique morphologies and gene expression patterns.

Figure 1.1: Examples of epithelial tubes. (A) Cross-sectional views of different types of epithelial tubes. (i) A multi-cellular tube; (ii) a tube composed of a single 'C'-shaped cell; (iii) a seamless single-cell tube. Apical surface is shown in green. (B) Longitudinal sections showing two types of seamless single-cell tubes. (i) A donut-shaped cell in which the lumen runs through the cell (topologically a toroid); (ii) a ramified cell in which the lumen terminates within the cell (topologically a sphere). (C) Drawings of apical junctions for various tube types.

A _____ cross section _____

(i) multicellular tube   (ii) single-cell tube with seam   (iii) seamless single-cell tube

B _____ longitudinal section _____

(i) donut-shaped   (ii) ramified

C _____ apical junctions _____

(i) multicellular   (ii) seamed   (iii) seamless   (iv) ramified
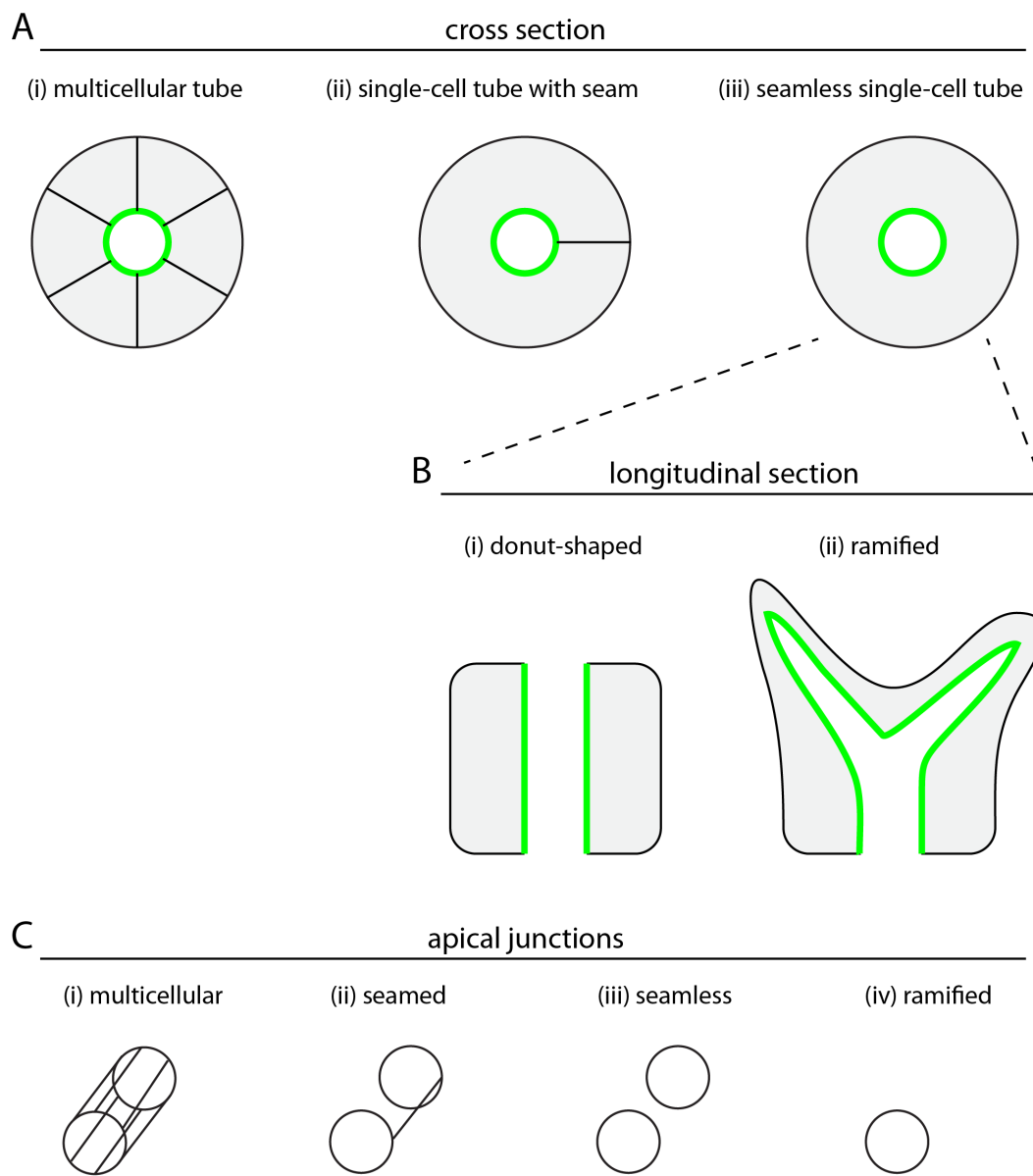
Figure 1.2: Mechanisms of tubulogenesis. (A) A sheet wrapping; (B) cavitation; (C) cord hollowing; (D) cell hollowing. Apical surfaces are shown in green.

A
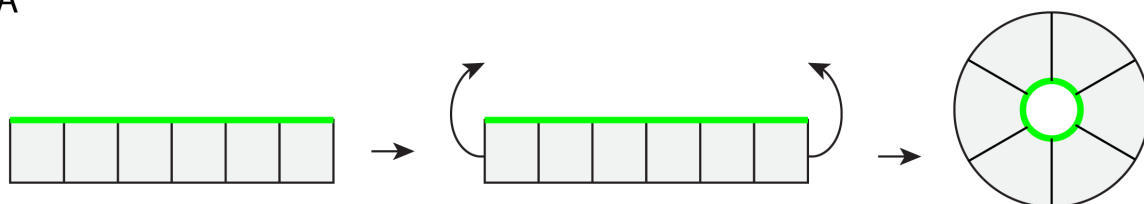
B
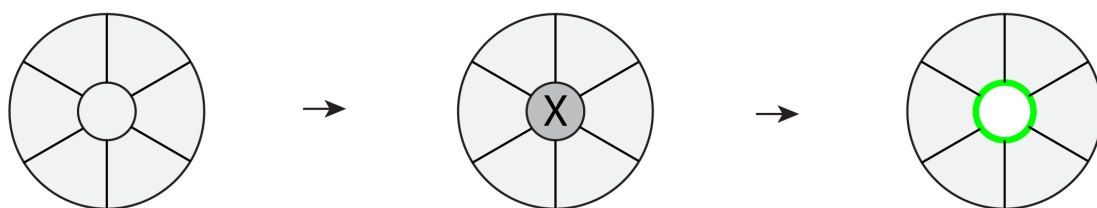
C
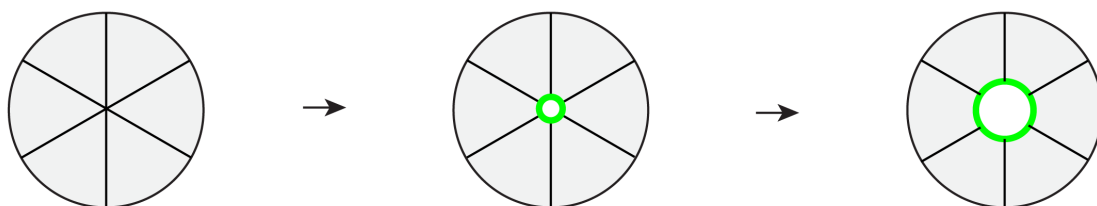
D
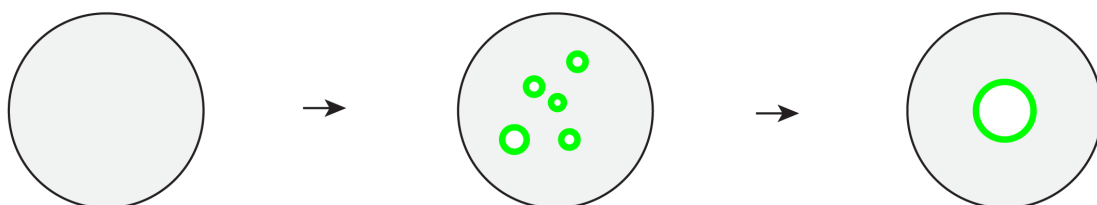
Figure 1.3: Epithelial anatomy of the *C. elegans* pharynx. (A) Nomarski image of the larval pharynx and valve. Anterior is to the left. The cuticle-rich lumen is indicated with an arrowhead. The basement membrane that surrounds the pharynx is indicated by an arrow. The grinder, a specialized structure for crushing bacteria, is marked with an asterisk and it part of the terminal bulb (t. bulb). (B) Upper: cartoon of the pharynx and valve. Positions of marginal cell groups along the anterior-posterior axis are indicated. Marginal cells (mc) shown in magenta; myoepithelial cells (pm) shown in blue. Lower: transverse views of the pharynx showing arrangement of epithelial cells around the Y-shaped lumen. The anterior pharynx is a multicellular tube. Note junctional remnant in pm2-5 from embryonic fusion events. pm8 and vpi1 are seamless tubes. The vpi2 group is a ring of three cells.

A

procorpus metacorpus isthmus t. bulb valve int

B

mc1 mc2 mc3

pm2-5 pm6-7 pm8 vpi1 vpi2
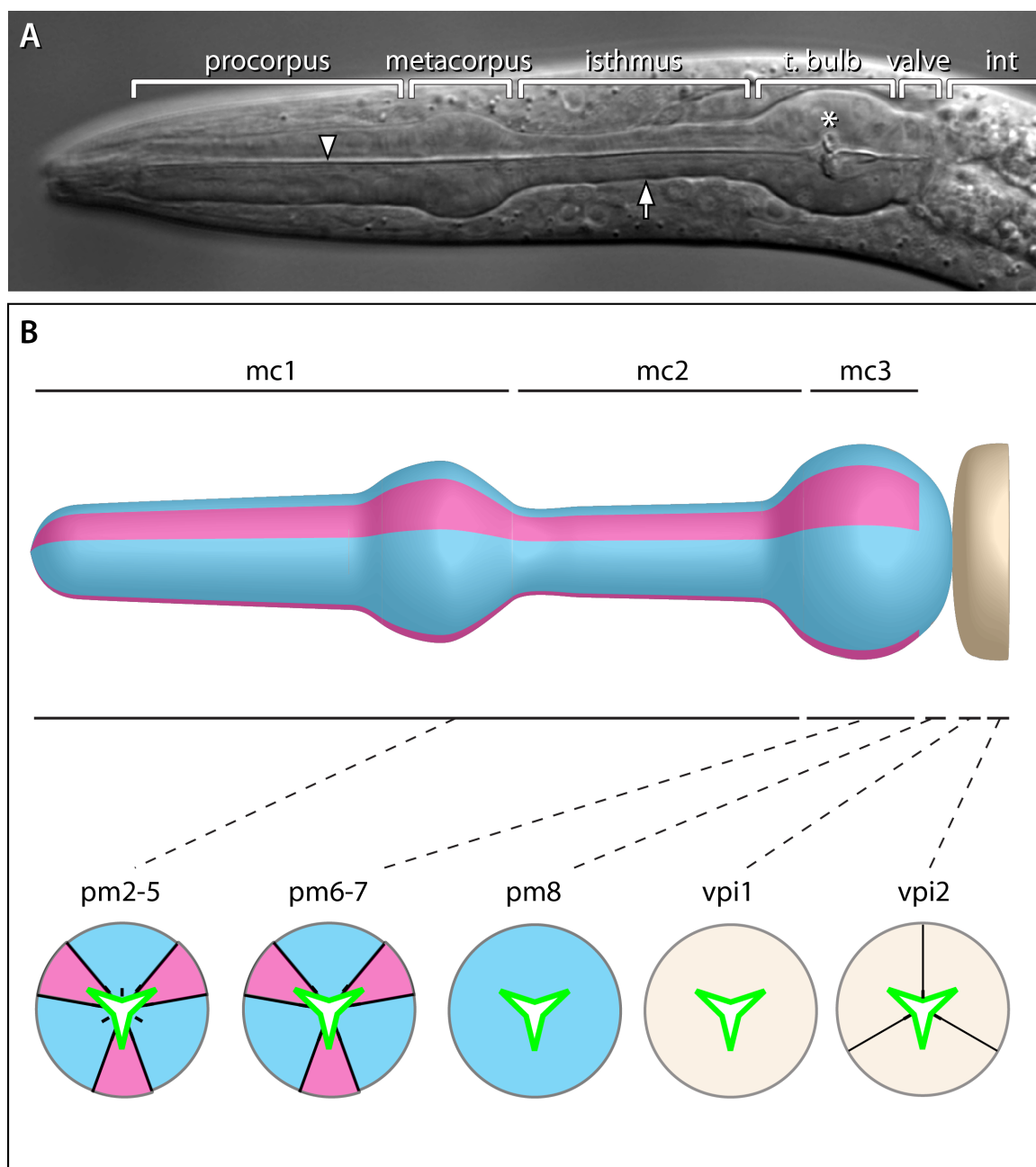
Chapter 2

NOTCH SIGNALING AND MORPHOGENESIS OF SINGLE-CELL TUBES IN THE *C. ELEGANS* DIGESTIVE TRACT

During organogenesis of the *C. elegans* digestive system, epithelial cells within a cyst-like primordium develop diverse and cell type-specific shapes through largely unknown mechanisms. We here analyze the morphogenesis of two adjacent epithelial cells in the cyst, called pm8 and vpi1, which become donut-shaped, or toroidal, single-cell tubes. pm8 and vpi1 delaminate from the dorsal epithelium and migrate across the cyst on a transient tract of laminin between ventral epithelial cells, while remodeling their apical junctions. pm8 appears to encircle the midline by wrapping around finger-like processes from neighboring cells. Finally, pm8 and vpi1 self-fuse to become toroids by expressing AFF-1 and EFF-1, respectively, two fusogens previously shown to promote cross-fusion between other cell types. Notch signaling is required for the expression of multiple genes, including *aff-1*, in pm8. In addition, Notch inhibits *eff-1* expression in pm8, thereby preventing cross-fusion between pm8 and vpi1. Thus, the tubulogenesis of pm8 and vpi1 involves highly orchestrated interactions with neighboring epithelial cells.[1]

2.1 Introduction

Epithelia formation is fundamental to the development of all animals. Epithelial cells are polarized, with basolateral domains separated from apical domains by adherens

---

[1]This chapter is reprinted from (Rasmussen et al., 2008), with permission from Elsevier.

junctions. The adherens junctions contain E-cadherin and other proteins that mediate cell adhesion, and the basal surface typically is associated with a basal lamina. Despite the organization and cohesion of epithelial cells, epithelia can be extensively remodeled in response to developmental signals. Planar epithelia can be remodeled into tubes, and epithelial tubes can develop branches (Lubarsky and Krasnow, 2003). Although oriented cell division or apoptosis can contribute to remodeling (Gong et al., 2004; Schreiber et al., 2005), in many cases remodeling involves non-dividing cells that change shape or position. For example, the elaborately branched tracheal tubes of *Drosophila* begin as sacs of epithelial cells that intercalate and change shape without dividing (Casanova, 2007). Epithelia can dissociate during epithelial to mesenchymal transitions (Thiery and Sleeman, 2006), or undergo transient restructuring to allow the passage of migrating cells. Examples of transepithelial migration include *Drosophila* germ cells that migrate through the posterior midgut epithelium to form the gonad (Kunwar et al., 2006), and the passage of human leukocytes through the epithelial lining of blood vessels to reach sites of infection (Petri and Bixel, 2006). These events demonstrate the remarkable ability of epithelial cells to change shapes by altering their adhesiveness.

The *C. elegans* pharynx provides an attractive model system for analyzing molecular mechanisms of epithelial remodeling during organogenesis. The pharynx is essentially a monolayered myoepithelial tube whose anatomy, specification and gene expression have been compared to the heart of higher animals. For example, the ascidian heart is a simple tube, consisting of a monolayer of myoepithelial cells (Oliphant and Cloney, 1972). The NK homeodomain transcription factors CEH-22 and Nkx2.5 function in nematode pharynx and vertebrate heart development, respectively, and zebrafish Nkx2.5 can rescue *C. elegans* mutants lacking CEH-22 (Chen and Fishman, 1996; Okkema and Fire, 1994; Okkema et al., 1997; Haun et al., 1998). In addi-

tion to muscle cells, the pharynx contains glands, neurons, and structural cells called marginal cells. An ultrastructural reconstruction of the adult pharynx showed these individual cells have remarkably complex, and reproducible shapes (Albertson and Thomson, 1976). Along the longitudinal axis of the pharynx, muscles and marginal cells are organized into distinct anterior/posterior groups based on region-specific morphologies. For example, the most anterior muscle is shaped like a fenestrated cylinder with openings that are nearly as large as the cell, while the most posterior muscle is a toroid. The pharynx is linked to the intestine through valve cells, the first of which is also a toroid.

Nearly all of the complex changes in pharyngeal cell shape begin within a cylindrical cyst of initially uniform, simple epithelial cells (Leung et al., 1999; Portereiko and Mango, 2001). During early embryogenesis, cells from two separate lineages aggregate to form a primordium that forms the pharynx and valve (Mango, 2007). In both lineages, the key step in specifying pharyngeal/valve fate is the expression of PHA-4, an organ selector gene that encodes a forkhead box transcription factor. PHA-4 is expressed in all pharyngeal and valve cells, and is necessary and sufficient for most early embryonic cells to adopt pharyngeal fates (Horner et al., 1998; Kalb et al., 1998; Mango et al., 1994). Midway through embryogenesis, cells in the primordium polarize to form an epithelial cyst that is primarily one cell in thickness (Leung et al., 1999). In cross sections of the cyst, most cells have a simple, wedge-shaped appearance: each cell has a narrow apical tip facing the midline of the cyst, and a broad basal surface associated with a basal lamina.

A complex remodeling of the cyst occurs over the next few hours of embryogenesis (Leung et al., 1999; Mango, 2007). The cylindrical cyst is transformed into a bilobed, tubular pharynx that contains a wide diversity of cell shapes and that is partitioned from the adjacent valve cells by a basal lamina. To understand how cell shapes are

determined within the cyst, we analyzed here the development of two toroidal, single-cell tubes called pm8 and vpi1. We show that morphogenesis involves Notch signaling, epithelial to mesenchymal transitions, migration through neighboring cells on a transient tract of laminin, and self-fusion. These results reveal numerous interactions that contribute to the final shapes of the cells.

2.2 Results

2.2.1 Background

The pharynx is a bilobed, myoepithelial tube containing pharyngeal muscles (pm), structural cells called marginal cells (mc), gland cells, and neurons (Figure 2.1A; see Mango, 2007, for description of pharyngeal anatomy and development). The pharynx connects to the intestine through a multicellular valve (vpi cells for <u>v</u>alve <u>p</u>harynx/<u>i</u>ntestine). The events analyzed here occur in the posterior lobe of the pharynx, called the terminal bulb, and in the adjacent valve cells. Most cells in the pharynx are arranged with threefold radial symmetry around the lumenal axis (Figure 2.1A and Movie S1, see the Supplemental Data available with this article online). Muscles, marginal cells, and valve cells show anterior/posterior differences in cell morphology, creating distinctive groups of one to six cells (groups pm1–8, mc1–3, vpi1–3; Albertson and Thomson, 1976). For example, mc3V is the ventral cell of the three group 3 marginal cells (Figure 2.1A). Although multiple cells surround the lumen of the pharynx/valve in a typical cross-section, there are two examples of single-cell tubes: pm8, the terminal cell in the pharynx, and vpi1, the first cell in the valve (Figures 2.1A–C). Our analysis of pm8 and vpi1 morphogenesis begins at about 6.5 hours after the 2-cell stage of embryogenesis, when the primordium of the pharynx/valve is a cylindrical cyst of polarized epithelial cells (Figures 2.1B,D). The apical surfaces of these cells face the midline of the cyst, where the pharyngeal/valve lumen forms,

and are outlined by junctional proteins such as AJM-1 (Figures 2.1D,E). The basal surfaces of these cells face the periphery of the cyst, and are associated with a basal lamina that contains laminin (Figure 2.1D).

2.2.2 Notch signaling regulates gene expression in pm8

Several genes have been described that are expressed in multiple or all pharyngeal and valve cells, however, the *ceh-24* gene is expressed uniquely in pm8 (Harfe and Fire, 1998). CEH-24 is an NK transcription factor related to CEH-22 (see Introduction), and previous studies identified a 117 bp enhancer from *ceh-24* that promotes pm8-specific expression (Harfe and Fire, 1998). We noticed that this enhancer contained a conserved GTGGGAA sequence that is a predicted binding site for LAG-1/CSL, the core DNA-binding protein in the Notch signaling pathway (Figure 2.7A; see Greenwald, 2005; Bray, 2006, for reviews on Notch). We found that LAG-1/CSL bound the wild-type enhancer in vitro, and that binding was dependent on the GTGGGAA sequence (Figure 2.7B). Transgenic *ceh-24*::GFP reporters constructed with either the wild-type enhancer sequence, or with a GTGGGAA to GAGGCAA mutation, were expressed in head neurons outside the pharynx, but only the wild-type enhancer drove robust expression in pm8 (Figures 2.2C and 2.7D; Table 2.1). Expression was dependent on Notch activity, as *lin-12 glp-1* double mutants that lack both of the *C. elegans* Notch proteins, LIN-12 and GLP-1, either did not express *ceh-24*::GFP (18/20 embryos) or showed only weak expression (2/20 embryos; Figure 2.2D; Table 2.1).

REF-1 is a *C. elegans* bHLH transcription factor that is distantly related to *Drosophila* E(spl) (Alper and Kenyon, 2001; Neves and Priess, 2005). The *ref-1* gene is a direct target of Notch signaling in several interactions in the early embryo, but is expressed in other cells independent of Notch (Neves and Priess, 2005). In

the wild-type epithelial cyst, we found that *ref-1*::GFP was expressed in pm8 and in the sister cells e2V and mc3V (Figure 2.2I and data not shown). *lin-12 glp-1* double mutants showed expression in e2V and mc3V, but not in pm8 (Figure 2.2J; Table 2.1). Additional experiments showed that pm8 expression required LAG-1/CSL, and appeared to involve either of the Notch ligands LAG-2/Delta or APX-1/Delta (Table 2.1 and see below).

The *myo-2* gene encodes a pharyngeal-specific myosin; the *myo-2* promoter lacks predicted LAG-1/CSL binding sites, and thus is unlikely to be a direct target of Notch signaling (data not shown). We generated an integrated transgenic strain expressing a nuclear-localized *myo-2*::GFP reporter (J. Gaudet, unpublished), and found that wild-type larvae reproducibly showed expression in each of the expected 13 muscle nuclei in the terminal bulb (6 pm5 + 3 pm6 + 3 pm7 + 1 pm8; Figure 2.2E; Table 2.1). Notch mutant larvae had defects in pm8 myogenesis (Figures 2.2F and 2.8B); for example, 97% of *lag-1* mutant larvae contained only 12 *myo-2*::GFP-expressing cells in the terminal bulb, and specifically lacked expression at the normal position of pm8 (Table 2.1). We conclude that Notch signaling induces the expression of a least two transcription factors in pm8, CEH-24 and REF-1, and is required for pm8 myogenesis.

2.2.3   Notch mutants are defective in both pm8 and vpi1 morphogenesis

lag-1 mutant larvae usually lacked a nucleus in the normal position of the pm8 nucleus, suggesting that Notch mutants have a defect in pm8 morphogenesis that is at least partially separate from the myogenesis defect. We used light and electron microscopy to compare the pharynx and valve in newly hatched, wild-type larvae with Notch mutant larvae. In newly hatched, wild-type larvae, the first valve cell (vpi1) forms a cup-like enclosure over the posterior end of pm8 (Figures 2.9A,C); in live animals,

pm8 and vpi1 appear tightly adherent and show no visible separation during body locomotion (our unpublished observations). pm8 and vpi1 make a small, direct contact near their apical surfaces, but are otherwise separated by a prominent basal lamina that almost completely separates the pharynx from the valve (Figure 2.9C). In Notch mutant larvae, cells at the pharynx/valve interface had several morphological defects including large gaps between cells (arrow in Figure 2.2B), broad contacts between pharyngeal cells and valve cells without an intervening basal lamina (Figure 2.9B and data not shown), and abnormal patterns of apical junctions (see Figures 2.4H,I). We were unable to identify cells with the normal morphology of pm8 or vpi1 in the mutant larvae, although other cells such as the pm6 and pm7 muscles appeared well differentiated (n=12; Figure 2.9B). Thus, these results suggest the Notch pathway has a role in the differentiation or morphogenesis of pm8, vpi1, and possibly other valve cells.

2.2.4   *Notch is activated in the postmitotic pm8 cell*

To determine when and where Notch interactions occurred, we first sought to identify the relevant ligand-expressing cells through laser-killing experiments. We found that descendants of the embryonic cell MSaapa that were not previously known to function in Notch signaling expressed the ligand LAG-2/Delta (Figure 2.3A) and were required for Notch-dependent *ref-1*::GFP expression in pm8 (Figure 2.3B). In immunostaining experiments, the first apparent contact between MSaapa descendants expressing *lag-2*::GFP and cells that express the receptor LIN-12/Notch occurred after the birth of pm8, approximately 6 hours after the 2-cell stage. A clone of four LIN-12-expressing cells is located in the left dorsal quadrant of the epithelial cyst; the most posterior cell in this group is pm8 (Figures 2.3C,D). At this stage, vpi1 is in the right dorsal quadrant of the cyst, and does not express detectable levels of LIN-12; the receptor

GLP-1/Notch was not detectable in vpi1 or pm8 (Figure 2.3C and data not shown). MSaapa descendants within the cyst express LAG-2/Delta, and one or two of these cells contact pm8 directly (Figure 2.3C). Lateral views of embryos at approximately the same stage showed Notch-independent expression of *ref-1*::GFP in the pharyngeal cells e2V and mc3V, but no other pharyngeal or valve cells (Figure 2.3D'). However, pm8 showed strong *ref-1*::GFP expression about 30 minutes later (Figure 2.3E'). These results suggest that Notch signaling is activated in the postmitotic pm8 cell, but not in vpi1 or any other valve cell, and that Notch thus has an indirect role in valve differentiation or morphogenesis.

2.2.5 pm8 and vpi1 morphogenesis

The initial stages of wild-type pm8 morphogenesis were visualized by immunostaining for LIN-12/Notch. For subsequent stages, we used the *ref-1* promoter to drive expression of a plasma membrane-localized GFP (*ref-1*::GFP-PM). pm8 initially is a wedge-shaped epithelial cell on the dorsal, left side of the cyst, and has a broad, midline-facing apical surface similar to other cyst cells (Figure 2.1E and Figure 2.3D). Shortly thereafter, pm8 nearly detaches from the dorsal basal lamina, and its apical surface is remodeled into a lamella that invades the ventral side of the cyst (Figures 2.3E and 2.4A,B; data not shown). Both the pm8 nucleus and bulk cytoplasm cross into the ventral side, leaving only a thin connection to the dorsal perimeter of the cyst (Figures 2.4A–D). pm8 invades the ventral side of the cyst to the left of the midline, but gradually spreads across the entire cross section of the cyst (Figure 2.4F and Movie S1).

vpi1 morphogenesis was examined by electron microscopy and expression of *eff-1*::EFF-1::GFP (see below). Similar to pm8, vpi1 initially is a wedge-shaped dorsal cell that extends a lamellar process into the ventral side of the cyst; the vpi1 lamella

is closely associated with the posterior surface of the migrating pm8 cell body (Figures 2.4E and 2.9D). In contrast to pm8, the nucleus and bulk cytoplasm of vpi1 remain on the dorsal side of the cyst. Both pm8 and vpi1 appear to redistribute cytoplasm throughout their respective cell bodies during late embryogenesis, becoming symmetrical tubes centered on the midline of the cyst (Figure 2.1C, inset, and data not shown).

2.2.6 pm8 and vpi1 migrate within the cyst on a transient path of laminin

In all embryos analyzed, pm8 and vpi1 migrated into the ventral side of the cyst specifically at the lateral interface between the ventral cells mc3V and vpi2V (see Figure 2.1B). In some examples of transepithelial migration in other systems, cells in the target epithelium disassociate prior to the arrival of migrating cells, thus creating openings for migration (Kunwar et al., 2006). Electron micrographs of the epithelial cyst before or during pm8 migration did not show obvious gaps between any ventral cells (data not shown). A second possibility is that the mc3V/vpi2V interface provides a guidance cue for pm8 migration. Consistent with this hypothesis, we found that a transient tract of laminin appears in the ventral cyst shortly before pm8 migration (Figures 2.5A,D), and disappears after pm8 migration (Figure 2.5E). Heterotrimeric laminin in *C. elegans* is composed of either of two α chains (EPI-1 and LAM-3), a β chain (LAM-1), and a γ chain (LAM-2) (Kramer, 2005). An antiserum specific for LAM-3 stained the tract in wild-type embryos, but not in *lam-3* mutant embryos (data not shown). In time-lapse movies of *lam-1*::LAM-1::GFP, the laminin tract appeared to spread inward from the ventral perimeter of the cyst over a 20 minute interval (Movie S2) before regressing. In later embryogenesis, a different and permanent zone of laminin appears along the posterior surface of pm8 that is part of the basal lamina between pm8 and vpi1 (Figures 2.5F and 2.9C). Using *ref-1*::GFP to identify both

mc3V and pm8, we found that the transient laminin tract appeared specifically at the mc3V/vpi2V interface, and that the tract disappeared concomitant with the ventral migration of pm8 (Figures 2.5G–I). The laminin tract was present at the mc3V/vpi2V interface in *lin-12 glp-1* mutants, indicating that it is specified independent of Notch signaling. Indeed, the tract persisted in 7.5 hour-old *lin-12 glp-1* mutant embryos (Figure 2.5B), long after it disappears from wild-type embryos (Figure 2.5E).

An antiserum against EPI-1 stained the tract, indicating that it contains both laminin α chains, LAM-3 and EPI-1. We found that *lam-3* and *epi-1* single mutants appeared to have normal pm8 migration (data not shown). However, pm8 was unable to migrate ventrally in *lam-3; epi-1* double mutants, and instead remained primarily on the dorsal side of the cyst (Figure 2.5J). Cell migration on laminin surfaces can involve the major laminin receptor, integrin. In *C. elegans*, *ina-1* is one of two genes encoding the alpha subunit of heterodimeric integrin, and *pat-3* encodes the sole beta subunit (Kramer, 2005). *pat-3(RNAi)* embryos had severe developmental defects that complicated an analysis of pm8 migration. However, most *ina-1* mutants were able to complete embryogenesis and hatch as deformed larvae. We found that *ina-1* mutants showed severe defects in pm8 migration (Figure 2.5K). In many larvae, pm8 appeared to have migrated abnormally, into the region normally occupied by valve cells and anterior intestinal cells (Figure 2.5K). The pm8 cell body was closely apposed to the basal lamina surrounding the valve and intestine, suggesting that pm8 might extend along basal laminae associated with these surfaces rather than the normal mc3V/vpi2V interface.

2.2.7   Tubulogenesis and self-fusion

A single-cell tube such as pm8 or vpi1 might, in principle, be either a toroid or a C-shaped cell. The apical surfaces of both types of tubes have circular intercellular

junctions at each end of the cell, but only the C-shaped cell has an autocellular apical junction (Figure 2.6A). pm8 and vpi1 have been shown to be toroids, rather than C-shaped cells, in adult *C. elegans* (Albertson and Thomson, 1976). We found that in 7.5 hour embryos pm8 and vpi1 had the apical junction pattern expected for toroidal cells (two unconnected circles; Figure 2.6B), and confirmed by electron microscopy that both cells are toroids (Figure 2.10). Although an epithelial cell can roll up into a C-shape, a toroid has a distinct topology that requires at least one self-fusion event. *C. elegans* development provides multiple examples where adjacent cells fuse together into a multinucleate syncytium, and most of these fusions require the *eff-1* gene (Mohler et al., 2002). EFF-1 acts homotypically to induce fusion; it is sufficient to promote fusion of heterologous cells that each express EFF-1 (Podbilewicz et al., 2006). Recent studies in *C. elegans* have identified a second fusogen, AFF-1, with a similar ability to fuse heterologous cells (Sapir et al., 2007). We found that *eff-1*::EFF-1::GFP was expressed at high levels in vpi1 beginning at about 7 hours (Figure 2.6B'), but was never expressed in pm8. In 7.5 hour *eff-1* mutant embryos, vpi1 had a novel, autocellular junction as characteristic of a C-shaped cell, while pm8 retained the wild-type, toroidal pattern of intercellular junctions (Figure 2.6B, inset). Conversely, aff-1::GFP was expressed in pm8 beginning at about 7.2 hours, but was never expressed in vpi1 (Figure 2.6C'). In 7.5 hour aff-1 mutant embryos, pm8 had a novel autocellular junction, while vpi1 retained the wild-type, toroidal pattern of intercellular junctions (Figure 2.6C, inset). These results suggest that in normal development both pm8 and vpi1 adopt C-shapes before self-fusing through AFF-1 and EFF-1 activities, respectively.

Because cells in the approximate positions of pm8 and vpi1 have highly abnormal patterns of apical junctions in Notch mutants, we examined EFF-1 expression in these embryos. Although *eff-1*::EFF-1::GFP is expressed only in vpi1 in wild-type

embryos, in *lag-1* mutant embryos the reporter was expressed in two adjacent cells at this position (Figures 2.6D,E), or in a single, abnormally large binucleate cell (Figure 2.6F). We identified one of the cells that expressed *eff-1*::EFF-1::GFP as pm8 based on its contact with group 7 muscle cells (data not shown). Conversely, neither pm8 nor vpi1 expressed *aff-1*::GFP in lag-1 mutants (Table 2.1). We conclude that Notch has two roles in pm8 and vpi1 tubulogenesis. First, Notch is required for pm8 to express AFF-1, allowing pm8 to self-fuse. Second, Notch is required to prevent pm8 from expressing EFF-1, thereby preventing pm8 from cross-fusing with the EFF-1-expressing vpi1 cell.

2.2.8 *Formation of the intracellular lumen in pm8 and vpi1*

If pm8 and vpi1 normally become C-shaped cells that then self-fuse into toroids, how are their C-shapes determined? Three group 3 marginal cells are immediately anterior to pm8 during pm8 and vpi1 morphogenesis, and one of these (mc3V) expresses the same *ref-1*::GFP-PM reporter as pm8 (see Figures 2.1A and 2.3E'). In analyzing pm8 morphogenesis, we discovered that all three marginal cells extend a finger-like process posteriorly along the midline of the cyst during pm8 and vpi1 morphogenesis (Figures 2.4A–D,F, and 2.10A; Movie S3). Thus, as the pm8 cell body moves into the left ventral side of the cyst, then spreads across the entire cross section of the cyst, it wraps around the three marginal cell fingers (Movie S4). The fingers appeared to stop at, or extend slightly beyond, the posterior surface of pm8, where they would presumably contact the thin, ventral lamella from vpi1; vpi1 showed a strong enrichment of filamentous actin at the midline during formation of its lumen that was not apparent in pm8 (Figure 2.4E). Previous studies have shown that the pharyngeal lumen begins as small opening along the midline of the epithelial cyst; as the lumen expands it acquires a Y-shape when viewed in cross section (Leung

et al., 1999). The three marginal cell fingers remained in the center of pm8 during lumenal expansion, moving apart to occupy the three tips of the Y-shaped lumen (Figure 2.4F). The marginal cell fingers formed apical junction connections with the apical face of pm8, but not vpi1, and persisted in the pm8 cell body throughout larval development. Thus, while the cylindrical apical surface of pm8 initially has only two, circular intercellular junctions (Figure 2.6B), in late embryos and larvae there are an additional three, paired lines of junctional material across this surface that correspond to the three fingers (Figures 2.6G,H). An intriguing possibility is that the marginal cells fingers template the lumenal channel through pm8, and possibly vpi1, as pm8 and vpi1 remodel their apical surfaces. However, we have not yet been able to test this hypothesis by removing all three marginal cells simultaneously; pm8 formed an abnormally shaped lumen when only mc3V was killed with a laser microbeam (2/2 embryos), or when the fate of mc3V was transformed by the *glp-1(e2072)* mutation (3/3 embryos examined by electron microscopy; see Priess et al., 1987).

2.3   Discussion

2.3.1   Establishment of the pharynx/valve boundary

We here analyzed the morphogenesis of pm8 and vpi1, two adjacent, single-cell tubes in the *C. elegans* digestive tract. pm8 and vpi1 differentiate within a cyst of initially similar epithelial cells that all express PHA-4. The morphogenetic events that define the pm8/vpi1 boundary compartmentalize the cyst into the functionally distinct organs of the pharynx and valve. Cells throughout the epithelial cyst initially have a radially-oriented apicobasal axis, and most cells retain this polarity after morphogenesis. For example, pharyngeal muscles have single sarcomeres, and in most of these muscles the myofilaments are oriented radially, extending from the pharyngeal lumen to the peripheral basal lamina. In contrast, the apicobasal axes of pm8 and vpi1 are

reoriented during morphogenesis. The basal surfaces of pm8 and vpi1 shift to face each other, and presumably form the basal lamina that nearly separates the two cells. This shift in polarity allows pm8 to have obliquely-oriented myofilaments; similar myofilaments occur at the terminus of the pharynx in diverse groups of nematodes, and are believed to function in moving foodstuffs during feeding (Doncaster, 1962; Mapes, 1965a). We speculate that it is advantageous for pm8 and vpi1 to be toroids, rather than simply C-shaped cells, because toroids present a symmetrical pm8/vpi1 interface for cell attachment and basal lamina deposition (see Figure 2.6A).

Formation of a toroid requires at least one fusion event; thus, pm8 and vpi1 must self-fuse, but not cross-fuse. We have shown that pm8 and vpi1 self-fuse by expressing different fusogens, an elegant solution to the problem of creating linked, single-cell tubes. vpi1 expresses a fusogen, EFF-1, that is sufficient to fuse heterologous cells that each express EFF-1 (Podbilewicz et al., 2006). We have shown that in *eff-1* mutants vpi1 is a C-shaped cell with an autocellular junction, indicating that EFF-1 normally promotes the self-fusion of vpi1. pm8 does not express EFF-1, but instead expresses a second fusogen, AFF-1, and requires *aff-1* activity to become a toroid. Thus, AFF-1 and EFF-1 cause self-fusion in pm8 and vpi1, in addition to promoting cross-fusion between other types of embryonic cells.

2.3.2   Epithelial to mesenchymal transition

pm8 and vpi1 are wedge-shaped, dorsal epithelial cells prior to becoming C-shaped cells and self-fusing. To form a C-shape around the cyst midline, both pm8 and vpi1 invade between cells in the ventral side of the cyst. Although vpi1 extends only a lamellar process through ventral cells, the nucleus and most of the pm8 cell body enter the ventral side. Notch activity appears to be involved in pm8 delamination from the dorsal basal lamina; pm8 normally detaches from the dorsal perimeter at

about the same time as Notch target genes are expressed in pm8, but does not appear to detach in Notch mutant embryos. The delamination and migration of pm8 can be considered an epithelial to mesenchymal transition (EMT). In most animals, EMT is a fundamental and widely used morphogenetic program that functions in gastrulation, and tissue and organ development; EMT also occurs in pathological states during wound healing and in tumor progression (Thiery and Sleeman, 2006). A well-documented role for EMT occurs in the development of the vertebrate heart (Eisenberg and Markwald, 1995). Within the primitive heart tube, epithelial (endocardial) cells that contribute to valve development and heat septation break adherens connections to their neighbors and invade the surrounding extracellular matrix (cardiac jelly). Notch signaling occurs within the endocardium, and is critical for EMT (Timmerman et al., 2004). In contrast to the prevalence of EMT in other systems, the *C. elegans* literature is almost devoid of examples of EMT. For example, most gastrulating cells in *C. elegans* are not epithelial, and lineage mechanisms ensure that most cells are born in their appropriate positions without extensive tissue remodeling (Nance et al., 2005). Because many basic processes in EMT are poorly understood, such as the restructuring of junctional complexes between cells, pm8 morphogenesis should prove a useful model system for genetic analysis.

2.3.3   Laminin and intraepithelial cell movements

The migration of pm8 and vpi1 between cells in the ventral epithelium of the cyst resembles transepithelial migration in other systems, such as human leukocytes and *Drosophila* germ cells (see Introduction). In all three systems, migration occurs between cells in the target epithelium. These events occur rapidly, requiring about 15 minutes for pm8 migration and from 5 to 16 minutes in some in vitro models of leukocyte invasion (Shaw et al., 2001). In *Drosophila*, the target epithelium appears

primed for invasion; apical junctions are remodeled to create intercellular gaps even in the absence of the invading germ cells (Kunwar et al., 2006). In contrast, invading leukocytes can induce junctional remodeling of the target epithelium (Shaw et al., 2001). In our present study, we found (1) that a tract of laminin appears between the ventral cells mc3V and vpi2V prior to pm8 and vpi1 migration, (2) that pm8 and vpi1 migration occurs specifically at the mc3V/vpi2V interface, and is associated with a disappearance of the laminin tract, and (3) that laminin function is essential for pm8 migration (vpi1 was not examined in this experiment). These results suggest that laminin provides a transient path for pm8 migration. We do not yet know whether the formation of the laminin tract is induced by signals from pm8 and/or vpi1, however, the tract forms independent of Notch. Future genetic studies should reveal the laminin receptor(s) involved in pm8 migration. If integrin were the sole receptor for laminin in pm8 migration, we would have expected a lack of migration in integrin mutants, rather than the overmigration, or aberrant migration observed. Interestingly, neurons in alpha6 integrin-null mice show an analogous overmigration phenotype (Georges-Labouesse et al., 1998). Although laminin is often implicated in animal cell migration, we know of no similar example of a transient laminin tract guiding migrating cells through a polarized epithelium. The tract in *C. elegans* forms and disappears within about 30 minutes, so it is possible similar, transient tracts might have been overlooked in epithelia in other systems. Indeed, we observed additional examples of laminin within *C. elegans* tissues that are not known to contain migratory cells (our unpublished observations). Thus, it will be interesting to determine whether laminin-dependent, short-range cell movements similar to those of pm8 and vpi1 are a common feature of epithelial remodeling.

2.3.4 Lumen formation in a single-cell tube

Single-cell tubes are found in diverse animal tissues, including the fine capillaries of the vertebrate vascular system, the termini of the *Drosophila* tracheal system, and the *C. elegans* excretory (renal) system (Lubarsky and Krasnow, 2003). Some of these tubes, such as the fusion cells of the *Drosophila* tracheal system, are toroids like the *C. elegans* pm8 and vpi1 cells (Samakovlis et al., 1996b). The lumen in some single-cell tubes is thought to form from the coalescence of cytoplasmic vacuoles (Lubarsky and Krasnow, 2003; Berry et al., 2003; Kamei et al., 2006). In our electron microscopic study, we did not find obvious cytoplasmic vacuoles in pm8 or vpi1 before or immediately after lumen formation (see Figure 2.9D). pm8 migrates into the ventral side of the epithelial cyst on the left side of the midline, and the pm8 cell body subsequently expands to span the diameter of the cyst. During these events, the three group 3 marginal cells extend fingers posteriorly along the midline. Thus, pm8 must actively or passively wrap around the fingers at the midline. An intriguing possibility is that the fingers play a morphogenetic role in templating the lumenal surface of pm8. However, we have not been able to test this hypothesis by removing all three of the marginal cells simultaneously. If the fingers do not play a direct role in templating the lumen, it is possible they have a mechanical function in holding cyst cells together while pm8 and vpi1 remodel their apical junctions.

2.3.5 Notch signaling and the tubulogenesis

The Notch pathway is required for proper pm8 and vpi1 tubulogenesis, and appears to have two distinct roles. First, Notch is required for pm8 to express the fusogen AFF-1. Although the presumptive ligand-expressing cells in the cyst appear to contact both pm8 and vpi1 (see Figure 2.3C), only pm8 expresses LIN-12/Notch, and only pm8 expresses the Notch targets *ceh-24* and *ref-1*. These results suggest that the

Notch pathway is activated only in pm8, and that defects in vpi1 morphogenesis in Notch mutants occur indirectly. Second, we have shown that expression of the EFF-1 fusogen is normally restricted to vpi1, but that pm8 and vpi1 both express EFF-1 in Notch mutants and can cross-fuse. Cross-fusion would prevent a basal lamina from forming between pm8 and vpi1, and thus account for the inappropriate, broad cellular contacts observed between pharyngeal and valve cells in Notch mutant embryos. Future studies should elucidate the transcriptional network linking Notch targets with fusogen expression and myogenesis. The regulatory regions of both *aff-1* and *eff-1* contain candidate LAG-1/CSL binding sites (our unpublished results), however, we do not yet know whether either gene is a direct target of Notch. pm8 does not appear to express FOS-1A, a transcription factor that regulates *aff-1* expression in a larval cell called the anchor cell (Sapir et al., 2007, and our unpublished results).

We conclude by noting that cells acquire several distinct, and reproducible morphologies during the differentiation of the pharynx/valve from an epithelial cyst. The remarkable number of events underlying the development of just two of these cells, pm8 and vpi1, hint at the complexity of organ differentiation. Because only a few postmitotic cells in the cyst express the receptors LIN-12/Notch or GLP-1/Notch, it appears that Notch does not play a major role in the morphogenesis of most other cyst cells. Thus, it is likely that there are several different pathways that specify cell shapes throughout the cyst, and it should be interesting in future studies to identify these pathways and determine how they are coordinated.

2.4   Experimental Procedures

2.4.1   Nematodes

Standard techniques were used to maintain and manipulate nematodes (Brenner, 1974). The following extrachromosomal or integrated arrays were created for this

study; details available upon request: *zuEx146*: [*ceh-24 (115bp)*::GFP (pKG63); *rol-6*], *zuEx165*: [*ceh-24 (115bp)(−CSL)*::GFP (pKG70); *rol-6*], *zuEx221*: [*ref-1 (153bp)*:: GFP-PM (pKG79); *rol-6*], *zuIs190*: [*myo-2*::GFP (pSEM474); *rol-6*]; the plasmid pSEM474 was kindly provided by Jeb Gaudet and Susan Mango. The following transgenes have been described: *zuEx132*: [*ref-1 (600bp)*::GFP] (Neves et al., 2007); *zuIs104*: [*ref-1 (1.8kb)*::REF-1::GFP] (Neves and Priess, 2005); *urEx131*: [*lam-1*::LAM-1::GFP] (Kao et al., 2006); *hyEx167*: [*aff-1*::GFP] (Sapir et al., 2007); *zzIs22*: [*eff-1*::EFF-1::GFP] (del Campo et al., 2005); and *syIs123*: [*fos-1a*::YFP::FOS-1A] (Sherwood et al., 2005). Mutant alleles used in this study are described in WormBase (`http://www.wormbase.org/`): LG1, *lam-3(n2561)*; LG II, *aff-1(tm2214)*, *eff-1(hy21)*, *eff-1(ok1021)*; LG III, *glp-1(q46)*, *ina-1(gm86)*, *lin-12(n941)*; LG IV, *epi-1(rh199)*, *lag-1(q385)*; LG V, *apx-1(zu347ts)*, *lag-2(q387)*, *lag-2(q411)*, *lag-2(q420ts)*. A strain was constructed with the *ref-1*::GFP-PM transgene that was heterozygous for the *lam-3(n2561)* and *epi-1(rh199)* mutations. Approximately 1/16 of the progeny of these animals had a novel and consistent defect in pm8 migration that was not observed in either of the homozygous single mutants; we infer that these embryos are homozygous for both mutations.

2.4.2 Transgenes

Standard techniques were used to manipulate DNA. All transgene constructs were made using PCR fusion techniques (Hobert, 2002). GFP reporter constructs for *ceh-24* and *ref-1* were derived from pAP10 (A. Paulson and S.E. Mango, unpublished). The *ceh-24* promoter was amplified using Pst I linkers and the following forward (F) and reverse (R) genomic sequences: *ceh-24* (F = gagctctttgcatctttttcac, R = gagaagtgttatcagtgttatcc; pKG63). *ref-1*::GFP-PM was constructed by cloning amplified genomic *ref-1* DNA (F= ctcaccaggggttatcaaaccaatatg, R=atcccaatggttcccatcactatc) into

the Hind III/Bam H1 sites of pJN152 GFP-PM (J. Nance, unpublished). Promoter/enhancer mutagenesis was performed using the QuikChange site-directed mutagenesis kit (Stratagene, La Jolla, CA, USA). Predicted start codons were obtained from the WormBase web site (`http://www.wormbase.org`). Constructs were injected at 40ng/μl together with *rol-6* DNA, at 100ng/μl, to generate extrachromosomal arrays (Mello and Fire, 1995). At least two independent lines were analyzed for each transgene, and at least twenty embryos were examined per line. The *myo-2*::GFP array was integrated by gamma-irradiation (Mello and Fire, 1995). Electrophoretic mobility shift assays (EMSA) shown in Figure 2.7 were performed essentially as described (Stroeher et al., 1994).

2.4.3 Immunofluorescence

The following antibodies/antisera were used: anti-LAM-3, anti-EPI-1 (Huang et al., 2003), mAbGJ1, mAbGJ2, anti-LIN-12 (gift from Stuart Kim), MH27 (Francis and Waterston, 1991), anti-GFP (Abcam ab6556). Worm and embryo fixation procedures were performed essentially as described (Lin et al., 1998; Leung et al., 1999). Unless stated otherwise, between 5 and 25 embryos were analyzed for all immunofluorescence experiments.

2.4.4 Microscopy

Electron microscopy was performed as described (Costa et al., 1997). Sets of 5–10 thin sections spaced by 0.5 to 1 micron intervals were taken from plastic-embedded clusters of 25–50 embryos. Embryos with the plane of section though the axis of the pharyngeal lumen were selected for detailed analysis.

Images shown in Figures 2.10 and 2.4F were from a set of serial sections through the terminal bulb of the pharynx and valve (J. Priess and J. N. Thomson, unpub-

lished). Fluorescence images in Figure 2.5G and Movies S1, Movie S2, Movie S4 were collected with a spinning disk confocal system (Yokogawa CSU-10) on a Nikon TE-2000 inverted microscope equipped with a Hamamatsu C-9100 camera, running Volocity 4.1 (Improvision, Lexington, MA).

2.4.5 DNA Binding

Electrophoretic mobility shift assays (EMSA) were performed essentially as described (Stroeher et al., 1994) with 25 nanograms of GST-LAG-1, 0.1 micrograms of poly (dI-dC) per reaction and 0.2 micromolar labeled probe. The GST-LAG-1 fusion protein used for EMSA has been described previously and contains amino-acid residues 192-663 of LAG-1 (Kovall and Hendrickson, 2004). The probe sequence was as follows: gaattctcgcgactCGTGGGAAaatgggcggaagggcacCGTGGGAAaatagttccaggaattc. This sequence has been used previously for EMSA with LAG-1 (Hwang et al., 2007) and the underlined region for EMSA with the CSL protein CBF1 (Zimber-Strobl et al., 1994). The wild-type competitor from the *ceh- 24* pm8 enhancer was used as follows: tggtgagcactttgtgtgaaggatctctttacTGTGGGAAccacccgagacgcatcattggggt. For the mutant competitor, TGTGGGAA was changed to TGAGGCAA.

2.5 Supplementary Material

The online supplement including Movies S1-S4 is available at `http://www.ncbi.nlm.nih.gov/pmc/articles/PMC2435507/`.

Reporter	Genotype	pm8 expression % (n)
ceh-24::GFP	WT	100 (50)
	lin-12(n676n930ts)	52 (72)
	lin-12(n941)glp-1(q46)	10 (20)
ceh-24(–CSL)::GFP	WT	15 (38)
ref-1(600bp)::GFP	WT	100 (35)
ref-1(1.8kb)::REF-1::GFP	*lin-12(n941)glp-1(q46)*	0 (83)
ref-1(600bp)::REF-1::GFP	*lin-12(n941)*	2 (64)
	lag-1(q385)/+	100 (18)
ref-1(600bp)::GFP	*lag-1(q385)*	0 (10)
	lag-2(q411)	100 (15)
	lag-2(q420ts)	100 (20)
	apx-1(zu347ts)	100 (21)
	lag-2(q387)	0 (12)
ref-1(1.8kb –CSL)::REF-1::GFP	WT	0 (25)
myo-2::GFP	WT	100 (110)
	lag-2(q420ts)	100 (36)
	lin-12(n941)/+	100 (44)
	lin-12(n941)	36 (78)
	lin-12(n941)glp-1(q46)	45 (206)
	lag-1(q385)	3 (89)
aff-1::GFP	WT	96 (67)
	lag-1(q385)	2 (62)

Table 2.1: Notch-regulated gene expression in pm8

Figure 2.1: Cell morphology and polarity in the pharynx/valve. (A) Diagram of some of the cells in the terminal bulb of the pharynx and in the valve. The three group 3 marginal cells are shown in purple, and names of the principle cells mentioned in the text are indicated. (B) Diagram of cell positions in the cyst (top) and pharynx/valve (bottom). Note the reorientation of the basal lamina-associated, basal surfaces of pm8 and vpi1. (C) pm8 in an adult and newly hatched larva (inset) visualized by *ref-1*::GFP-PM; white lines indicate perimeter of terminal bulb. (D) Optical longitudinal section through the middle of an embryo showing the epithelial cyst (bracket). (E–E") High magnification of region corresponding to double-headed arrow in panel D after immunostaining for apical junctions (AJM-1) and LIN-12/Notch to visualize pm8 (see also Figure 2.3D). Note that pm8 contacts, but does not cross, the midline (arrow). Polygonal shapes are the apical surfaces of various cells in the cylindrical array around the midline. Bars = 2 μm (C), 10 μm (D), 2.5 μm (E–E").

A terminal bulb

pharynx   valve intestine

pm8   vpi1

lumen   pm7

mc3V   pm8   vpi2V

B epithelial cyst

pm8 vpi1

midline

mc3V vpi2V

basal lamina

pharynx   valve

lumen   mc3V pm8 vpi1 vpi2V

C adult pm8

lumen

D dorsal

apical junctions (AJM-1)
laminin (LAM-3)

midline

epithelial cyst

ventral

E apical junctions

E′ pm8 LIN-12

E″ pm8 merge
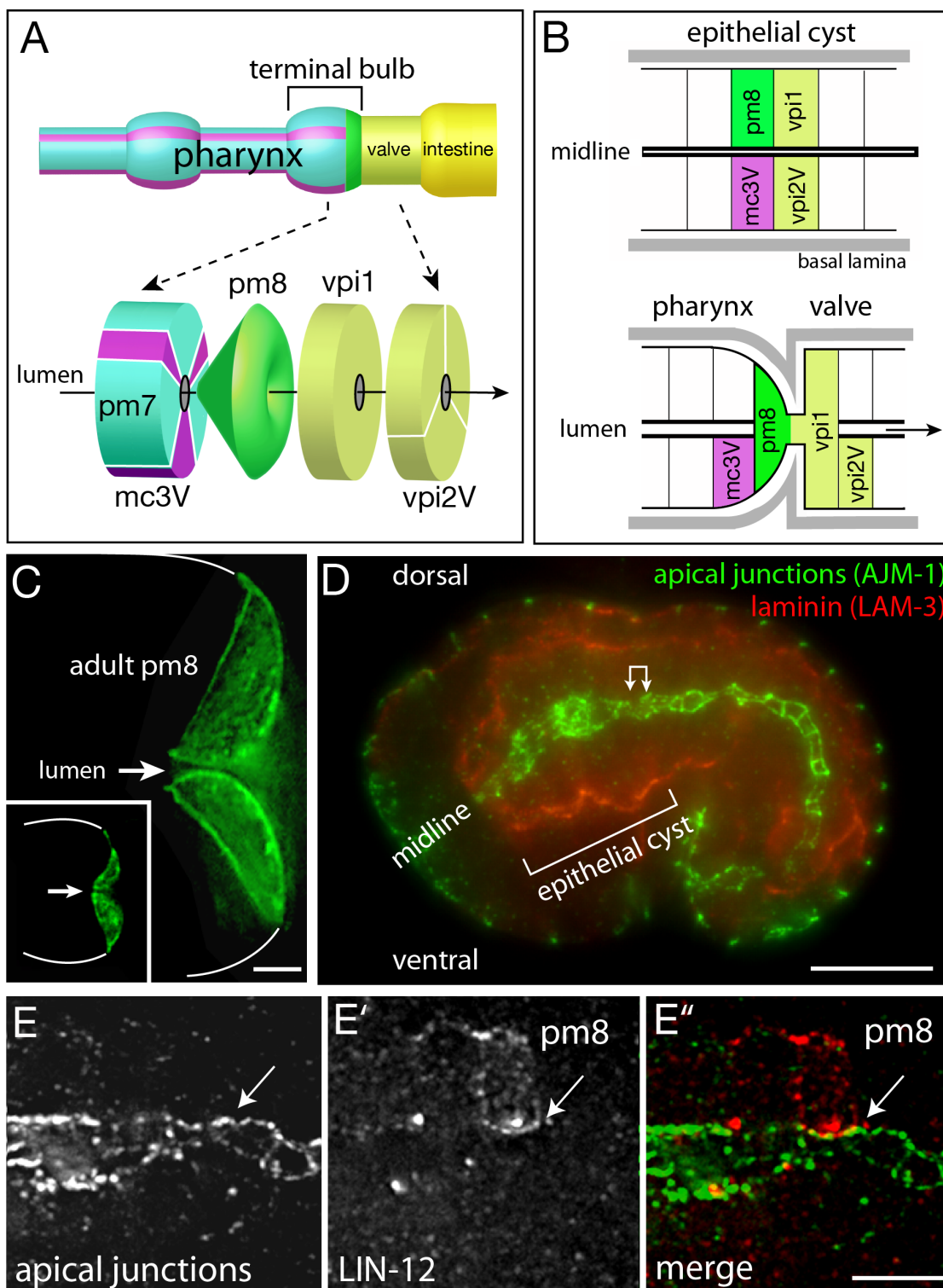
Figure 2.2: Notch-dependent gene expression in pm8. The columns show wild-type (left) and *lin-12 glp-1* mutant (right) animals either after hatching at 14 hours (A–F), or at 7 hours in embryogenesis (G–J). Transgenic reporters are as listed; white lines indicate perimeter of the pharynx (C,D) or epithelial cyst (I,J). Nuclei labeled "n" in panels C and D are neurons outside the pharynx that express *ceh-24*::GFP. Bars = 5 μm (A–F), 10 μm (G–J). Embryos are approximately 50 μm in length.

wild type   *lin-12 glp-1*

A valve B

pharynx

C pm8   D n n n n

ceh-24::GFP   *ceh-24*::GFP

E pm5 pm6 pm7 pm8 F pm5 pm6 pm7

myo-2::GFP   *myo-2*::GFP

G pm8   H

I pm8 mc3V e2V J mc3V e2V
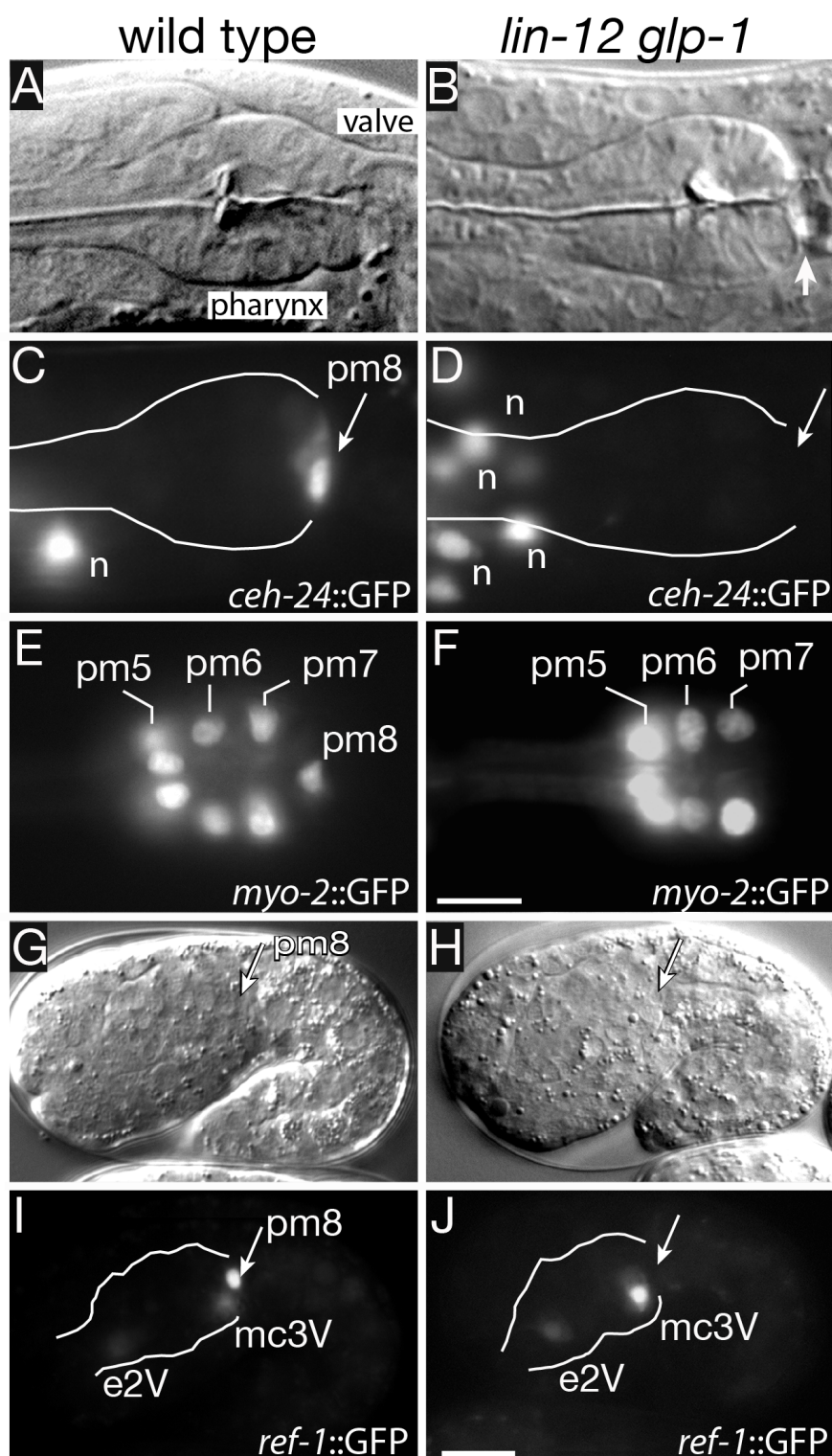
ref-1::GFP   *ref-1*::GFP

Figure 2.3: Notch signaling in the epithelial cyst. (A–A') Ventral view of an embryo before formation of the cyst showing *lag-2* expression in MSaapa. (B) *ref-1*::GFP expression in a cyst-stage, wild-type embryo after killing MSaapa; embryo shown is the same stage and orientation as in Figure 2.2I. *ref-1*::GFP expression in pm8 was observed after killing the following cells: MS (0/4 embryos), MSaa (0/4- MS and MSaa are precursors of pm8), MSap (6/6), MSaap (0/4), MSaapa plus MSaapp (0/3), MSaapp (5/5), MSaapa (4/4 when the ablated cell entered the body cavity, 0/3 when it remained outside). (C–C") Dorsal view of a 6 hour embryo immunostained for GFP (*lag-2*::GFP) and LIN-12/Notch; white lines indicate boundary of epithelial cyst. The approximate position of vpi1 is indicated based on light microscopy of living embryos at this stage and orientation. (D–D") Lateral view of embryo at about the same stage as panel C; *ref-1*::GFP is expressed in the Notch-independent cells e2V and mc3V, but not in pm8. (E–E") Embryo approximately 20 minutes later than in panel D showing *ref-1*::GFP in pm8. Note lamella from pm8 (arrow in panel E) extending ventrally across the midline of the cyst (dashed line).
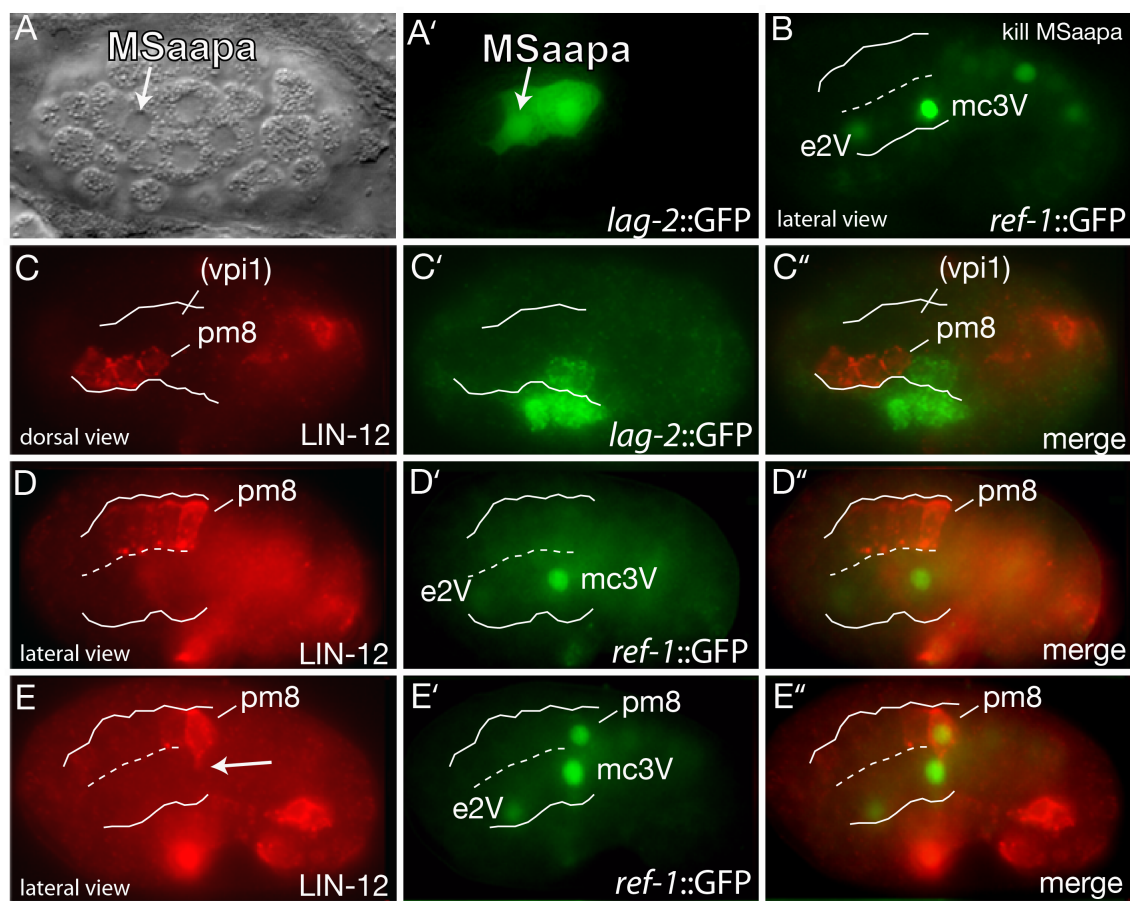
Figure 2.4: Ventral migration and lumen formation in pm8 and vpi1. (A–D) *ref-1*::GFP-PM expression in pm8 and the group 3 marginal cell mc3V in successively older embryos. Images are optical sections through the midline of the cyst. (E–E") vpi1 expressing *eff-1*::EFF-1::GFP and stained with phalloidin to visualize F-actin at the midline (arrow). (F) Electron micrograph and diagram of a cross section through pm8 in an embryo near hatching. The three marginal cell fingers (numbered 1–3) are evident in the Y-shaped lumenal channel (white) of pm8. (G) Apical junctions in a wild-type, third stage (L3) larva.. Apical surfaces of cell like pm7 resemble broad triangles, while the group 3 marginal cells (numbered 1–3) have long, thin apical surfaces. Note how fingers from the marginal cells extend through the apical surface of pm8. The region indicated by the double-headed arrow is diagrammed to show a superposition of the pm8 and vpi1 cell bodies on their apical surfaces; apical junctions are drawn in black. (H, I) Same region as in panel F in wild-type (H) and *lin-12 glp-1* mutant (I) embryos near hatching. Bars = 1 μm (F), 5 μm (F–H).

A — dorsal; pm8; mc3V; ventral

B — pm8; mc3V

C — pm8; mc3V

D — pm8; mc3V

E — EFF-1::GFP; vpi1   E' — F-actin   E" — merge; vpi1   E''' — vpi1; pm8

F — pm8; 1; 2; lumen; 3; nucleus; ventral

G — 1; pm8; vpi1; int; pm6; 2; pm7; 3; pm8; vpi1; 1; 2; 3

H — pm8; vpi1; pm6; int; pm7

I — pm7; pm6; int; *lin-12 glp-1*
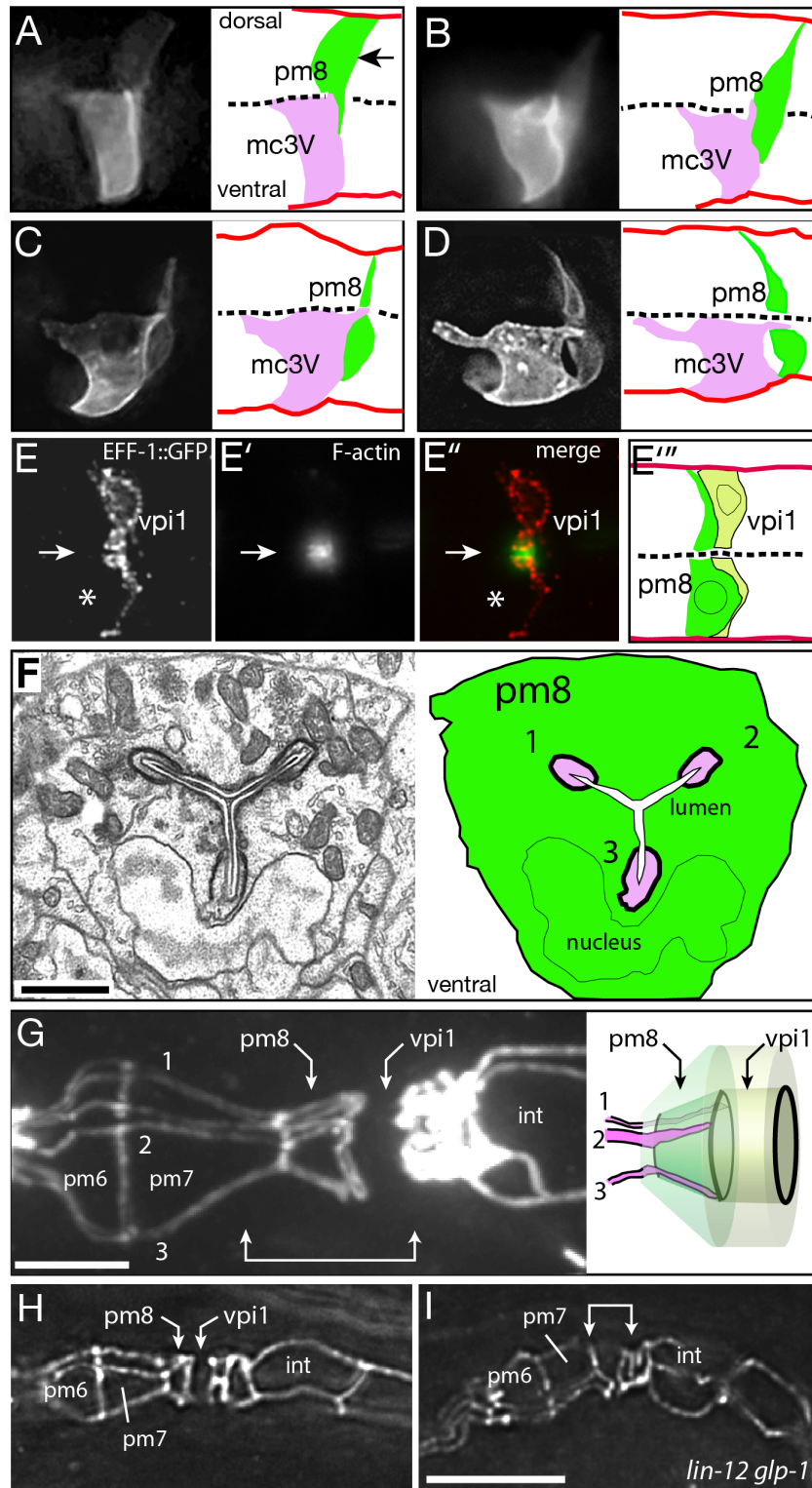
Figure 2.5: pm8 migrates ventrally on a laminin tract. (A) A 7 hour embryo stained for laminin. Laminin is present in the basal lamina surrounding the cyst (bracket). A transverse tract of laminin is evident in the posterior, ventral half of the cyst (arrow indicates the cyst midline). (B) *lin-12 glp-1* embryo at 7.5 hours. (C–F) Sequence of successively older wild-type embryos showing the appearance (D) and disappearance (E) of the laminin tract, followed by the deposition of laminin on the posterior surface of pm8 after morphogenesis (F). (G–I) Single embryos immunostained for LAM-3 and GFP (*ref-1*::GFP-PM) before (G), during (H), and near the completion (I) of pm8 migration. Arrows indicate the midline of the cyst. (J) *lam-3; epi-1* double mutant at about 9 hours; pm8 has failed to migrate to the ventral side. This embryo has a shape similar to younger, 7.5 hour wild-type embryos because of defects in body morphogenesis, but has the well-formed tail spike (arrow) characteristic of wild-type 9 hour embryos. (K) *ina-1* mutant larva showing pm8 extension into the valve/anterior intestine; similar defects occur in 74% of the hatched animals (n=46). Bars = 10μm (A,B) and 5 μm (G–I).

LAM-3   *ref-1*::GFP   merge

lam-3; epi-1

ina-1
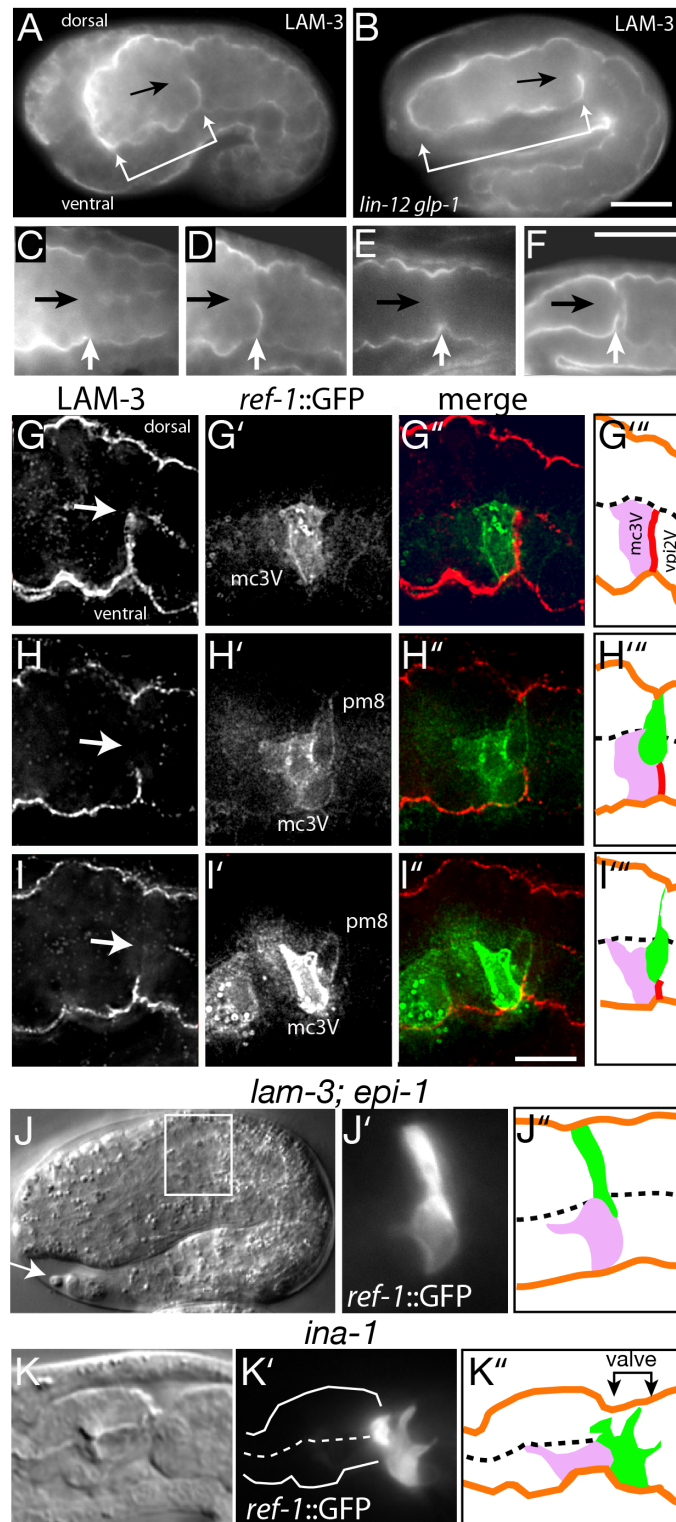
Figure 2.6: Self-fusion of pm8 and vpi1. (A) Diagram comparing (1) a box-like cell with a simple, flat apical surface, (2) a topologically equivalent C-shaped cell, and (3) a topologically distinct toroid with a cylindrical apical surface; apical junctions are shown as bold lines. (B–B") Apical junctions at the pharynx/valve boundary in a 7.5 hour wild-type embryo stained for the apical junction marker AJM-1 (panel B) and for *eff-1*::EFF-1::GFP (panel B'). In this longitudinal view, the intercellular junctions at the ends of pm8 and vpi1 appear as vertical lines (panel B). The inset in (B) shows the same region in an *eff-1* mutant with an autocellular junction linking the intercellular junctions in vpi1, but not pm8. (C–C") Same region and stage as in panel B, showing *aff-1*::GFP expression in pm8 and an autocellular junction in pm8 in an *aff-1* mutant (inset). (D,D') *lag-1* embryo with binucleate cell expressing *eff-1*::EFF-1::GFP. (E,E') *lag-1* embryo showing a mononucleate cell expressing *eff-1*::EFF-1::GFP.(F–F") different focal plane of the same embryo in panel (E) showing a second *eff-1*::EFF-1::GFP-expressing cell. Note that both cells have a ventral-directed process but neither cell extends completely through the cyst. Bars = 2.5 μm (B–F).

A. C-shaped cell, toroid, apical surface, autocellular junction, intercellular junctions

B. pm8, vpi1 — *eff-1*

B'. vpi1 — *eff-1*::EFF-1::GFP

B". vpi1 — merge

C. pm8, vpi1 — *aff-1*

C'. pm8 — *aff-1*::GFP

C". pm8 — merge

lag-1

D. EFF-1::GFP

D'. merge

E. EFF-1::GFP

E'. merge

F. DNA

F'. EFF-1::GFP

F". merge
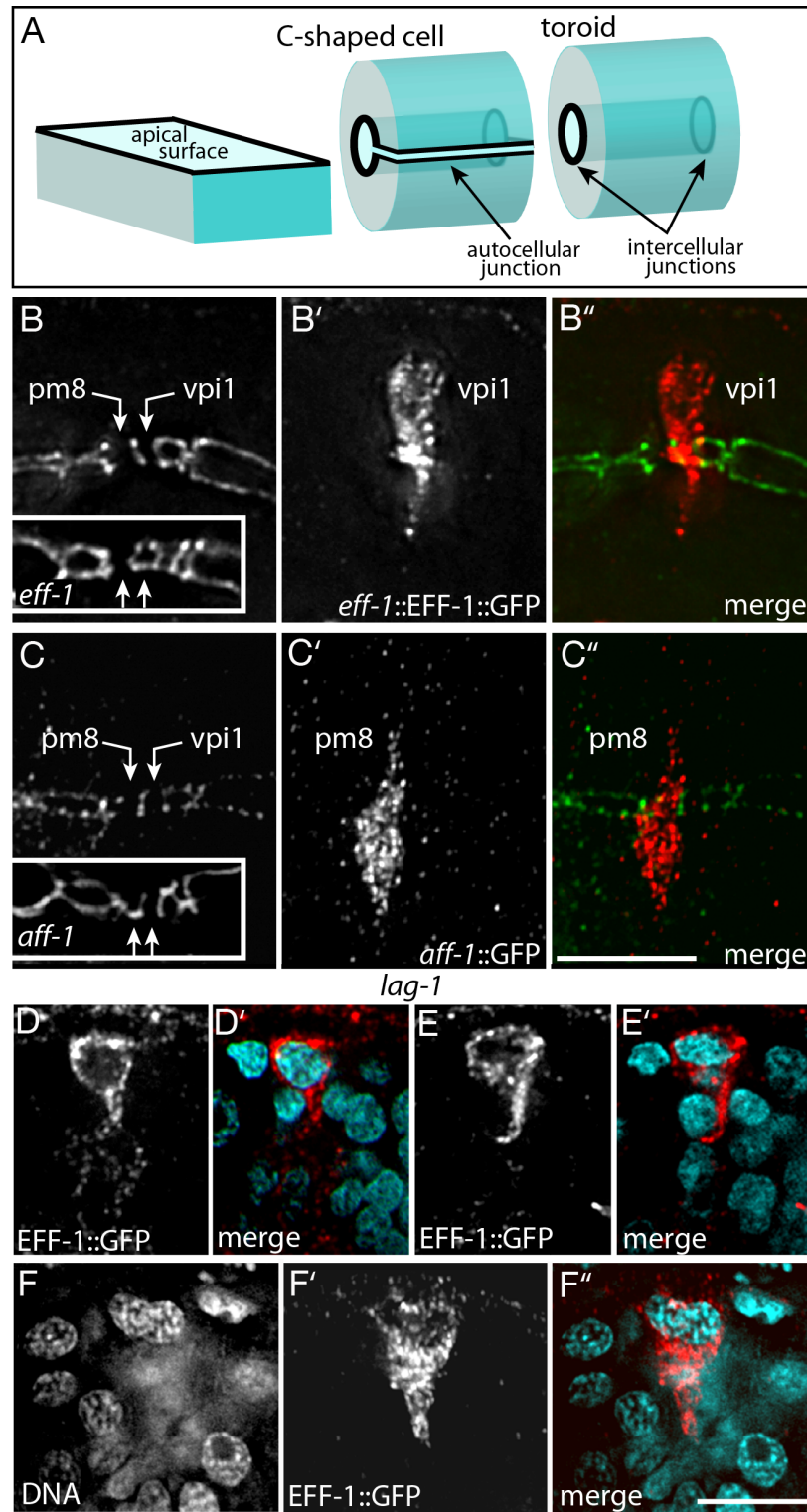
Figure 2.7: *ceh-24* is a direct target of Notch signaling. (A) The 115 bp pm8 enhancer from the *C. elegans ceh-24* gene (Harfe and Fire, 1998) aligned with sequences upstream of *ceh-24* orthologs in *C. briggsae*, *C. remanei* and *C. brenneri* (*C.b.*, *C.r.*, and *C.br.*, respectively; bases shared by three or more sequences are shown in uppercase). (B) EMSA competition experiment using sequences from the wild-type *ceh-24* pm8 enhancer shown in panel A, or with the LAG-1/CSL site mutated from GTGGGAA to GAGGCAA. The labeled probe is a previously described sequence that contains two LAG-1/CSL sites and that binds LAG- 1 *in vitro* (Hwang et al., 2007). Open triangles indicate bound probe. (C, D) Wild-type embryo expressing a *ceh-24*::GFP reporter with GTGGGAA mutated to GAGGCAA; expression is observed in neurons outside the pharynx (arrowhead), but not in pm8 (arrow).

A

ceh-24

```
C.e   GAGctCTTtgCATcTTtTTCACTT-----TTGATTGGt-------GAGCACTTTgTGTGA
C.b   GAGctCTTctCATaTTCTTCACTTt----TTGATTGGc-------GAGCACTTT-TGTGA
C.r   GAGtcCTTctCATcTcCTTCACTT-----TTGATTGGc-------GAGCACTTT-TGTGA
C.br  tAGgaggcagCtctcTCTTCACTTttttgTTGATTGGaagtgggaGAGCACTTT-TGTGA

C.e   AGGATCTCTTTACTGTGGGAACCaCCCGAgaCgcATcATtgg---ggtGGATAACACt-g
C.b   AGGATCTCTcTACTGTGGGAACCgCCCGAcgCatATcATggg---ggaGGcTAACA---a
C.r   AGGATCTCTTTACTGTGGGAACCaCCCGAcgCttcTtATttctttatgaGATAACACttt
C.br  AGGATCTCTTTACTGTGGGAACCtatatgatCtgAggAaatcatc---GGATAACACgag
```
LAG-1/CSL

```
C.e   ATAACACTTcTcT
C.b   ATAACACTccTgT
C.r   tcccattTTgTtT
C.br  ATAACACTTgctT
```

B

+ LAG-1/CSL

wild-type competitor | mutant competitor

0   1x   50x 100x | 1x   50x 100x

probe

C

D

mutated LAG-1 site

Figure 2.8: Muscle differentiation in the terminal bulb. (A,B) Light and fluorescent micrographs of newly-hatched wild-type (A) and *lin-12 glp-1* (B) larvae expressing *myo-2*::GFP; brackets indicate position of valve. The image of the wild-type larva shows 5 of the 13 expressing nuclei, including pm8. The mutant larva has 13 expressing nuclei, however, the most posterior nucleus is in the valve/anterior intestine cell region. The outline of this cell is faintly visible; note thin cytoplasmic connection to pharynx (asterisk). 10% (n=93) of *lin-12 glp-1* larvae with 13 *myo-2*::GFP-positive nuclei showed a similar mislocalization of the candidate pm8 cell. (C–C'''). *myo-2*::GFP expression in the terminal bulb of *ced-4 lin-12 glp-1* mutant larva. This analysis addressed whether the candidate pm8 cell in some *lin-12 glp-1* embryos was a non-pm8 cell normally programmed for cell death. Wild-type embryos contain 13 positive nuclei in the terminal bulb (Table 2.1), while 76% (n= 50) of *ced-4* single mutant larvae defective in apoptosis contain 14 positive nuclei, indicating that at least one cell normally programmed for death can become a muscle. If this undead cell was the source of the 13th muscle in Notch mutants, then *ced-4 lin-12 glp-1* larvae should never have more than 13 positive nuclei. Instead, 15% of the triple mutant larvae had 14 nuclei as shown. This suggests that some pm8 cells can undergo at least partial myogenesis in *lin- 12 glp-1* embryos, but not in *lag-1* embryos (Table 2.1).

wild type

lin-12 glp-1
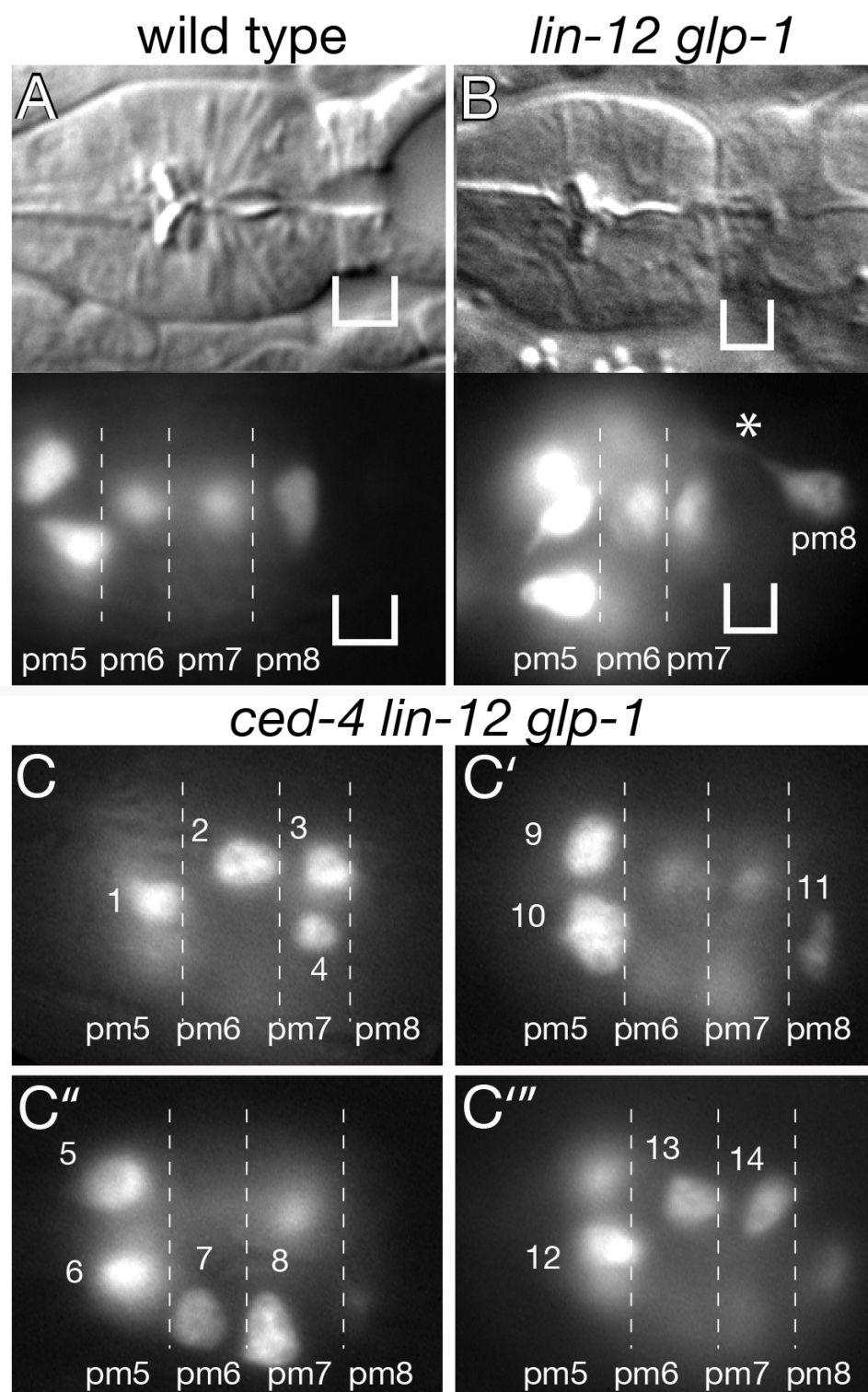
ced-4 lin-12 glp-1

Figure 2.9: Electron micrographs of longitudinal sections through the pharynx/valve. (A) Newly-hatched wild-type larva; the pm8 and vpi1 cell bodies are outlined in bold. (B) Newly-hatched *lin-12 glp-1* mutant larva. The developing grinder in pm6 (grey) permits an unambiguous identification of this cell type, and hence the adjacent pm7 cells. Note that the lumen at the pharynx/valve boundary is abnormal, and that the pm7 cell is in direct contact with valve cells (arrow); thus pm8 is not in its correct position. A candidate pm8 cell is indicated. (C) High magnification of the pm8/vpi1 interface from the larva shown in panel A. Note that a basal lamina (bl) nearly separates pm8 from vpi1. A similar partitioning between the pharynx and valve has been observed in diverse nematodes (e.g., Lee, 1968). (D) Wild-type embryo at about 7 hours. pm8 has migrated ventrally and vpi1 has extended ventrally along the pm8 cell body. Red dots indicate cytoplasmic vesicles in several cells other than pm8 and vpi1. These vesicles have been described previously in cells throughout the digestive tract and termed "apical vesicles" (Leung et al., 1999).

wild type

A

1.0 μm

pm7

vpi1

pm8

valve

lumen

int

lin-12 glp-1

B

1.0 μm

pm6

pm6

pm7

pm7

pm8 ?

gl

valve

int

newly hatched larva

C

0.5 μm

AJ

AJ

lumen

pm8

basal lamina

pm7

vpi 1

embryo

D

2.0 μm

vpi 1

valve

gl

int

mc3V

pm8

gl
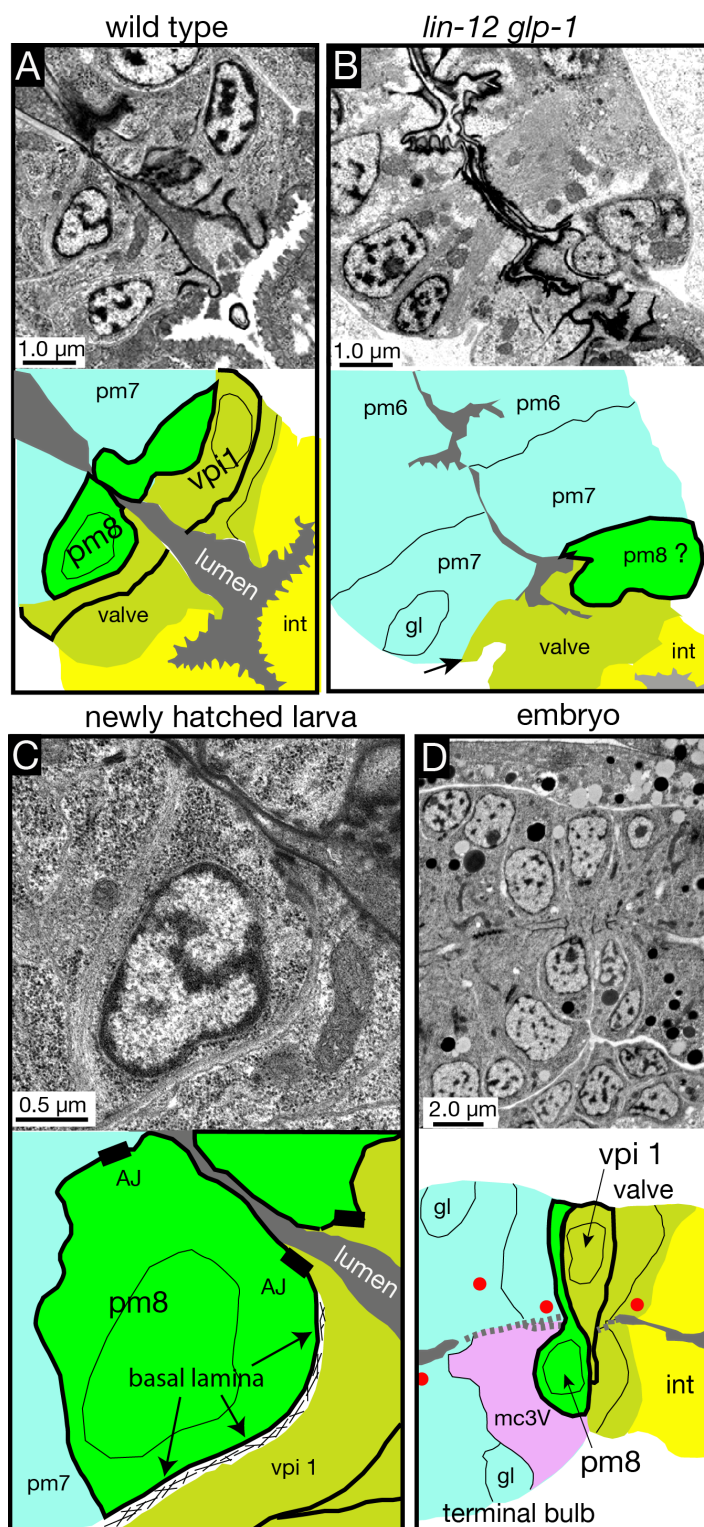
terminal bulb

Figure 2.10: pm8 and vpi1 become toroids during embryogenesis. Electron micrographs of cross sections through the pharynx/valve region of a wild-type embryo near hatching; these images are from serial thin sections through the terminal bulb where all cells were identified. The plane of section is slightly oblique, such that panel A includes the ventral, anterior neighbors of pm7, part of the mc3V cell body, and the gland cells (gl). Note that pm8 and vpi1 are continuous, donut-shaped cells without autocellular junctions. The apical junctions linking the group 3 marginal cell fingers (1–3) to the apical surface of pm8 appear as electron-dense zones. The lumen in both pm8 and vpi1 has developed the Y-shape characteristic of this stage of embryogenesis (Leung et al., 1999).

1.0 µm
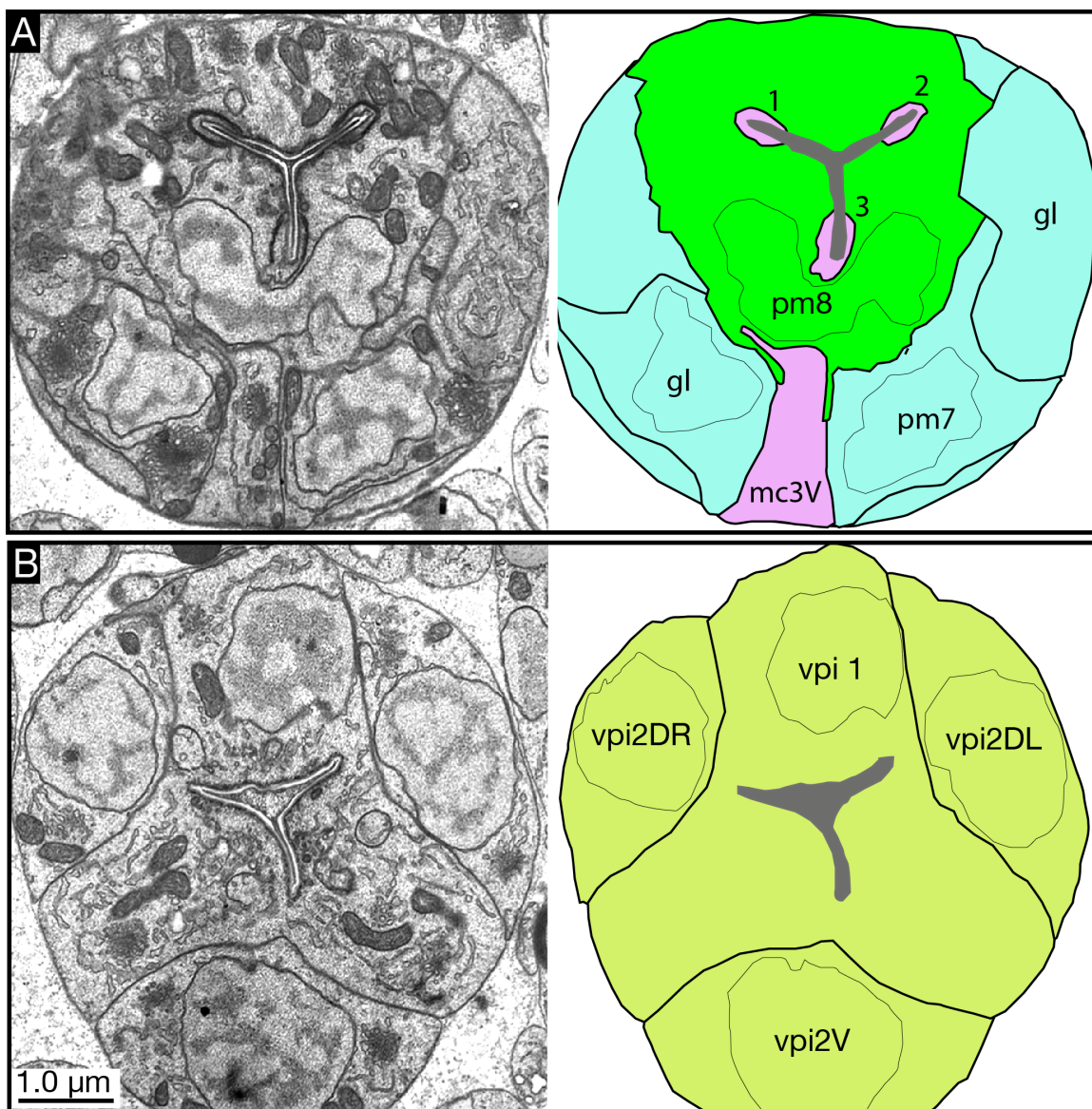
Chapter 3

LAMININ IS REQUIRED TO ORIENT EPITHELIAL POLARITY IN THE *C. ELEGANS* PHARYNX

The development of many animal organs involves a mesenchymal to epithelial transition, in which cells develop and coordinate polarity through largely unknown mechanisms. The *C. elegans* pharynx is an epithelial tube in which cells polarize around a central lumen, and provides a simple system to understand the coordination of epithelial polarity. We show that pharyngeal precursor cells initially group into a bilaterally symmetric, rectangular array of cells we call the double plate through the action of cell fate regulators. The double plate cells polarize, with asymmetrical localization of PAR proteins, before apically constricting to form a cylindrical cyst. We show that the polarity of the double plate cells is oriented by laminin, providing in vivo evidence that laminin has a early role in cell polarity that can be distinguished from its later role in basement membrane integrity.

3.1 Introduction

Cells exhibit multiple asymmetries during animal development, suggesting that successive cues exist that create and change cell polarity. For example, the one-cell *C. elegans* embryo develops anterior-posterior polarity cued by the sperm-contributed centrosome, but blastomeres at the four-cell stage exhibit inner-outer polarity cued by cell contacts (reviewed by Nance and Zallen, 2011). Perhaps the most dramatic changes in cell polarity occur during tissue and organ morphogenesis, when large groups of mesenchymal cells coordinately polarize to form epithelial sheets or tubes,

an event termed MET (Mesenchymal to Epithelial Transition; Chaffer et al., 2007). Work on cultured cells has long suggested that extracellular matrix components such as collagen and laminin might function as polarity cues for developing epithelia (Ekblom, 1989).

Laminin is a secreted, heterotrimeric protein, consisting of α, β, and γ subunits, and is an integral basement membrane component (reviewed by Miner and Yurchenco, 2004). The expression of certain laminin isoforms is causally related to the development of some aggressive, malignant epithelial cancers (reviewed by Marinkovich, 2007). Cells use laminin receptors, such as integrins and dystroglycans, to bind and polymerize laminin at the cell surface. Evidence that laminin might function as a polarizing cue during MET has come primarily from work on cultured mammalian kidney cells. After several days in three-dimensional culture, Madin-Darby canine kidney (MDCK) cells form epithelial cysts that differentiate apical surfaces facing an internal lumen. MDCK cysts can develop inverted polarity when grown without basement membrane-containing substrate, or after expression of a dominant-negative Rac1 (O'Brien et al., 2001; Wang et al., 1990). Addition of high levels of exogenous laminin can rescue this inverted polarity, suggesting that laminin can orient MDCK polarity (O'Brien et al., 2001). In contrast, antibodies against laminin α1 were shown to block epithelial polarization in kidney organ culture (Klein et al., 1988). Thus, it is unclear whether laminin acts to initiate, or orient, epithelial polarity during MET in vitro.

The in vivo analysis of laminin function is complicated by the presence multiple isoforms of the laminin subunits in many animals (Miner and Yurchenco, 2004). Consistent with its central role in basement membrane assembly, however, mutations in single laminin isoforms cause severe developmental or tissue abnormalities in mice and humans (Miner and Yurchenco, 2004). In *C. elegans*, mutants lacking either of two

α subunits, *lam-3* or *epi-1*, have complex terminal phenotypes, including ruptured tissues, ectopic cell adhesions, and abnormally positioned adherens junctions (Huang et al., 2003). Developmental studies have not resolved whether these abnormalities result from primary defects in cell polarity, or from more general requirements for basement membranes in tissue integrity and support.

In the present study, we analyzed how embryonic cells that form the *C. elegans* pharynx acquire and coordinate their polarity, and how laminin affects these events. The pharynx is a tubular, epithelial organ that contains myoepithelial cells, support epithelial cells, glands, and neurons (Albertson and Thomson, 1976). The pharynx develops from pharyngeal precursor cells (PPCs) that cluster together as a primordium in the interior of the embryo. Through unknown mechanisms, the primordium undergoes a MET to transform into a cylindrical epithelial cyst. The cyst represents the architectural foundation for later pharyngeal differentiation, prefiguring the basic symmetry and patterning of the mature pharynx. Although some pharyngeal cells migrate and/or develop elaborate shapes (Mörck et al., 2003; Raharjo et al., 2011; Rasmussen et al., 2008), most of the cells in the mature pharynx retain their basic shapes and positions in the cyst. As with many examples of polarized cells in animal development, one of the first markers of polarity in the cyst is the asymmetric distribution of PAR-3 complex proteins (PAR-3, PAR-6, PKC-3; Nance and Zallen, 2011). PAR-3 complex proteins localize along the central, apical axis of the cyst (Bossinger et al., 2001; Leung et al., 1999; McMahon et al., 2001), and PAR-3 is required for the apical localization of key polarity regulators in the cyst (Achilleos et al., 2010). However, the cues that orient and coordinate the localization of PAR-3 complex proteins in the cyst are unknown.

Using live imaging, we show that the tubular cyst is preceded by the grouping of PPCs into a morphogenetic intermediate we call the double plate. PPC polarization

and PAR localization begin in the double plate, which transforms into a cyst by apical constriction. We show that laminin serves as a cue to orient the polarity of double plate PPCs. Although laminin is critical for morphogenesis of the pharynx, laminin does not appear to have a similar role in the morphogenesis of the intestine, a second epithelial tube. Thus, different epithelial organs appear to utilize at least partially distinct polarity cues, and pharyngeal development provides a model for analyzing laminin-based signaling.

3.2   Results

3.2.1   Pharyngeal precursor cells form a bilaterally symmetric, double plate

The pharynx forms from pharyngeal precursor cells (PPCs) that express PHA-4, a FoxA transcription factor essential for pharyngeal-specific differentiation (Figure 3.1A; Horner et al., 1998; Kalb et al., 1998; Mango et al., 1994). Approximately 400 minutes after the first cell division of the embryo, the PPCs undergo a MET to become a cylindrical cyst of polarized cells (Figure 3.1A; see also Figure 3.7A; Mango, 2009). In the light microscope, the cyst appears to separate from surrounding body tissues by a narrow space, and gaps appear along the central axis of the cyst that eventually coalesce or expand to form the lumen (Figure 3.1A, arrowhead). By electron microscopy, the cyst cells appear wedge-shaped in cross section, with narrow, apical tips and broad peripheral surfaces (Leung et al., 1999). For live imaging of cyst formation, we used a PPC-specific nuclear reporter (*pha-4*::HIS::GFP) and a ubiquitous plasma membrane reporter (*pie-1*::mCherry::PH(PLC1δ1)). Conventional mounting techniques for *C. elegans* embryos allows optical sectioning through longitudinal planes (Figures 3.1A,D), but can compress either the left-right or dorsal-ventral axis and makes the wedge-shapes of cyst cells difficult to score. Thus, we developed a technique to mount embryos for transverse optical sectioning (Figure 3.1D; see Experimental Procedures).

The PPCs are descendants of four early embryonic blastomeres that are born on the ventral surface of the embryo, but after multiple cycles of cell division and ingression all PPCs are internal (Figure 3.1A; Sulston et al., 1983). In transverse optical sections, the ingressing PPCs appear to converge into a dorsal-ventral oriented, rectangular array of cells between about 150 and 310 minutes into development (Figure 3.2A). The array extends dorsally within the embryo as internal PPCs divide and additional PPCs ingress from the ventral surface. Although there are shifts in nuclear positions within the growing array, inspection of the cell boundaries showed that the array remains almost exclusively two cells wide. Thus, we term the array of PPCs the "double plate" stage, and refer to the plane between the left and right halves of the double plate as the midplane (Figure 3.2A; see also Figure 3.2C).

We wanted to determine how bilateral symmetry was maintained during growth of the double plate. Previous studies showed that most embryonic cell divisions are oriented longitudinally (anterior-posterior), rather than left-right, and that cell positions in the pharyngeal cyst and at later stages are correlated with the positions of some early PPCs (Santella et al., 2010; Sulston et al., 1983). Thus, bilateral symmetry of the double plate might derive simply from the original, left-right positions of the PPCs (Figure 3.2C). Consistent with previous studies, we found that PPCs on the left and right sides of the double plate were respective descendants of early left and right PPCs on the ventral surface of the embryo (Figure 3.2C). Moreover, embryonic cells that flank the left and right sides of the early PPCs are precursors of body wall muscles (BWMs), and we found that these BWMs flank the left and right sides, respectively, of the double plate PPCs (Figures 3.2C,D). Although most PPC divisions in the double plate had the expected anterior-posterior orientation, we found that at least two PPCs consistently divided left-right (Figure 3.2B). The left and right daughters of these PPCs remained on their respective sides of the midplane, indicating that

the symmetry of the double plate is not maintained solely by an absence of left-right divisions.

We next addressed whether the bilateral symmetry of the double plate might arise from a lack of PPC motility, thus maintaining early, left-right differences in cell positions. To test this possibility, we examined pharyngeal development in *mex-1(RNAi)* embryos. Loss of *mex-1* function causes mislocalization of the transcription factor SKN-1 (Bowerman et al., 1993). SKN-1 is required to specify the fate of an early blastomere called MS, whose left and right daughters contribute to the left and right sides, respectively, of the double plate, and *mex-1* mutants can have five MS-like blastomeres (Mello et al., 1992). If PPCs remained in place after birth, *mex-1* mutants should form multiple groupings of PPCS separated by BWMs. Instead, terminal stage *mex-1(RNAi)* embryos formed a single block of pharyngeal cells without intervening BWMs (Figure 3.2E). These results suggest that PPCs have an ability to move and aggregate with other PPCs.

We examined *wrm-1* mutants to ask whether cell fate differences between left and right PPCs contributed to the bilateral symmetry of the double plate. Previous studies showed that some gene expression differences between the left and right daughters of MS and their descendants depend on the transcription factor POP-1/TCF-1 and proteins such as WRM-1 that regulate POP-1 activity (Hermann et al., 2000; Rocheleau et al., 1999). We cultured temperature-sensitive *wrm-1(ne1982)* mutants at the restrictive temperature (25°C) until the birth of the MS daughters, then down-shifted to the permissive temperature (15°C) and tracked the behavior of the daughters and their descendants. We found that MS daughters were born in their normal, left-right positions, and that the early descendants of both cells ingressed at the normal times. However, the border between the early left-right descendants quickly became more irregular than in wild-type embryos (Figures 3.2F,G). At later stages, PPCs in the

temperature-shifted *wrm-1(ne1982)* embryos formed a cluster that did not resemble the normal double plate; the cluster was more than 2 cells wide, and remained ventral rather than extending dorsally (Figures 3.2H,I).

Because the transcription factor PHA-4/FoxA is thought to be required for most, if not all, aspects of pharyngeal-specific differentiation (Mango, 2009), we examined formation of the double plate in *pha-4(q490)* mutants. We found that the early division pattern and ingression of the PPCs appeared wild-type in *pha-4(q490)* embryos (data not shown), and that all of the PPCs ingressed (Figure 3.1D). After ingressing, the mutant PPCs assembled into an array that approximated the shape of the double plate, and that was surrounded by BWM precursors (Figure 3.3B and data not shown). However, the width of the array was more variable than in wild-type embryos, often with three or more cells dorsally and only one cell ventrally (Figures 3.3A,B). Moreover, some PPCs were observed to cross the midplane and remain on the contralateral side (Figure 3.3B). Together, these results suggest that the birthplaces and ingression patterns of the early PPCs are not sufficient to explain the shape of the double plate, and that the formation and maintenance of the double plate instead requires cell fate regulators.

3.2.2   The double plate transforms into a cyst by apical constriction

The rectangular double plate of PPCs must ultimately adopt the cylindrical shape of the cyst. A previous study based on nuclear PPC positions described formation of the cyst as an inflation event that separated left from right groups of nuclei (Santella et al., 2010). Indeed, in transverse views of the double plate, many left and right PPC nuclei appeared to move away from each other during cyst formation (Figure 3.3A). However, imaging of the PPC cell membranes showed that the nuclear movement is concomitant with marked changes in cell shape that occur over about 60 minutes

and begin at ∼330 minutes in development (Figure 3.4A). The midplane-facing surfaces of double plate PPCs shrink while the peripheral surfaces show relatively little change in size, resulting in radially elongated, wedge-shaped PPCs whose nuclei are displaced toward the peripheral surface (Figures 3.4A,B). Thus, these results show that the midplane-facing cell surfaces of the double plate become the apical surfaces of the cyst. Formation of wedge-shaped cells in several systems involves apical constriction, which can be driven by the actomyosin cytoskeleton (reviewed by Sawyer et al., 2010). We imaged cyst formation with reporters for non-muscle myosin and F-actin, and found that the level of both reporters increased progressively at the midplane/apical surfaces as the PPCs developed wedge shapes (Figures 3.4C,D). Both reporters initially showed a slight enrichment along the basal surfaces of the double plate PPCs, but this diminished with time (Figures 3.4C,D,D'). Thus, the double plate transforms into a cyst by the polarized contraction of the midplane, or future apical, surface.

In some epithelial tissues, including the *C. elegans* intestine, asymmetric localization of centrosomes and PAR-3 complex proteins are early markers of apical polarity (Buendia et al., 1990; Leung et al., 1999). To determine when double plate PPCs first become polarized, we scored the position of the centrosome in each PPC relative to the center of the nucleus, measuring whether the centrosome was proximal, or distal, to the midplane. Centrosomes initially showed an equal proximal-distal distribution, as expected from the predominantly anterior-posterior divisions of the PPCs (Figure 3.4F). However, by ∼310 minutes there was a shift in centrosome positions toward the midplane, before any apparent enrichment of non-muscle myosin or filamentous actin at the midplane (Figure 3.4F). Similarly, PAR-6 showed a reproducible enrichment at the midplane at ∼310 minutes (Figure 3.5A). We next compared the relative enrichment at the midplane of PAR-6 and NMY-2 in embryos co-expressing markers

for both proteins, and found that PAR-6 enrichment precedes detectable NMY-2 enrichment (Figure 3.4G); this contrasts with early embryos, where PAR-6 and NMY-2 become enriched simultaneously (Munro et al., 2004).

3.2.3   PPC polarization does not require contact with non-PPCs

In considering possible polarity cues for the PPCs, we first addressed whether cells surrounding the PPCs are essential for polarization. We found that some of the ectopic PPCs in *mex-1(RNAi)* embryos develop at the surface of the embryo without ingressing, and that many of these cells had no contact with non-PPCs. In immunostaining experiments, we found that the surface PPCs localized the basal marker laminin to their exterior surfaces, and localized a late, lumenal marker to their interior surfaces (Figures 3.6A and 3.8). Next, we used live imaging to track the surface-localized PPCs in *mex-1(RNAi)* embryos expressing reporters for PAR-6 and PPC nuclei. Consistent with the immunostaining results, PAR-6 became highly enriched at the interior face of the surface-localized PPCs (Figure 3.6B). Thus, PPCs do not require contact with non-PPCs in order to develop a normal, apical-basal axis of polarity.

3.2.4   Laminin orients polarity in double plate PPCs

The deposition of laminin at the periphery of surface-localized PPCs in *mex-1* embryos was of interest because laminin appears to function as a polarizing cue for cultured MDCK cells (see Introduction). Immunostaining of wild-type embryos with antibodies against LAM-3/laminin α and PAR-3 showed that puncta of laminin localized to the peripheral, basal surfaces of double plate PPCs at the first detectable PAR-3 asymmetry (Figure 3.5D). In live embryos, we found that a laminin reporter (LAM-1::GFP) was enriched at or near the peripheral/basal surfaces of double plate PPCs at about the same time PAR-6 showed enrichment in separate experiments

(Figures 3.5A,B). In live embryos expressing both LAM-1::GFP and mCherry::PAR-6, the basal enrichment of LAM-1 preceded apical enrichment of PAR-6 by at least 15 minutes (Figure 3.5F). In addition, we found that the β-integrin PAT-3, a candidate laminin receptor, was expressed in double plate PPCs, and was highly enriched at basal surfaces at a similar time as laminin (Figures 3.5C,E and data not shown). These results suggest that PPCs develop basal polarity at, or prior to, asymmetric PAR localization.

To determine whether laminin has a role in polarizing the double plate PPCs, we examined embryos homozygous for *lam-1(ok3139)*, a predicted null allele in the sole gene encoding the laminin β subunit (Figure 3.9; see Experimental Procedures). *lam-1(-)* embryos have abnormal basement membranes, but localize at least some basement membrane components to the peripheral surface of the pharynx (Figure 3.10; see also Huang et al., 2003). Although the terminal morphology of *lam-1(-)* embryos appears highly abnormal by light microscopy, they appear to produce all of the major differentiated cell types (Figures 3.6D,E), consistent with previous studies on other mutations in laminin subunits (Huang et al., 2003; Kao et al., 2006). In particular, pharyngeal tissue differentiated that contained internal lines of material resembling the normal, cuticle-lined pharyngeal lumen. However, the *lam-1(-)* pharynx usually had two or more such lines, in contrast to the single wild-type lumen (Figures 3.6D,E; n=96/97). The pharyngeal lumen normally branches radially into a Y-shaped profile late in wild-type embryogenesis (Leung et al., 1999). However, transverse views of the *lam-1(-)* mutants showed that the ectopic lumenal material was not a radial outgrowth of the lumen, but instead appeared to be an entirely separate lumen(s), surrounded by PPCs (Figures 3.6F,G). The lumenal defect did not result from a hyperplasia of pharyngeal tissue, as *lam-1(-)* embryos contained 88 ± 2 PPCs (n=4) compared to the wild-type number of 86 (Kalb et al., 1998). In contrast

to these pharyngeal defects, *lam-1(-)* mutants formed a relatively normal intestine with a single lumen (Figures 3.6H,I).

We analyzed the ontogeny of the multiple, internal lumens in *lam-1(-)* mutants by examining PAR-3 and PAR-6 localization in live and fixed embryos. We found that the mutants formed a double plate of PPCs, similar to wild-type embryos (Figure 3.7G, arrows). Surprisingly, however, both PAR-3 and PAR-6 mislocalized to the peripheral, basal surfaces of the mutant double plate PPCs at the time these proteins normally localize to the midplane (Figures 3.7A–D). By examining PAR-6 localization in conjunction with a general membrane reporter, we confirmed that the basal PAR-6::GFP was within the mutant PPCs, rather than in adjacent BWMs (Figures 3.7E,F). Therefore, we conclude that laminin mutants have an early defect in PPC polarity, with many PPCs exhibiting inverted polarity. To test if the polarity inversion might result from inappropriate signaling from neighboring cells, we examined PAR-3 localization in surface-localized PPCs of *mex-1(RNAi); lam-1(-)* embryos and found that these PPCs showed a similar, inverted polarity (Figure 3.6C).

Live-imaging of double plate PPCs in *lam-1(-)* embryos showed that the basal, PAR-6-containing cell surfaces appeared to move into the interior of the developing pharynx (data not shown). Using reporters for non-muscle myosin and cell membranes, we found that the basal surfaces of the *lam-1(-)* PPCs constricted at about the same time as apical PPC surfaces normally constrict. Remarkably, neighboring PPCs spread around and eventually enclosed the basal sites, displacing them to the interior of the pharynx (Figure 3.7G–G"). Thus, PPCs in *lam-1(-)* embryos have an early defect in apical-basal polarity that is masked by subsequent morphogenetic events.

3.2.5 Laminin can act non-cell autonomously to orient PPC polarity

Because several embryonic tissues have been reported to express laminin, including the pharynx, intestine, and body wall muscles, we wanted to determine which cells must express *lam-1* to properly orient PPC polarity (Kao et al., 2006). We constructed a homozygous *lam-1(ok3139)* strain that carried an extrachromosomal array (*zuEx288*) containing a wild-type *lam-1(+)* gene plus a cell-autonomous marker (SUR-5::GFP); such transgenic arrays are lost stochastically during cell divisions, resulting in animals mosaic for gene expression. As expected, animals with SUR-5::GFP expression in most or all cells had a normal pharynx with a single lumen (Figure 3.6J; n=46/47), and animals lacking expression had the multiple lumen defect (n=60/61). We then searched for rare, mosaic animals that lacked SUR-5::GFP in all pharyngeal cells, but that retained expression in other cell groups. We found that the pharynx had a single lumen in 6/8 animals with SUR-5::GFP expression only in intestinal cells, and 14/17 animals with expression only in skin (hypodermal) cells and body wall muscles (Figures 3.6K,L). These results suggest that laminin expressed by non-PPCs can diffuse through the embryo and accumulate on the available, basal surface of PPCs, where it acts as a polarity cue.

3.3 Discussion

Epithelial tubes such as the *C. elegans* pharynx are near universal components of animal organs, and the mechanisms of tube formation have been studied in several systems (reviewed by Lubarsky and Krasnow, 2003). Some tubes, such as the vertebrate neural tube, form by the apical constriction and folding of polarized epithelial sheets (Nishimura and Takeichi, 2008). Other tubes, such as the zebrafish endoderm and mammalian dorsal aorta, form by the aggregation of non-polarized cells, the generation of a common axis of polarity, and subsequent hollowing (Horne-Badovinac

et al., 2001; Strilić et al., 2009). Here, we showed that morphogenesis of the *C. elegans* pharynx incorporates both developmental motifs.

Morphogenesis of the pharyngeal cyst proceeds through a bilaterally symmetric intermediate, the double plate, where PPCs first develop apical/basal polarity. The mature *C. elegans* pharynx has threefold symmetry, but has an underlying bilateral symmetry evident in the cell lineages of MS descendants that produce about half of the pharynx (Albertson and Thomson, 1976; Sulston et al., 1983). For example, symmetrical epithelial cells in the mature pharynx called mc3DL and mc3DR are descendants of the left and right daughters of MS, respectively, and their fates appear to be determined by a lineage mechanism rather than cell position (Priess et al., 1987). These epithelial cells do not contact each other in the mature pharynx, and are separated from their nearest common ancestor by seven cell divisions. How then, are these cells able to occupy precisely symmetrical positions? We suggest that the double plate structure allows specific pairs of left and right precursor cells to maintain, and possibly adjust, their proximity throughout the early stages of pharynx formation, until they are physically separated during cyst morphogenesis.

The PPCs appear to actively aggregate into the double plate primordium, because ectopic, supernumerary PPCs in *mex-1* mutants can form a single block of pharyngeal cells that excludes other cell types such as BWMs and intestinal cells. The bilateral symmetry of the double plate likely involves differential cell adhesion, because left and right PPCs stay on their respective sides as the double plate develops, even when they are born through left-right cell divisions. We showed that *wrm-1*, an integral component of the POP-1/TCF pathway (Rocheleau et al., 1999), is required for the rectangular shape and bilateral symmetry of the double plate. The POP-1/TCF pathway operates in the early embryo to create numerous differences between anterior-posterior sister cells (reviewed by Herman and Wu, 2004). However, because

the division axes of most early cells are oblique, many anterior-posterior sisters differ in their left-right positions, resulting in left-right differences in gene expression. For example, only left descendants of the MS blastomere express the Notch ligand LAG-2/Delta, but both left and right descendants can express LAG-2/Delta when the POP-1/TCF pathway is disrupted (Hermann et al., 2000). Thus, analogous left-right differences in early cell adhesion could shape the double plate, and an important goal of future studies will be to identify the molecular basis for those differences.

The double plate transforms into a cylindrical cyst, apparently by PPCs constricting their midplane, or future apical, surfaces; the apical surfaces decrease in size concomitant with an increase in F-actin and non-muscle myosin. The basal surfaces of the PPCs show relatively little change in size during apical constriction, suggesting they might adhere to neighboring cells or extracellular matrix. Indeed, we showed that the PPCs are surrounded by laminin before constriction, that they express a candidate laminin receptor, PAT-3/β-integrin, and that the basal surface can change size markedly in laminin mutants. Because only the apical surfaces constrict in wild-type embryos, the radial distance between the apical and basal surfaces necessarily increases; the narrowing of the apical tip likely displaces the nucleus toward the periphery, causing the apparent inflation of nuclear positions described previously (Santella et al., 2010).

Coordinated polarization of large groups of cells is a hallmark of epithelial development, and allows tubular epithelia to form a single, continuous lumen. Our results show that laminin provides a critical cue for the coordinate polarization of epithelial cells in the pharynx, although not for epithelial cells in the intestine. A previous study showed that mutants lacking LAM-3, one of two laminin α proteins in *C. elegans,* develop ruptures in the pharyngeal basement membrane, and that some pharyngeal cells appear to adhere to surrounding tissues through these gaps (Huang

et al., 2003). However, all of the mutant pharyngeal cells appeared to connect to a central lumen, as do the wild-type pharyngeal cells. Although pharyngeal cells in *lam-1* mutants connect to a lumenal surface, we showed that there are multiple lumenal surfaces in the mutant pharynx, arising from polarity defects at the earliest stages of cyst formation. Double plate PPCs appear to polarize randomly in *lam-1* mutants, with many localizing PAR-3 and PAR-6 to the periphery. Remarkably, this peripheral surface can be repositioned into the interior of the developing pharynx, by the ectopic constriction and rearrangement of neighboring PPCs. These polarity defects occur hours before differentiation of the normal pharyngeal basement membrane is complete (Mullen et al., 1999), arguing that they do not arise as secondary consequences of general basement membrane abnormalities.

Several embryonic cell types, including PPCs, normally express laminin. Our analysis of laminin mosaics shows that laminin supplied by non-PPCs is sufficient to orient PPC polarity. Consistent with previous observations, this result suggests that secreted laminin can diffuse through the embryo (Huang et al., 2003). Laminin accumulates at the exposed, peripheral surface of the PPCs, possible excluded from lateral membranes by adhesion between PPCs. We have no evidence that laminin receptors are localized asymmetrically in the double plate PPCs prior to laminin enrichment. Indeed, we found that that PAT-3/β-integrin localizes to the basal surface at about the same time as laminin, and that laminin function is required for PAT-3 localization (Figure 3.11).

Similar to *C. elegans,* the *Drosophila* genome encodes single copies of some laminin subunits, allowing the analysis of mutants that lack all secreted laminin (Urbano et al., 2009). Nevertheless, previous studies of laminin mutants in both systems did not find defects in coordinating epithelial polarity (Huang et al., 2003; Kao et al., 2006; Urbano et al., 2009), nor did we observe defects in *C. elegans* intestinal epithelial polarity in

the present study. Thus, laminin could function as a polarity signal in only certain epithelia, like the pharynx. For example, *C. elegans* intestinal cells cease dividing and polarize earlier than pharyngeal cells, possibly because of their role in metabolizing yolk to support tissue development (Bossinger and Schierenberg, 1996), and thus intestinal development might require earlier polarity cues. Alternatively, some epithelia might employ multiple signals that function redundantly with laminin, such as other basement membrane proteins. A third possibility is that some epithelia recognize inappropriate features of their environment as polarity cues when laminin is absent. By analogy, when the sperm-supplied centrosome is not available to polarize the one-cell *C. elegans* embryo, the meiotic spindle at the opposite pole of the egg appears to cue inverted polarity (Wallenfang and Seydoux, 2000). Similarly, *Drosophila* wing epithelial cells polarize in the absence of planar cell polarity components, but fail to coordinate their polarity at the tissue level (Wong and Adler, 1993). These observations suggest that cells are primed to become polarized, and can be susceptible to inappropriate triggers. Although basement membrane defects in laminin mutants might allow some PPCs to make inappropriate contacts with surrounding tissues, we do not believe that those tissues induce the inverted PPC polarity. Significantly, we showed that surface-localized PPCs in *mex-1(RNAi);lam-1(-)* embryos that do not contact any non-PPCs develop inverted polarity and PAR localization. Thus, the present study provides in vivo evidence that laminin acts as a polarizing cue for some, but not all epithelia. We conclude that the *C. elegans* pharynx should provide a useful genetic model for dissecting laminin-based signaling, prior to the general requirements for laminin in basement membrane assembly and tissue integrity.

3.4 Experimental Procedures

3.4.1 Nematodes

C. elegans were cultured as described (Brenner, 1974). Mutant alleles used (details available at `http://www.wormbase.org`): LG III, *unc-119(ed3), wrm-1(ne1982)*; LG IV, *lam-1(ok3139,ok3221), nT1[qIs51], unc-5(e53)*; LG V, *fog-2(q71) pha-4(q490), stu-3(q265) rol-9(sc148)*. Transgenes used: *stIs10088* [*hlh-1(3.3kb)*::HIS-24::mCherry] (Murray et al., 2008), *pxIs10* [*pha-4*::GFP::CAAX] (Portereiko and Mango, 2001), *pxIs6* [*pha-4*::GFP::HIS-11] (Portereiko and Mango, 2001), *stIs10389, wgIs37* [PHA-4::TY1::EGFP::3xFLAG] (J. Murray, unpublished; Zhong et al., 2010), *zuIs45* [*nmy-2*::NMY-2::GFP] (Nance et al., 2003), *xnIs3* [*par-6*::PAR-6::GFP] (Totong et al., 2007), *pie-1*::mCherry::PAR-6 (Schonegg et al., 2007), *urEx131* [*lam-1*::LAM-1::GFP] (Kao et al., 2006), *qyIs43* [PAT-3::GFP; *ina-1*(genomic)] (Hagedorn et al., 2009), *ltIs44* [*pie-1*::mCherry::PH(PLC1δ1)] (Kachur et al., 2008), *zuEx276, zuIs270* [*pha-4*::GFP::dMoesin-ABD], *zuEx254* [*lin-12(pm8)*::mCherry::CAAX; *lin-12(pm8)*::GFP ::HIS-11] and *zuEx288* [*lam-1(+);* SUR-5::GFP]. *mex-1(RNAi)* was performed by feeding. Developmental staging of embryos was performed as described (Sulston et al., 1983).

3.4.2 Transgene Construction

To create pSSR18[*pha-4*::GFP::dMoesin-ABD], the dMoesin-ABD fragment from pJWZ6 (Ziel et al., 2009) was PCR amplified and fused to GFP by cloning. The GFP-dMoesin-ABD fragment was PCR amplified with primers oSSR32 (5'-CCTAG Gattttcaggaggacccttgct-3') and oSSR33 (5'-GGGCCCcggccgactagtaggaaaca-3') and cloned into the AvrII and ApaI sites of pJIM20 (Murray et al., 2008). *zuEx276* was created by injection of pSSR18 at 20 ng/μl and pJN254 at 100 ng/μl (Nance

et al., 2003) into *unc-119(ed3)* worms, and integrated by gamma-irradiation to create *zuIs270*. To create pJR09[*lin-12(pm8)*::GFP::HIS-11], the fourth intron of *lin-12* was PCR amplified with primers oJR018 F (5'-GCATGCggcacttttaagacacccaac-3') and oJR018 R (5'-GCTAGCgggacacacgcaaatgtatg-3') and cloned into the SphI and NheI sites of pAP.10 (Gaudet and Mango, 2002). *zuEx254* was created by injection of pJR09 at 20 ng/μl, pJR17[*lin-12(pm8)*::mCherry::CAAX] at 20 ng/μl, and pRF4 at 100 ng/μl Mello et al. (1991) into N2 worms.

3.4.3   Imaging

Embryos were mounted for longitudinal optical sectioning as described (Sulston et al., 1983). For transverse sectioning with confocal microscopy, approximately 1" square pieces of 35 micron Nitex mesh (Dynamic Aqua-Supply Ltd., Surrey, Canada) were treated with 1% Osmium tetroxide (Sigma) overnight and then washed extensively; this treatment reduces Nitex autofluorescence. Embryos were pipetted in a small volume of liquid onto a piece of the Nitex filter on top of a 3% agarose pad. The embryos/filter were covered with a coverslip and sealed with petroleum jelly. Time-lapse movies were acquired with a spinning disk confocal system (Yokogawa CSU-10) on a Nikon TE-2000 inverted microscope equipped with a Hamamatsu C9100 camera, running Volocity 5.3.3 (Improvision, Lexington, MA). A 60X oil immersion objective (Nikon) was used for longitudinal optical sectioning, and a 60X water immersion objective (Nikon) for transverse sectioning. Image stacks were analyzed, measured and adjusted for brightness and contrast using ImageJ (`http://rsbweb.nih.gov/ij/`) or Adobe Photoshop. Brightness and contrast were adjusted for each timepoint separately. Quantification of midplane enrichment of NMY-2 and PAR-6 was performed by analyzing maximum intensity projections of longitudinal views of embryos co-expressing NMY-2::GFP and mCherry::PAR-6. The integrated intensities in two

5x12 micron regions (PPC midplane and PPC lateral) were corrected for camera noise, and then normalized to the initial timepoint. The midplane enrichment at time i was calculated as: $(PPC_{mid;t=i}/PPC_{lateral;t=i})/(PPC_{mid;t=0}/PPC_{lateral;t=0})$.

3.4.4   Immunofluorescence

Fixation and staining of embryos was performed as described (Leung et al., 1999). The following primary antibodies and antisera used were: chicken α–LAM-3, α–EPI-1 (Huang et al., 2003), rabbit α–GFP (Abcam), α–UNC-52 (GM1; Mullen et al., 1999), α–LET-2 (Graham et al., 1997), mouse α–PAR-3 (Nance et al., 2003), MH25 (Francis and Waterston, 1985), MH27 (Francis and Waterston, 1991), mAbGJ1 [α–LAM-3], mAbGJ2 [pan-laminin] (Rasmussen et al., 2008), IFA (Pruss et al., 1981) and mAbPL1 (G. Hermann and J.P., unpublished). For quantification of centrosome orientation, image stacks were acquired of PHA-4::GFP-expressing embryos immunostained with α–GFP and IFA antibodies (a marker of centrosomes; Leung et al., 1999). Centrosomes were considered midplane-facing if they fell in a 180º sector facing the midplane. Using this assay, 50% of randomly oriented centrosomes would score as midplane-facing.

3.4.5   Characterization of lam-1 Mutants

lam-1 deletion alleles ok3139 and ok3221 were generated by the international C. elegans Gene Knockout Consortium. ok3139 was outcrossed five times and maintained over the GFP-marked balancer nT1[qIs51] or the visible marker unc-5(e53). Alleles ok3139 and ok3221 were sequenced and found to both contain frameshifts in exon 6 of lam-1, N-terminal to the coiled-coil domains required for assembly of the laminin subunits (Miner and Yurchenco, 2004); thus, these mutations are predicted to eliminate heterotrimer secretion. Embryos homozygous for either allele are embryonic lethal,

and *lam-1(ok3221)* embryos show a multi-lumen phenotype similar to that described here for *lam-1(ok3139)* (data not shown). The *ok3139* mutation was fully rescued by the fosmid WRM0633dC11 that contains the wild-type *lam-1* locus. For mosaic analysis, *lam-1(ok3139)/nT1[qIs51]* adults were injected with WRM0633dC11 at 10 ng/μl, pTG96 at 100 ng/μl (Yochem et al., 1998), and pRF4 at 50 ng/μl (Mello et al., 1991); viable *ok3139* homozygotes were isolated and maintained from this strain. The multi-lumen phenotype of *lam-1(ok3139)* was also rescued by LAM-1::GFP, but these animals died as L1 larvae.

Figure 3.1: Pharyngeal cyst development in wild type and *pha-4* mutants. Longitudinal, optical sections through the center of wild-type (A) and *fog-2(q71) pha-4(q490)* embryos (B) at ∼420 mins in development. Embryos express a nuclear reporter (green, *pha-4*::HIS-GFP) in all pharyngeal precursor cells (PPCs) and in intestinal cells (int). Because the PPC reporter does not express the PHA-4 protein, it does not rescue the *pha-4* mutation and the "PPCs" in the mutant embryo do not differentiate as pharyngeal cells. Arrows in A indicate the periphery of the pharyngeal cyst, and the arrowhead indicates a gap along the central, future lumenal axis of the cyst. (C) Partial cell lineage diagram indicating the origins of early cells mentioned in this study; BWMs = Body Wall Muscles, a non-pharyngeal type of muscle. (D) Optical sections used in this paper superimposed on a cartoon of an embryo midway through development (adapted from Priess and Hirsh, 1986); D=Dorsal, V=Ventral, A=Anterior, and P=Posterior. Bars = 5 μm.

A wild type

B *pha-4(q490)*

PPCs   int

PPCs   int

C fertilized egg
AB   MS
int
PPCs   BWMs
PPCs   BWMs

D transverse plane
D
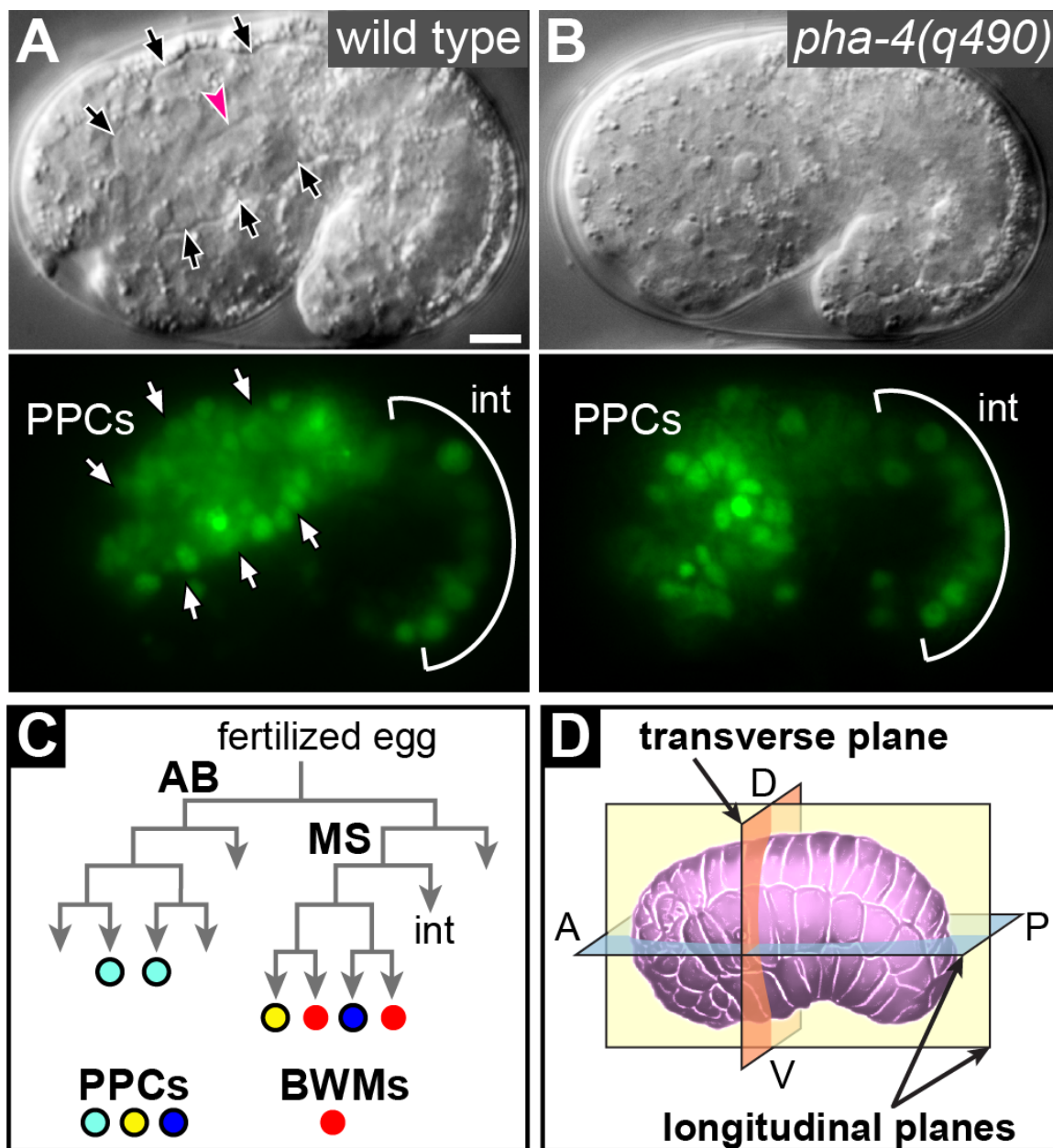A   P
V
longitudinal planes

Figure 3.2: PPCs organize into a bilaterally symmetric double plate. (A and B) Confocal fluorescence image sequence of single, live embryos expressing a PPC-specific nuclear reporter (green, *pha-4*::HIS-GFP) and a general membrane reporter (red, memb). Images are transverse optical sections oriented as in Figure 3.1D; images were collected approximately 15 μm from the anterior pole of the embryo. PPCs are ingressing from the left and right ventral (bottom) sides into the interior of the embryo, then extending dorsally (up). (B) Examples of left-right PPC divisions in the double plate; cells are indicated before (single arrow) and after (double arrow) division; the dashed line indicates the midplane of the double plate. (C) Cartoon of the ventral surface of a 24-cell embryo ($\sim$100 mins), and of a transverse section through an embryo at the double plate stage ($\sim$290 mins). Nuclei with black outlines are PPCs and color-coded as in Figure 3.1C, red nuclei are BWM precursors. (D) Transverse optical section of a live, $\sim$250 min embryo expressing the same PPC and membrane reporters as in A and B, but with an additional reporter for BWMs (red, *hlh-1*::HIS-mCherry). (E) Longitudinal optical section through a terminal stage *mex-1(RNAi)* embryo (anterior is up). (F and G) Ventral, surface views of live wild-type and *wrm-1(ts)* embryos raised at the restrictive temperature until the MS cell division, then imaged at the permissive temperature. Images show before (top) and after (bottom) the fifth cell division of the MS-derived PPCs, coded as in Figure 3.1C; white lines indicate sister cells. Note irregular left-right positioning of cells in the *wrm-1(ts)* embryo. (H and I) Live *wrm-1(ts)* embryos raised at the permissive temperature (H), or temperature shifted (I) as in G; reporters and optical sectioning as in A. Note failure of PPCs to form a double plate after shifting from the restrictive temperature (n=15/15 embryos). Bars = 5 μm (A,C,E,H,I), 2.5 μm (B,F,G).

A transverse view
t=0' (~150') PPCs
36'
60'
84'
108'
144'

B t=0' (~310')
8'
16'
24'
32'

C
anterior
MS
R   L
posterior
ventral view
24-cell stage

dorsal
R   L
ventral
transverse view
double plate stage

D BWMs
HLH-1
PPCs
HLH-1

E *mex-1*
PPCs
int
PHA-4
BWMs
HLH-1
merge

F WT

G *wrm-1, 25°C*

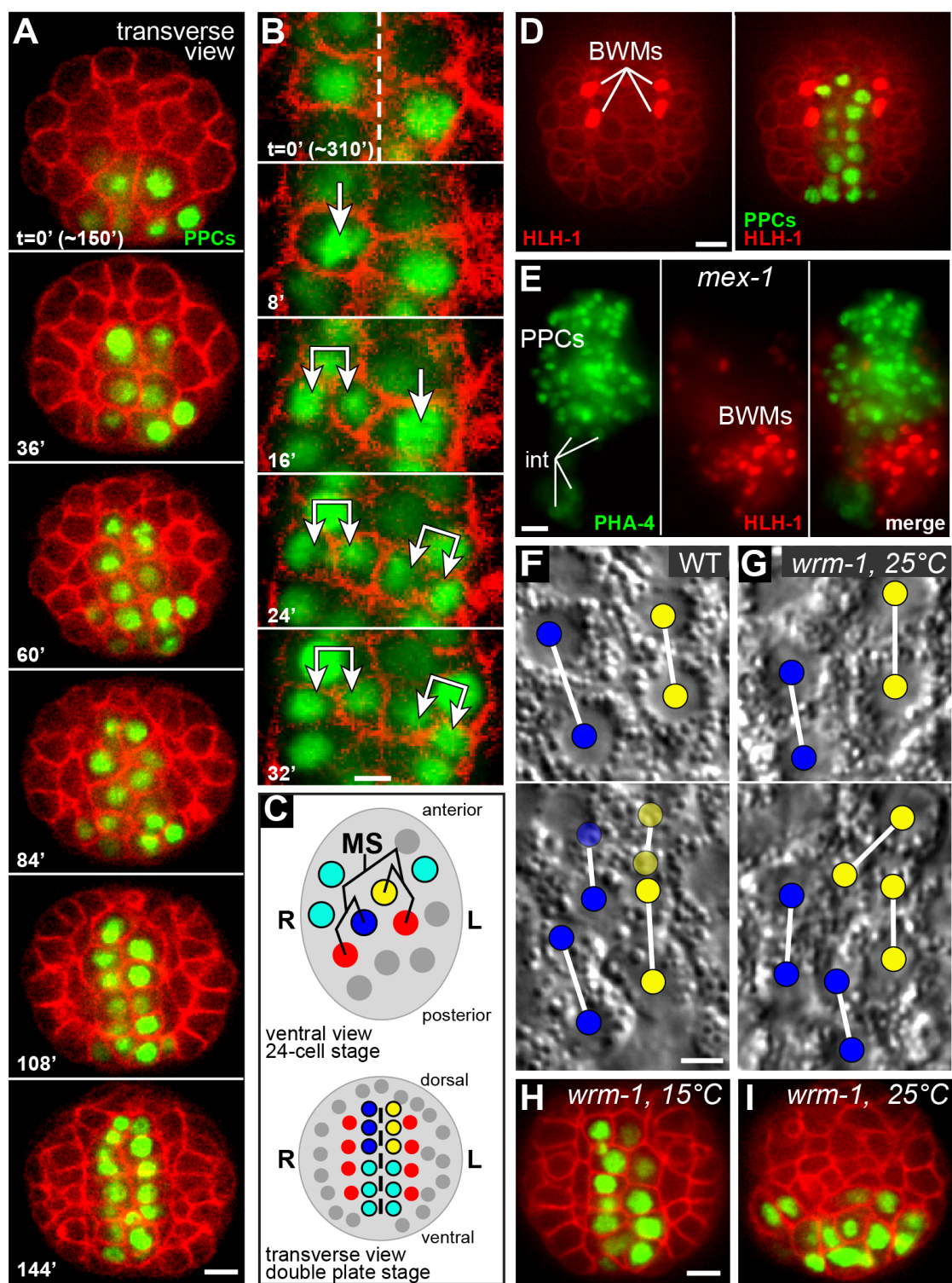**H** *wrm-1, 15°C*

I *wrm-1, 25°C*

Figure 3.3: PHA-4 is required to maintain bilateral symmetry of the double plate. (A) Transverse optical sections through a live wild-type embryo showing the PPCs (green, *pha-4*::HIS-GFP) transition from double plate to cyst. (B) *fog-2(q71) pha-4(q490)* embryo showing the inappropriate left-right crossing of a PPC (arrow) and the failure to form a cyst. Bar = 5 μm.
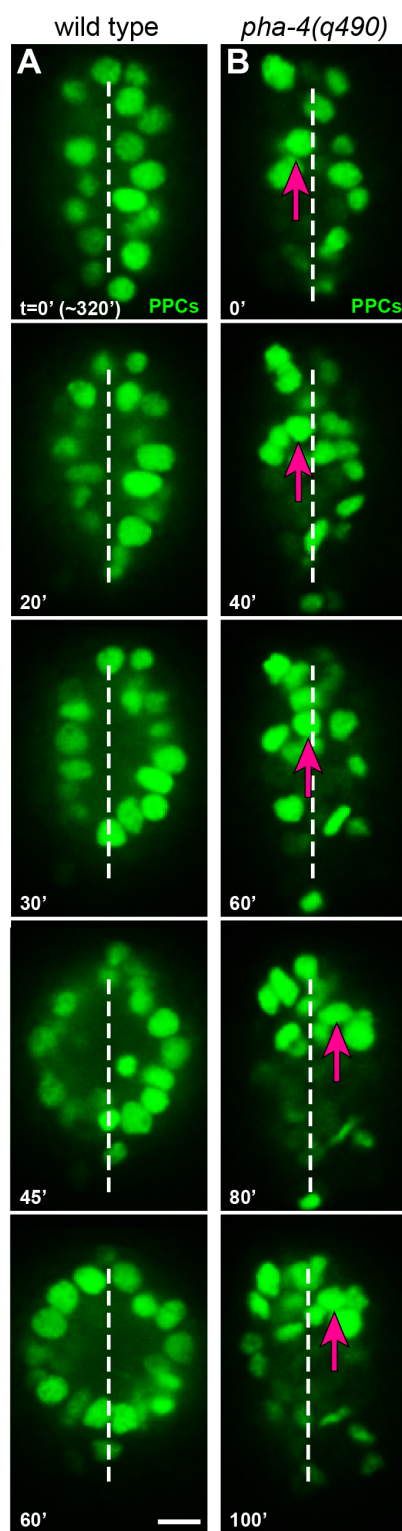
wild type | pha-4(q490)

Figure 3.4: Cyst formation by apical constriction of double plate cells. (A–D) Transverse optical sections of live embryos showing the transition from double plate to cyst; arrows indicate the left and right periphery of the double plate. (A) Image sequence showing all cell membranes (memb). (B) Image sequence showing a single, tagged PPC (*zuEx254*). (C) F-actin expression (*pha-4*::GFP::dMoesin-ABD) expression in the PPCs; note enrichment along the midplane/apical surface. (D) Non-muscle myosin expression (*nmy-2*::NMY-2::GFP). (D') Magnified view of the periphery of the double plate (arrow with bracket in D) showing non-muscle myosin is initially enriched at the periphery of PPCs before it concentrates apically. (E) Average membrane length (in microns) of midplane and peripheral PPC surfaces. Error bars indicate 95% confidence intervals. (F) The left panel is a longitudinal view of the pharynx showing the positions of centrosomes (red, IFA) and PPC nuclei (blue, DAPI) relative to the midplane through the double plate. Note cluster of midplane-facing centrosomes in the top left PPCs. Anterior is up. The right panel quantifies centrosome positions over time. n>55 centrosomes analyzed per timepoint. (G) Quantification of midplane enrichment of PAR-6 and NMY-2 in embryos co-expressing *pie-1*::mCherry::PAR-6 and *nmy-2*::NMY-2::GFP (average of 4 embryos). Error bars indicate 95% confidence intervals. Bars = 5 μm (A,C,D), 2.5 μm (B,F), 1 μm (D').

A   310'   memb
340'
370'
400'

B

C   F-actin

D   non-muscle myosin

D'

E   peripheral
membrane length
4
3
2
1
0
0'   20'   40'   60'
time (t₀ = ~310')
midplane

F   Centrosomes
% midplane-facing
60
40
20
240'   290'   310'
DNA

G   PAR-6
midplane enrichment
1.6
1.4
1.2
1.0
0'   20'   40'   60'   80'
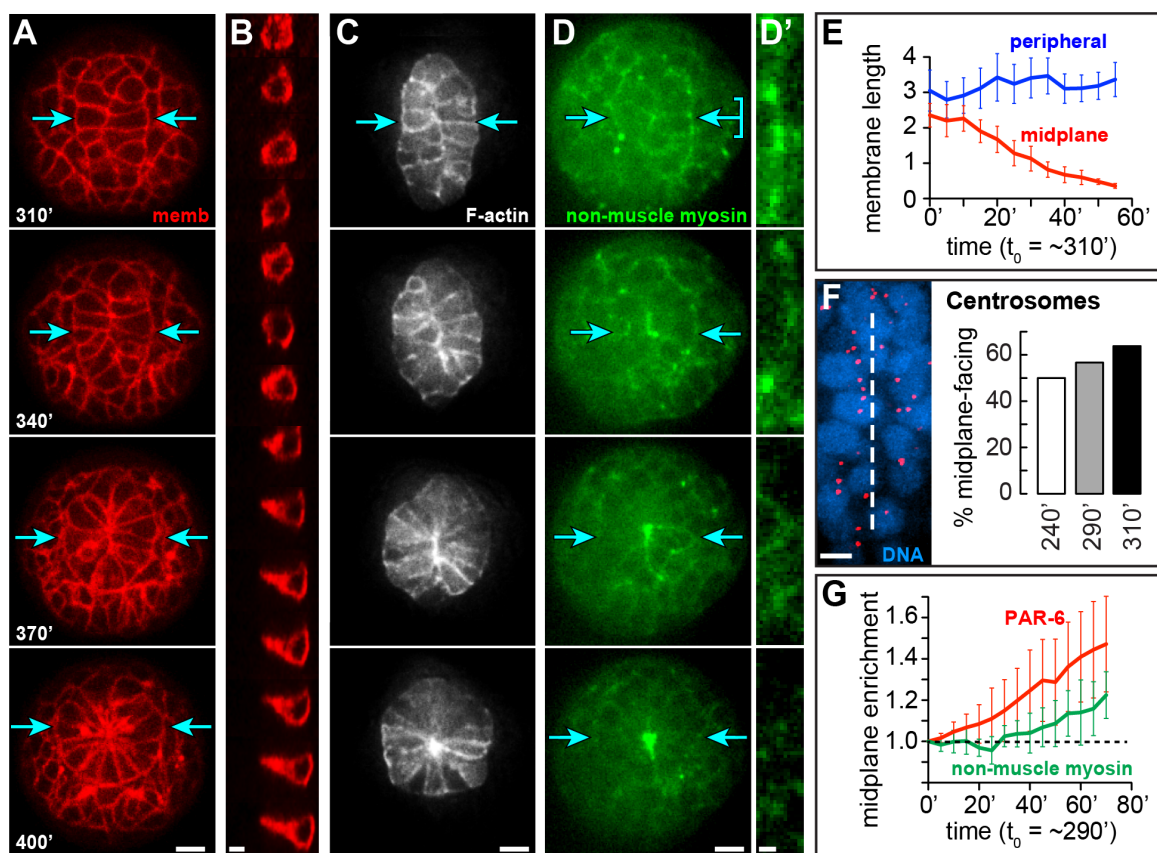time (t₀ = ~290')
non-muscle myosin

Figure 3.5: Onset of apical and basal polarity in double plate PPCs. (A–C) Transverse optical sections of live embryos showing the transition from double plate to cyst; arrows indicate the left and right periphery of the double plate. Embryos express the following reporters: (A) PAR-6 (*pie-1*::mCherry::PAR-6), (B) LAM-1/laminin β (*lam-1*::LAM-1::GFP), and (C) PAT-3/β-integrin (*pat-3*::PAT-3::GFP). (D and E) Ventral, longitudinal views of embryos immunostained for PAR-3 and either LAM-3/laminin α (D), or PAT-3/β-integrin (E); embryos were selected as showing the first detectable asymmetry of PAR-3 in the PPCs (bracketed). Note that both LAM-3 and PAT-3 show enrichment at the periphery of the PPCs. (F) Top, kymograph display of an embryo co-expressing *pie-1*::mCherry::PAR-6 and *lam-1*::LAM-1::GFP; panels show the width of the double plate and surrounding BWMs. Note that relative levels of PAR-6 fluctuate at the midplane before 35', but LAM-1 shows sustained enrichment at the periphery. Graphs at bottom show fluorescence intensity linescans across the kymographs at 35' and 60'; the dashed line indicates the midplane. Bars = 5 μm (A–F).
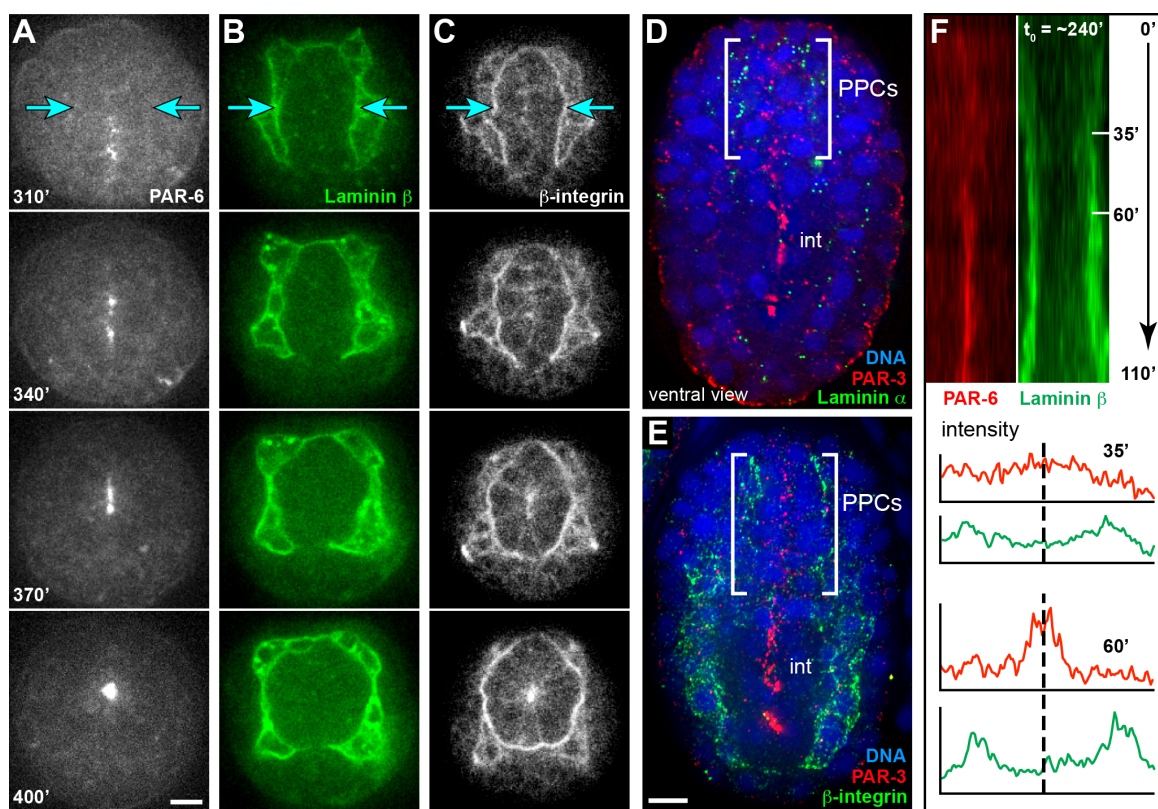
Figure 3.6: Laminin is required to specify a single, lumenal surface. (A) High magnification view of PPCs at the surface of a *mex-1(RNAi)* embryo (PPC nuclei are visible in lower panel). The embryo was immunostained for LAM-3/laminin α (white), PPCs (green, *pha-4*::PHA-4::GFP) and a lumenal marker (red, mAbPL1). Note that laminin accumulates at the external periphery of the surface PPCs (arrowheads), and that lumenal markers differentiate one cell diameter in from this surface. (B) Image sequence of surface PPCs in a live *mex-1(RNAi)* embryo expressing reporters for PAR-6 (red, *pie-1*::mCherry::PAR-6) and PPC nuclei (green, *pha-4*::PHA-4::GFP). (C) Surface PPCs in an immunostained *mex-1(RNAi); lam-1(ok3139)* embryo showing PAR-3 (red) and PPC nuclei (green, *pha-4*::PHA-4::GFP). Note the surface accumulation of PAR-3. (D and E) Brightfield images of late stage wild-type and *lam-1(ok3139)* embryos. Arrowheads indicate the cuticle-lined pharyngeal lumen; note multiple lines in the *lam-1(-)* mutant. (F and G) Immunostained wild-type and *lam-1(-)* embryos at 470 min showing PPC nuclei (green, *pha-4*::PHA-4::GFP) and a marker for the pharyngeal lumen (red, mAbPL1). Insets are reconstructed, cross sectional views through the pharynx, showing that each lumen is surrounded by PPCs. (H and I) Brightfield and fluorescent images of the intestine in live wild-type and *lam-1(-)* embryos at ∼280 min, showing localization of PAR-6 (red, *par-6*::PAR-6::GFP) to the single, lumenal surface (arrow). Although *lam-1(-)* embryos showed mispositioning of some intestinal cells, 28/28 embryos examined localized PAR-3 or PAR-6 only to the apical surfaces of intestinal cells. (J–L) Images of newly hatched *lam-1(-)* larvae that are mosaic for a *lam-1(+)* transgene (*zuEx288*); the right panel shows expression of the fluorescent reporter (*sur-5*::SUR-5::GFP) indicating presence of *zuEx288*. Note formation of a single pharyngeal lumen (arrowhead) when *zuEx288* is present only in the intestine (K) or hypodermis and body wall muscles (L). Bars = 2.5 μm (A–C), 5 μm (D–L).

mex-1(RNAi)

wild type

lam-1(-)

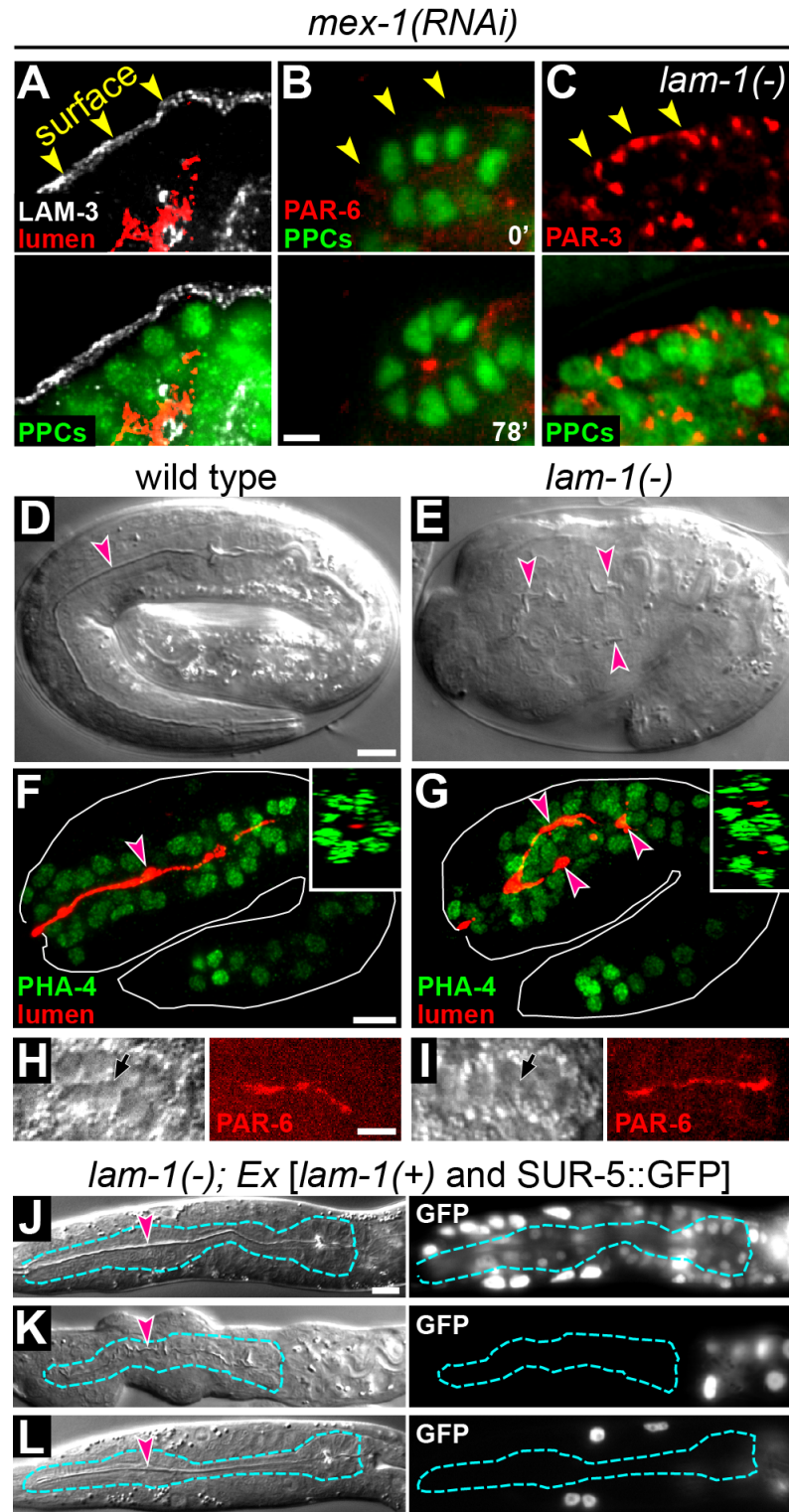*lam-1(-); Ex* [*lam-1(+)* and SUR-5::GFP]

Figure 3.7: Laminin orients PPC polarity. (A and B) Dorsal, longitudinal optical sections of immunostained wild-type and *lam-1(ok3139)* embryos. Images show PPC nuclei (green, *pha-4*::PHA-4::GFP) and PAR-3 localization (red) as maximum intensity projections through the double plate; arrows indicate the midplane. Note multiple lines of PAR-3 in the *lam-1(-)* embryo (n=18/18). (C and D) PAR-6 localization (*par-6*::PAR-6::GFP) in single longitudinal, optical sections through the double plate of live wild-type and *lam-1(-)* embryos. Note that PAR-6 localization begins, and persists, at the periphery of the double plate in the *lam-1(-)* embryos (n=16/16). (E and F) High magnification images showing part of a longitudinal optical section through the double plate of live wild-type (top) and *lam-1(-)* embryos showing PAR-6 (red, *par-6*::PAR-6::GFP) and plasma membranes (green, memb). Line scans through the double plate are shown below. (G–G") Images showing transverse optical sections of a live *lam-1(-)* embryo with reporters for non-muscle myosin (green, *nmy-2*::NMY-2::GFP) and plasma membranes (red, memb). Images in G" are high magnification views of PPCs at the periphery of the double plate (bracketed region in G and G'). The cartoons show tracings of individual, color coded PPCs within the double plate (grey region), taken from movie frames at left. Bars = 2.5 μm (A–F, G"), 5 μm (G,G').

wild type
A — PAR-3 / DNA / PPCs

lam-1(-)
B — PAR-3 / DNA / PPCs

wild type
C — PAR-6
t=0' (~280')
20'
40'
50'

lam-1(-)
D — PAR-6
0'
30'
50'
70'

wild type
E — PAR-6 / memb
intensity — PAR-6 / memb
PPCs

lam-1(-)
F — PAR-6 / memb
intensity — PAR-6 / memb
PPCs

lam-1(-)
G — non-muscle myosin
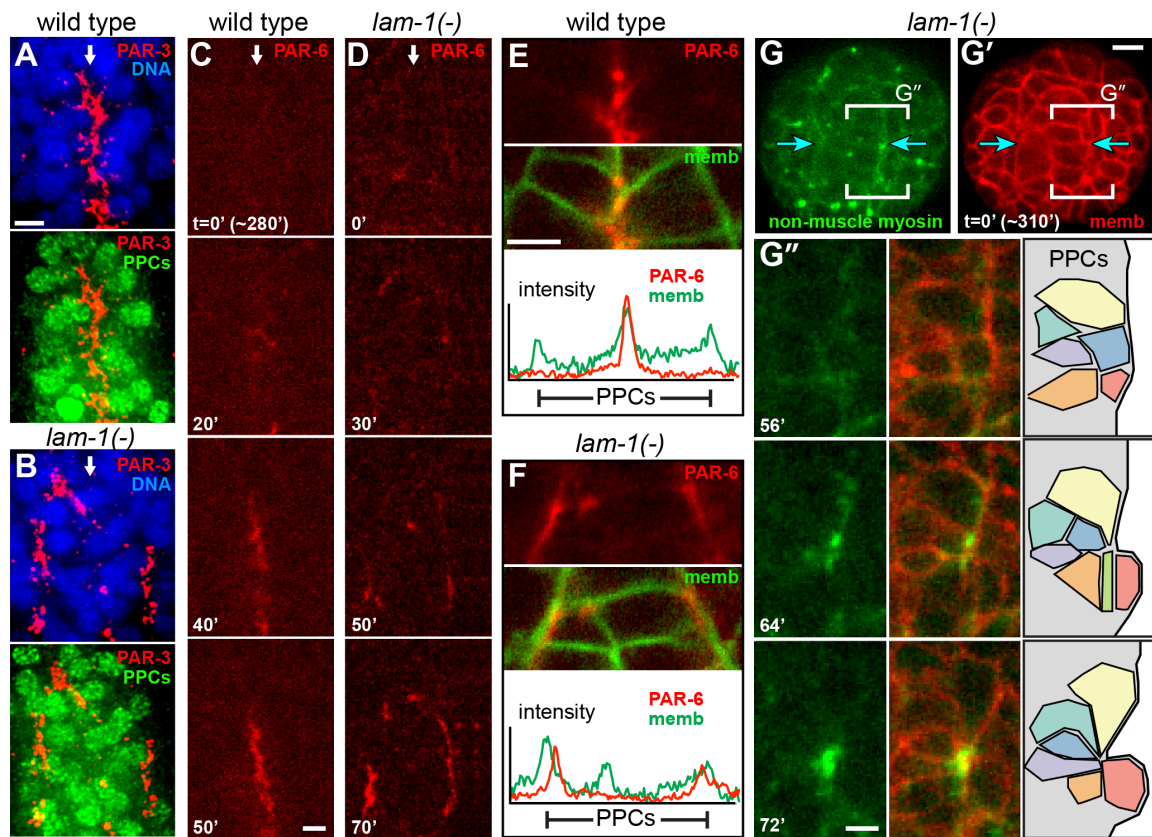G' — t=0' (~310') memb
G" — PPCs
56'
64'
72'

Figure 3.8: mAbPL1 is a marker of the pharyngeal lumen. (A–D) Immunostained embryos at sequentially older stages showing progressive apical/lumenal localization of the antigen stained by mAbPL1. White arrows indicate the margins of the pharynx.
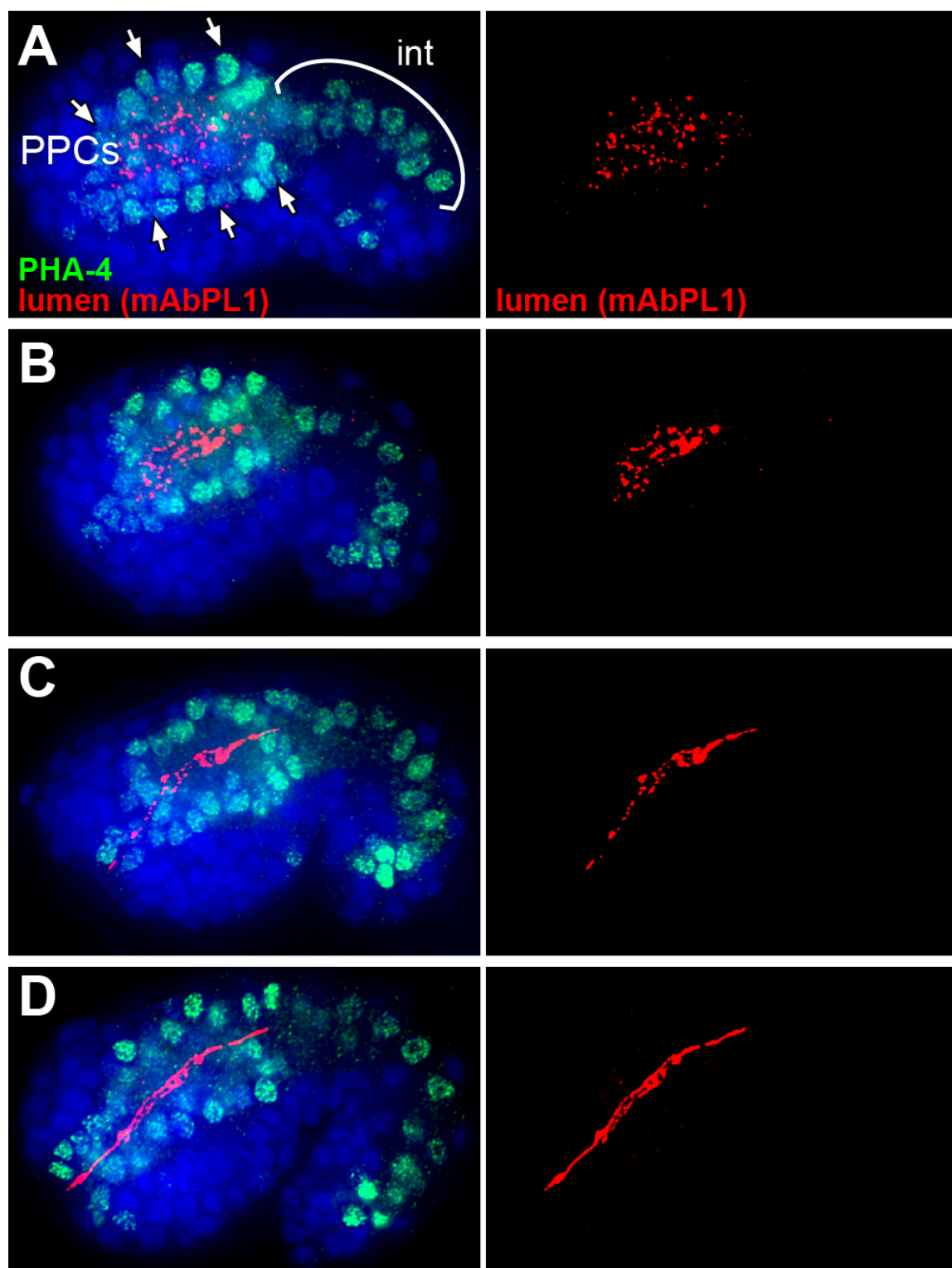
PHA-4
lumen (mAbPL1)

Figure 3.9: Characterization of *lam-1(ok3139)* mutants. (A) Schematic of the LAM-1 protein showing the laminin domains (see Aumailley et al., 2005, for nomenclature of the laminin domains). Diagram of the *lam-1* gene shows the positions of mutations in strains used for this study; alleles *ok3139* and *ok3221* cause frameshift mutations in exon 6. (B and C) Embryos from a *lam-1(ok3139)/nT1[qIs51]* adult immunostained for GFP (the *qIs51* transgene gives strong intestinal GFP expression in embryos of this stage) and laminin. Note that *lam-1(ok3139)* embryos lack all laminin staining.
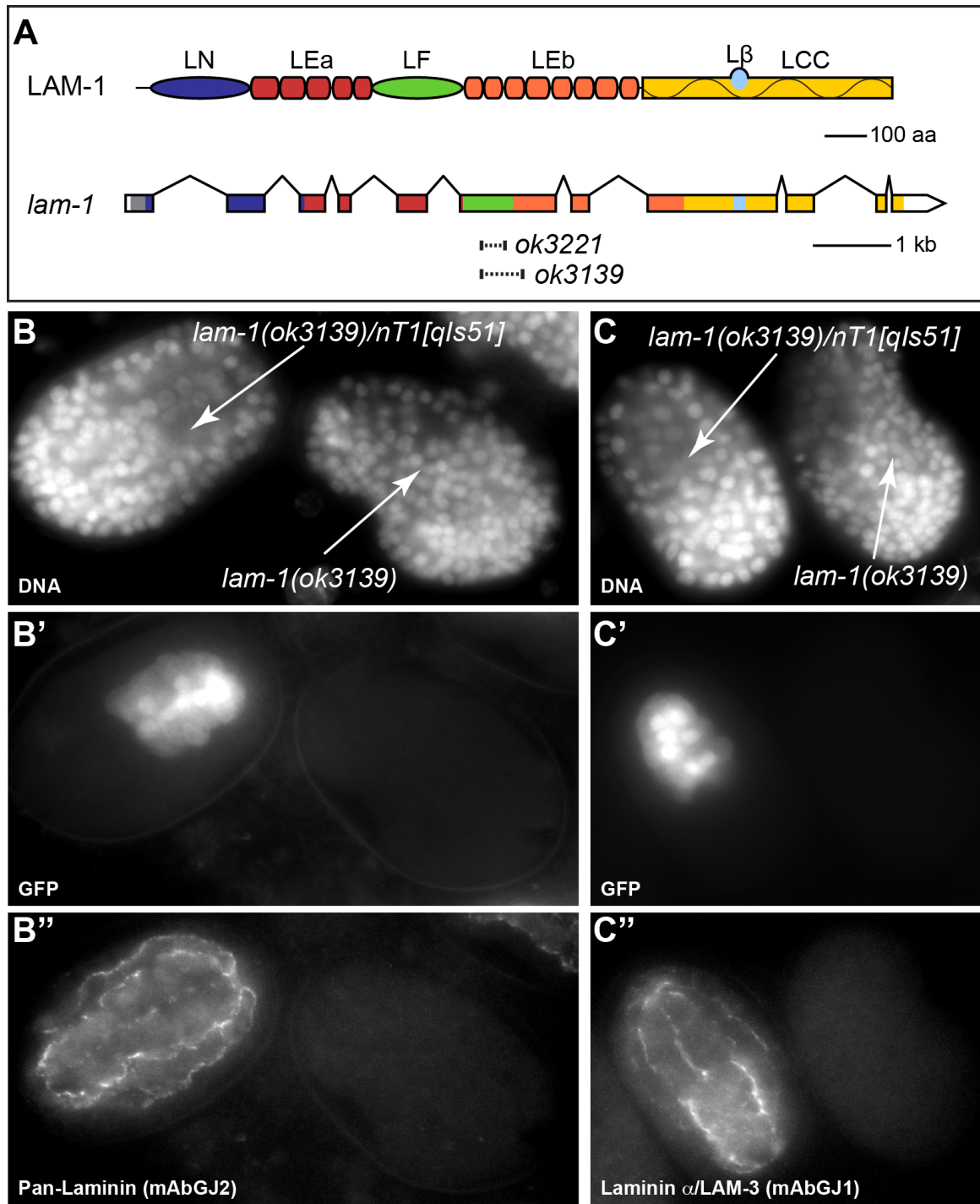
Figure 3.10: Laminin is required for pharyngeal basement membrane integrity in late embryos. Longitudinal views of late stage (>470 min) *lam-1(ok3139); zuEx288[lam-1(+) and SUR-5::GFP]* (A,C,E) and *lam-1(ok3139)* (B,D,F) embryos immunostained for PAT-3/β-integrin (A and B), UNC-52/Perlecan (C and D) and LET-2/Type IV collagen (E and F). Note that in the *lam-1(ok3139)* embryos PAT-3, UNC-52 and LET-2 localize to the outer surfaces of the pharynx, but appear disorganized. White arrows indicate the margins of the pharynx.
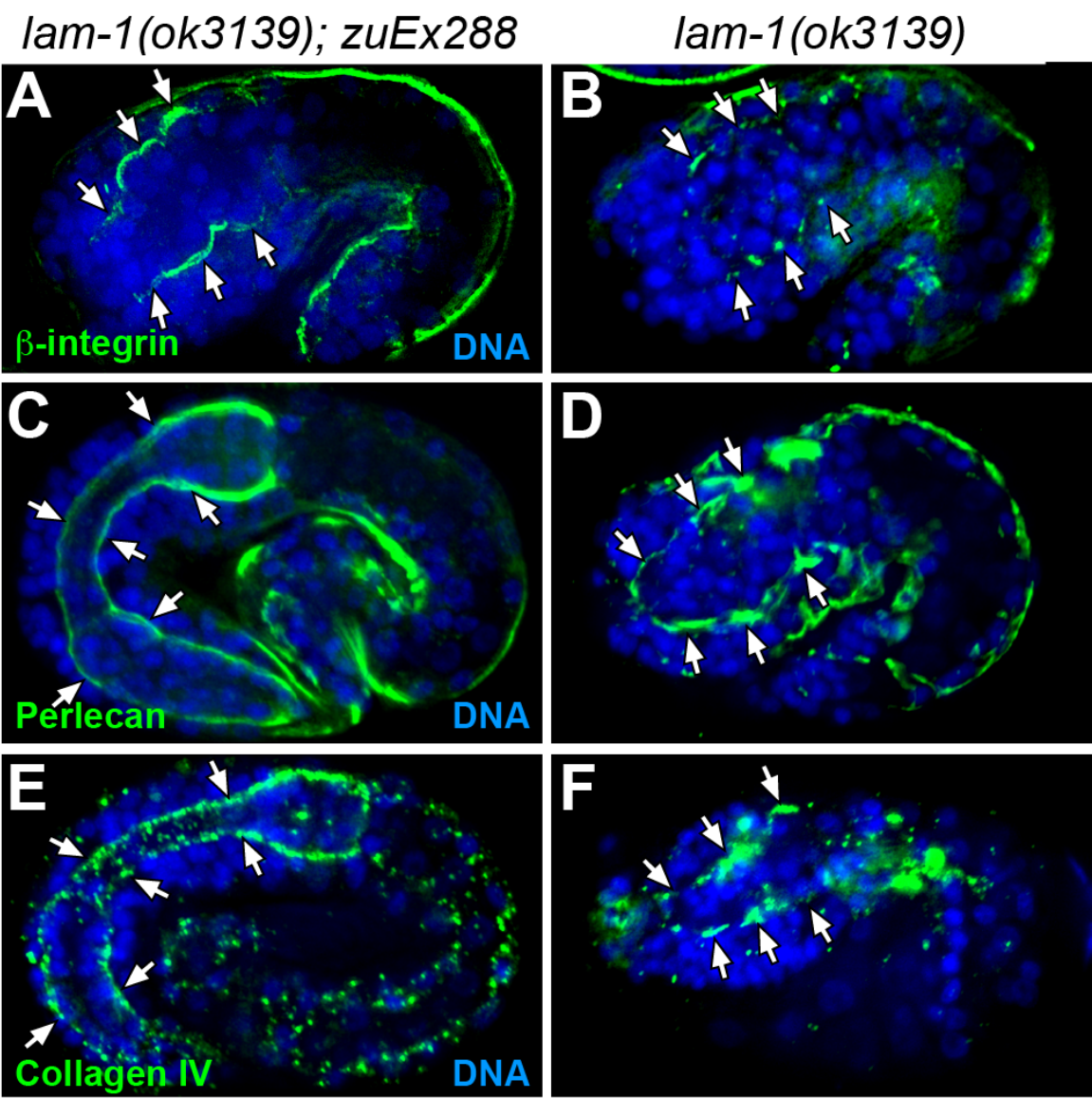
lam-1(ok3139); zuEx288   *lam-1(ok3139)*

Figure 3.11: Laminin is required for polarized localization of β-integrin in double plate PPCs. (A) Longitudinal views of double plate stage embryos from a *lam-1(ok3139); zuEx288*[*lam-1(+)* and SUR-5::GFP] adult immunostained for GFP (to score for the presence of *zuEx288*) and PAT-3/β-integrin. Note that PAT-3 appears uniformly localized along the PPC membranes in the *lam-1(ok3139)* embryo in contrast to the polarized localization in the *lam-1(ok3139); zuEx288* embryo. The brackets indicate the margins of the double plate PPCs.

A *lam-1(ok3139); zuEx288*

PPCs

PPCs

lam-1(ok3139)

DNA

A'

GFP

A"

β-integrin/PAT-3
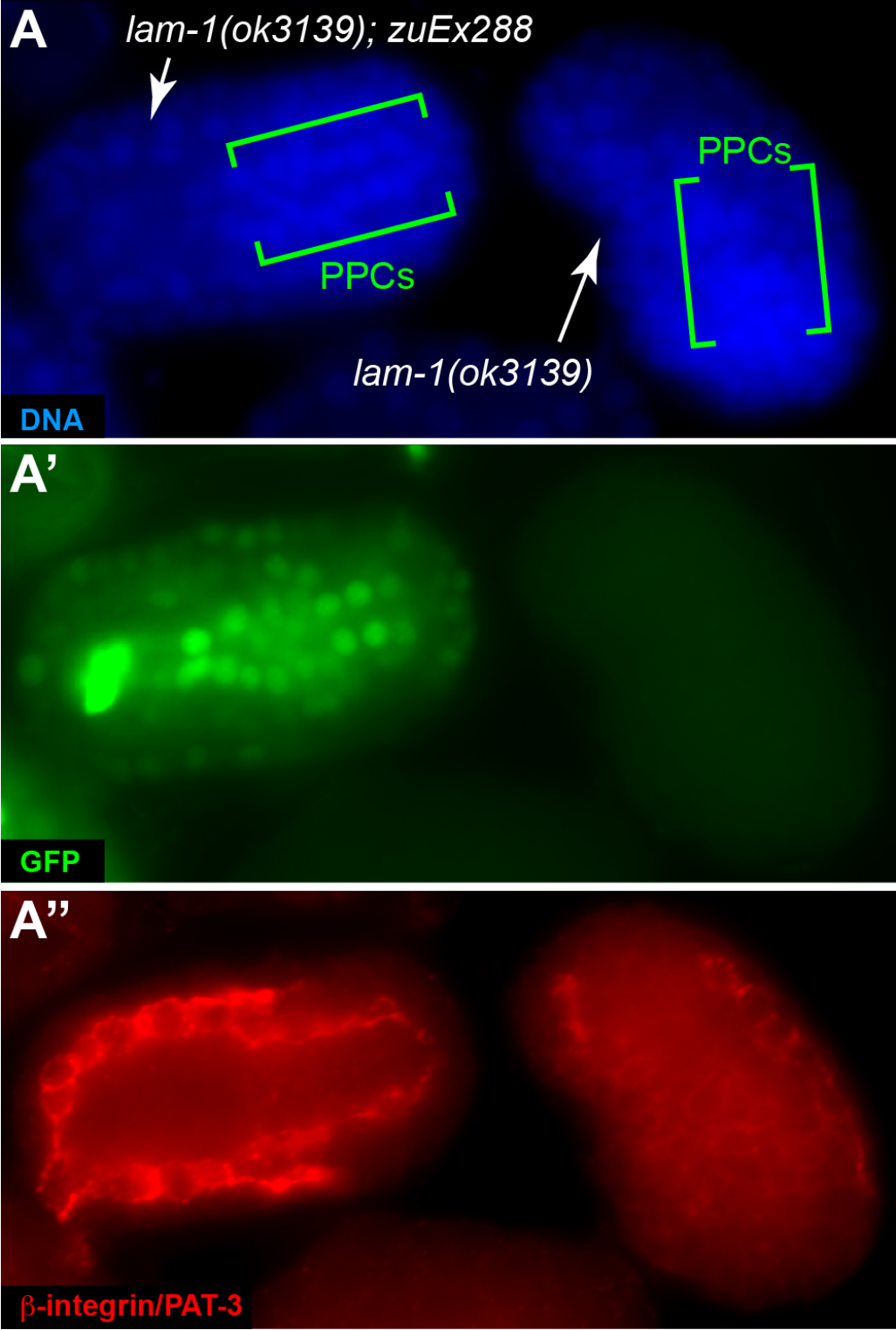
Chapter 4

PERSPECTIVES AND FUTURE DIRECTIONS

This thesis helped further our understanding of morphogenesis of the *C. elegans* pharynx; however, many mysteries remain.

In Chapter 2, I found that single cells can self-fuse (also referred to in the literature as auto-fusion). Although cell fusion happens in many systems, including humans, the only genetic system to study developmental fusogens is *C. elegans*. Almost a third of somatic cells in *C. elegans* fuse with a neighbor during development (Sapir et al., 2008) and previous studies had found that manipulated cells in *C. elegans* could self-fuse (Sharma-Kishore et al., 1999). In addition to the self-fusion of pm8 and vpi1, recent studies have found that single cells outside the pharynx can also self-fuse. The duct cell of the excretory system requires AFF-1 to form a toroid (Stone et al., 2009) and reshaping of menora-like neuronal arbors requires EFF-1 (Oren-Suissa et al., 2010).

Fusogens are powerful molecules, sufficient to fuse cultured and embryonic cells, and are therefore likely under tight transcriptional and post-transcriptional control. Most of the cell fusions in the worm require EFF-1. EFF-1 is expressed in a diversity of cell types, including epithelia, neurons, and myoepithelia, over a wide range of developmental time. How is the precise spatiotemporal control of EFF-1 expression regulated? I found that Notch signaling is required to inhibit EFF-1 expression in pm8, which is possibly mediated by the REF-1 family of bHLH transcription factors (Neves and Priess, 2005). Unknown mechanisms activate EFF-1 expression in vpi1. Many different types of transcription factors regulate EFF-1 expression, both positively and negatively (reviewed by Podbilewicz, 2006). These observations suggest

that the *eff-1* regulatory region is likely complex, and how and where these upstream transcription factors bind within the regulatory region is poorly understood. Fusogens are also likely regulated at the post-transcriptional level. For example, fusion of the dorsal hypodermal cells appears to initiate via a fusion pore adjacent to the adherens junctions Mohler et al. (1998). How are fusogens targeted to specific membrane domains within a cell? Do they interact with polarity complexes? Once fusion is initiated, how is the fusion pore expanded and do fusogens have a role in disassembly of the adherens junctions? Future studies using antibodies or GFP translational reporters will hopefully help resolve this.

Do toroidal cells in other systems also form by self-fusion? This question may be difficult to resolve in the short-term. Although recent work has identified the first homolog of EFF-1/AFF-1 outside of nematodes (Avinoam et al., 2011), few systems have the detailed anatomical knowledge of *C. elegans*, nor the genetic tools.

To form toroids, pm8 and vpi1 wrap around the midline to create an intracellular lumen. The formation of the pm8 lumen may be templated by neighboring marginal cells, however, vpi1 apparently does not require marginal cells to form its lumen (unpublished observations). As several tubular systems contain apical matrix (see Chapter 1), lumen formation could, in principle, be templated by extracellular material along the midline. By electron microscopy, the pharyngeal lumen does appear to contain matrix, however, no components of the pharyngeal matrix are known to be expressed at the time of pm8 and vpi1 morphogenesis. Apical matrix in the pharynx could act as a guidance cue for multiple morphogenetic processes in addition to toroid formation of pm8 and vpi1, such as long-range migrations along the anterior-posterior axis that occur (Sulston et al., 1983; Santella et al., 2010).

In Chapter 3, I found that laminin can orient the axis epithelial polarity in the pharynx. A similar reversal of polarity has been noted in certain cancers (Adams

et al., 2004). How does laminin work as a polarity cue? This likely involves recognition and assembly of laminin on the basal surface of pharyngeal cells by a transmembrane receptor, such as integrins, followed by reorganization of the cytoskeleton. Zygotic loss-of-function mutations in the sole gene encoding β-integrin, *pat-3*, do not result in defects in pharyngeal polarity, suggesting that either maternal PAT-3 is sufficient to orient pharyngeal polarity or that other receptors are involved. In another system where laminin can orient cell polarity (see Chapter 1), it appears to involve a β-integrin/Rac1/non-muscle-myosin regulatory cascade (O'Brien et al., 2001; Yu et al., 2005, 2008), however, little else is known. *C. elegans* has three genes coding for Rac that function redundantly and it is currently unknown if they are required to orient pharyngeal polarity (Lundquist, 2006). New molecules involved in this process could potentially be identified by forward genetics selecting for the multi-lumen phenotype. As laminin has been found to act as a polarity cue for neurons in vivo, it will be interesting to determine if common mechanisms are used to orient these different cell types (Randlett et al., 2011).

The pharynx is also an attractive system to understand the relationship between changes in organ shape and basement membrane dynamics that occur during growth of all animals. Recent use of photoconvertible laminin and collagen revealed that basement membranes can slide relative to tissues (Ihara et al., 2011). As the basement membrane around the pharynx appears malleable at cyst stage, it is likely being slid, bent, and turned over by the pharyngeal cells. The pharyngeal basement membrane must also be remodeled during post-embryonic growth of the pharynx, when the organ expands dramatically without further cell divisions, which has begun to be investigated (Jafari et al., 2010).

BIBLIOGRAPHY

Achilleos, A., Wehman, A. M. and Nance, J. (2010). PAR-3 mediates the initial clustering and apical localization of junction and polarity proteins during C. elegans intestinal epithelial cell polarization. Development *137*, 1833–1842.

Adams, S. A., Smith, M. E. F., Cowley, G. P. and Carr, L. A. (2004). Reversal of glandular polarity in the lymphovascular compartment of breast cancer. J Clin Pathol *57*, 1114–1117.

Albertson, D. G. and Thomson, J. N. (1976). The pharynx of Caenorhabditis elegans. Philos Trans R Soc Lond B Biol Sci *275*, 299–325.

Alper, S. and Kenyon, C. (2001). REF-1, a protein with two bHLH domains, alters the pattern of cell fusion in C. elegans by regulating Hox protein activity. Development *128*, 1793–1804.

Aumailley, M., Bruckner-Tuderman, L., Carter, W. G., Deutzmann, R., Edgar, D., Ekblom, P., Engel, J., Engvall, E., Hohenester, E., Jones, J. C. R., Kleinman, H. K., Marinkovich, M. P., Martin, G. R., Mayer, U., Meneguzzi, G., Miner, J. H., Miyazaki, K., Patarroyo, M., Paulsson, M., Quaranta, V., Sanes, J. R., Sasaki, T., Sekiguchi, K., Sorokin, L. M., Talts, J. F., Tryggvason, K., Uitto, J., Virtanen, I., von der Mark, K., Wewer, U. M., Yamada, Y. and Yurchenco, P. D. (2005). A simplified laminin nomenclature. Matrix Biol *24*, 326–332.

Avery, L. and Thomas, J. (1997). Feeding and defecation. In C. elegans II, (Riddle, D., Blumenthal, T., Meyer, B. and Priess, J., eds), pp. 679–716, Cold Spring Harbor, NY: Cold Spring Harbor Laboratory Press.

Avinoam, O., Fridman, K., Valansi, C., Abutbul, I., Zeev-Ben-Mordehai, T., Maurer, U. E., Sapir, A., Danino, D., Grnewald, K., White, J. M. and Podbilewicz, B. (2011). Conserved eukaryotic fusogens can fuse viral envelopes to cells. Science *332*, 589–592.

Bacaj, T., Tevlin, M., Lu, Y. and Shaham, S. (2008). Glia are essential for sensory organ function in C. elegans. Science *322*, 744–747.

Baer, M., Chanut-Delalande, H. and Affolter, M. (2009). Cellular and molecular mechanisms underlying the formation of biological tubes. Curr Top Dev Biol *89*, 137–62.

Bagnat, M., Cheung, I. D., Mostov, K. E. and Stainier, D. Y. (2007). Genetic control of single lumen formation in the zebrafish gut. Nat Cell Biol *9*, 954–60.

Bagnat, M., Navis, A., Herbstreith, S., Brand-Arzamendi, K., Curado, S., Gabriel, S., Mostov, K., Huisken, J. and Stainier, D. Y. (2010). Cse1l is a negative regulator of CFTR-dependent fluid secretion. Curr Biol *20*, 1840–5.

Bär, T., Güldner, F. H. and Wolff, J. R. (1984). "Seamless" endothelial cells of blood capillaries. Cell Tissue Res *235*, 99–106.

Baum, P. and Garriga, G. (1997). Neuronal migrations and axon fasciculation are disrupted in ina-1 integrin mutants. Neuron *19*, 51–62.

Berry, K. L., Bulow, H. E., Hall, D. H. and Hobert, O. (2003). A C. elegans CLIC-like protein required for intracellular tube formation and maintenance. Science *302*, 2134–7.

Bird, A. F. (1971). The Structure of Nematodes. Academic Press.

Blum, Y., Belting, H., Ellertsdottir, E., Herwig, L., Lüders, F. and Affolter, M. (2008). Complex cell rearrangements during intersegmental vessel sprouting and vessel fusion in the zebrafish embryo. Dev Biol *316*, 312–22.

Bossinger, O., Klebes, A., Segbert, C., Theres, C. and Knust, E. (2001). Zonula adherens formation in Caenorhabditis elegans requires dlg-1, the homologue of the Drosophila gene discs large. Dev Biol *230*, 29–42.

Bossinger, O. and Schierenberg, E. (1996). The use of fluorescent marker dyes for studying intercellular communication in nematode embryos. Int J Dev Biol *40*, 431–9.

Bowerman, B., Draper, B. W., Mello, C. C. and Priess, J. R. (1993). The maternal gene skn-1 encodes a protein that is distributed unequally in early C. elegans embryos. Cell *74*, 443–52.

Bowerman, B., Eaton, B. A. and Priess, J. R. (1992). skn-1, a maternally expressed gene required to specify the fate of ventral blastomeres in the early C. elegans embryo. Cell *68*, 1061–1075.

Bray, S. J. (2006). Notch signalling: a simple pathway becomes complex. Nat Rev Mol Cell Biol *7*, 678–89.

Brenner, S. (1974). The genetics of Caenorhabditis elegans. Genetics *77*, 71–94.

Broitman-Maduro, G., Lin, K. T.-H., Hung, W. W. K. and Maduro, M. F. (2006). Specification of the C. elegans MS blastomere by the T-box factor TBX-35. Development *133*, 3097–3106.

Broitman-Maduro, G., Owraghi, M., Hung, W. W. K., Kuntz, S., Sternberg, P. W. and Maduro, M. F. (2009). The NK-2 class homeodomain factor CEH-51 and the T-box factor TBX-35 have overlapping function in C. elegans mesoderm development. Development *136*, 2735–2746.

Bryant, D. M., Datta, A., Rodríguez-Fraticelli, A. E., Peränen, J., Martín-Belmonte, F. and Mostov, K. E. (2010). A molecular network for de novo generation of the apical surface and lumen. Nat Cell Biol *12*, 1035–45.

Bryant, D. M. and Mostov, K. E. (2008). From cells to organs: building polarized tissue. Nat Rev Mol Cell Biol *9,* 887–901.

Buechner, M. (2002). Tubes and the single C. elegans excretory cell. Trends Cell Biol *12*, 479–484.

Buechner, M., Hall, D. H., Bhatt, H. and Hedgecock, E. M. (1999). Cystic canal mutants in Caenorhabditis elegans are defective in the apical membrane domain of the renal (excretory) cell. Dev Biol *214*, 227–241.

Buendia, B., Bré, M. H., Griffiths, G. and Karsenti, E. (1990). Cytoskeletal control of centrioles movement during the establishment of polarity in Madin-Darby canine kidney cells. J Cell Biol *110*, 1123–1135.

Calvo, D., Victor, M., Gay, F., Sui, G., Luke, M. P., Dufourcq, P., Wen, G., Maduro, M., Rothman, J. and Shi, Y. (2001). A POP-1 repressor complex restricts inappropriate cell type-specific gene transcription during Caenorhabditis elegans embryogenesis. EMBO J *20*, 7197–7208.

Carlsson, P. and Mahlapuu, M. (2002). Forkhead transcription factors: key players in development and metabolism. Dev Biol *250*, 1–23.

Casanova, J. (2007). The emergence of shape: notions from the study of the Drosophila tracheal system. EMBO Rep *8*, 335–9.

Chaffer, C. L., Thompson, E. W. and Williams, E. D. (2007). Mesenchymal to epithelial transition in development and disease. Cells Tissues Organs *185*, 7–19.

Chen, J. N. and Fishman, M. C. (1996). Zebrafish tinman homolog demarcates the heart field and initiates myocardial differentiation. Development *122*, 3809–3816.

Chitwood, B. G. and Chitwood, M. B. (1950). Introduction to Nematology. University Park Press.

Costa, M., Draper, B. W. and Priess, J. R. (1997). The role of actin filaments in patterning the Caenorhabditis elegans cuticle. Dev Biol *184*, 373–384.

Costa, M., Raich, W., Agbunag, C., Leung, B., Hardin, J. and Priess, J. R. (1998). A putative catenin-cadherin system mediates morphogenesis of the Caenorhabditis elegans embryo. J Cell Biol *141*, 297–308.

Datta, A., Bryant, D. M. and Mostov, K. E. (2011). Molecular regulation of lumen morphogenesis. Curr Biol *21*, R126–R136.

del Campo, J. J., Opoku-Serebuoh, E., Isaacson, A. B., Scranton, V. L., Tucker, M., Han, M. and Mohler, W. A. (2005). Fusogenic activity of EFF-1 is regulated via dynamic localization in fusing somatic cells of C. elegans. Curr Biol *15*, 413–423.

Doncaster, C. (1962). Nematode feeding mechanisms. I. Observations on Rhabditis-and Pelodera. Nematologica *8*, 313–320.

Eisenberg, L. M. and Markwald, R. R. (1995). Molecular regulation of atrioventricular valvuloseptal morphogenesis. Circ Res *77*, 1–6.

Ekblom, P. (1989). Developmentally regulated conversion of mesenchyme to epithelium. FASEB J *3*, 2141–2150.

Folkman, J. and Haudenschild, C. (1980). Angiogenesis in vitro. Nature *288*, 551–6.

Francis, G. R. and Waterston, R. H. (1985). Muscle organization in Caenorhabditis elegans: localization of proteins implicated in thin filament attachment and I-band organization. J Cell Biol *101*, 1532–49.

Francis, R. and Waterston, R. H. (1991). Muscle cell attachment in Caenorhabditis elegans. J Cell Biol *114*, 465–79.

Gaudet, J. and Mango, S. E. (2002). Regulation of organogenesis by the Caenorhabditis elegans FoxA protein PHA-4. Science *295*, 821–5.

Gaudet, J., Muttumu, S., Horner, M. and Mango, S. E. (2004). Whole-genome analysis of temporal gene expression during foregut development. PLoS Biol *2*, e352.

Georges-Labouesse, E., Mark, M., Messaddeq, N. and Gansmüller, A. (1998). Essential role of alpha 6 integrins in cortical and retinal lamination. Curr Biol *8*, 983–986.

Gervais, L. and Casanova, J. (2010). In vivo coupling of cell elongation and lumen formation in a single cell. Curr Biol *20*, 359–66.

Gong, Y., Mo, C. and Fraser, S. E. (2004). Planar cell polarity signalling controls cell division orientation during zebrafish gastrulation. Nature *430*, 689–693.

Good, K., Ciosk, R., Nance, J., Neves, A., Hill, R. J. and Priess, J. R. (2004). The T-box transcription factors TBX-37 and TBX-38 link GLP-1/Notch signaling to mesoderm induction in C. elegans embryos. Development *131*, 1967–78.

Graham, P. L., Johnson, J. J., Wang, S., Sibley, M. H., Gupta, M. C. and Kramer, J. M. (1997). Type IV collagen is detectable in most, but not all, basement membranes of Caenorhabditis elegans and assembles on tissues that do not express it. J Cell Biol *137*, 1171–1183.

Greenwald, I. (2005). LIN-12/Notch signaling in C. elegans. In Wormbook, (The C. elegans Research Community, ed.), pp. 1–16, `http://www.wormbook.org`.

Hagedorn, E. J., Yashiro, H., Ziel, J. W., Ihara, S., Wang, Z. and Sherwood, D. R. (2009). Integrin acts upstream of netrin signaling to regulate formation of the anchor cell's invasive membrane in C. elegans. Dev Cell *17*, 187–198.

Harfe, B. D. and Fire, A. (1998). Muscle and nerve-specific regulation of a novel NK-2 class homeodomain factor in Caenorhabditis elegans. Development *125*, 421–9.

Harrell, J. R. and Goldstein, B. (2011). Internalization of multiple cells during C. elegans gastrulation depends on common cytoskeletal mechanisms but different cell polarity and cell fate regulators. Dev Biol *350*, 1–12.

Haun, C., Alexander, J., Stainier, D. Y. and Okkema, P. G. (1998). Rescue of Caenorhabditis elegans pharyngeal development by a vertebrate heart specification gene. Proc Natl Acad Sci U S A *95*, 5072–5.

Herman, M. A. and Wu, M. (2004). Noncanonical Wnt signaling pathways in C. elegans converge on POP-1/TCF and control cell polarity. Front Biosci *9*, 1530–9.

Hermann, G. J., Leung, B. and Priess, J. R. (2000). Left-right asymmetry in C. elegans intestine organogenesis involves a LIN-12/Notch signaling pathway. Development *127*, 3429–40.

Hildebrand, J. D. (2005). Shroom regulates epithelial cell shape via the apical positioning of an actomyosin network. J Cell Sci *118*, 5191–5203.

Hildebrand, J. D. and Soriano, P. (1999). Shroom, a PDZ domain-containing actin-binding protein, is required for neural tube morphogenesis in mice. Cell *99*, 485–497.

Hobert, O. (2002). PCR fusion-based approach to create reporter gene constructs for expression analysis in transgenic C. elegans. Biotechniques *32*, 728–730.

Horne-Badovinac, S., Lin, D., Waldron, S., Schwarz, M., Mbamalu, G., Pawson, T., Jan, Y., Stainier, D. Y. and Abdelilah-Seyfried, S. (2001). Positional cloning of heart and soul reveals multiple roles for PKC lambda in zebrafish organogenesis. Curr Biol *11*, 1492–1502.

Horner, M. A., Quintin, S., Domeier, M. E., Kimble, J., Labouesse, M. and Mango, S. E. (1998). pha-4, an HNF-3 homolog, specifies pharyngeal organ identity in Caenorhabditis elegans. Genes Dev *12*, 1947–52.

Huang, C. C., Hall, D. H., Hedgecock, E. M., Kao, G., Karantza, V., Vogel, B. E., Hutter, H., Chisholm, A. D., Yurchenco, P. D. and Wadsworth, W. G. (2003). Laminin alpha subunits and their role in C. elegans development. Development *130*, 3343–58.

Hwang, B., Meruelo, A. and Sternberg, P. (2007). C. elegans EVI1 proto-oncogene, EGL-43, is necessary for Notch-mediated cell fate specification and regulates cell invasion. Development *134*, 669–79.

Ihara, S., Hagedorn, E. J., Morrissey, M. A., Chi, Q., Motegi, F., Kramer, J. M. and Sherwood, D. R. (2011). Basement membrane sliding and targeted adhesion remodels tissue boundaries during uterine-vulval attachment in Caenorhabditis elegans. Nat Cell Biol *13*, 641–651.

Jafari, G., Burghoorn, J., Kawano, T., Mathew, M., Mörck, C., Axäng, C., Ailion, M., Thomas, J. H., Culotti, J. G., Swoboda, P. and Pilon, M. (2010). Genetics of extracellular matrix remodeling during organ growth using the Caenorhabditis elegans pharynx model. Genetics *186*, 969–982.

Jazwinska, A., Ribeiro, C. and Affolter, M. (2003). Epithelial tube morphogenesis during Drosophila tracheal development requires Piopio, a luminal ZP protein. Nat Cell Biol *5*, 895–901.

Jiang, L., Rogers, S. L. and Crews, S. T. (2007). The Drosophila Dead end Arf-like3 GTPase controls vesicle trafficking during tracheal fusion cell morphogenesis. Dev Biol *311*, 487–499.

Kachur, T. M., Audhya, A. and Pilgrim, D. B. (2008). UNC-45 is required for NMY-2 contractile function in early embryonic polarity establishment and germline cellularization in C. elegans. Dev Biol *314*, 287–299.

Kalb, J. M., Lau, K. K., Goszczynski, B., Fukushige, T., Moons, D., Okkema, P. G. and McGhee, J. D. (1998). pha-4 is Ce-fkh-1, a fork head/HNF-3alpha,beta,gamma homolog that functions in organogenesis of the C. elegans pharynx. Development *125*, 2171–80.

Kaltenbach, L. S., Updike, D. L. and Mango, S. E. (2005). Contribution of the amino and carboxyl termini for PHA-4/FoxA function in Caenorhabditis elegans. Dev Dyn *234*, 346–354.

Kamei, M., Saunders, W. B., Bayless, K. J., Dye, L., Davis, G. E. and Weinstein, B. M. (2006). Endothelial tubes assemble from intracellular vacuoles in vivo. Nature *442*, 453–6.

Kao, G., Huang, C. C., Hedgecock, E. M., Hall, D. H. and Wadsworth, W. G. (2006). The role of the laminin beta subunit in laminin heterotrimer assembly and basement membrane function and development in C. elegans. Dev Biol *290*, 211–219.

Khatoon, N. and Erasmus, D. A. (1971). The Ultrastructure of the Pharynx of Cosmocerca ornata (Nematoda). Zeitschrift fur Parasitenkunde (Berlin, Germany) *36*, 1–14.

Klein, G., Langegger, M., Timpl, R. and Ekblom, P. (1988). Role of laminin A chain in the development of epithelial cell polarity. Cell *55*, 331–41.

Kovall, R. A. and Hendrickson, W. A. (2004). Crystal structure of the nuclear effector of Notch signaling, CSL, bound to DNA. Embo J *23*, 3441–51.

Kramer, J. M. (2005). Basement membranes. In Wormbook, (The C. elegans Research Community, ed.), pp. 1–15, `http://www.wormbook.org`.

Kunwar, P. S., Siekhaus, D. E. and Lehmann, R. (2006). In vivo migration: a germ cell perspective. Annu Rev Cell Dev Biol *22*, 237–65.

Labouesse, M. (2006). Epithelial junctions and attachments. In Wormbook, (The C. elegans Research Community, ed.), pp. 1–21, `http://www.wormbook.org`.

Lee, D. L. (1968). The ultrastructure of the alimentary tract of the skin-penetrating larva of Nippostrongylus brasiliensis (Nematoda). Journal of Zoology *154*, 9–18.

Lee, M., Lee, S., Zadeh, A. D. and Kolodziej, P. A. (2003). Distinct sites in E-cadherin regulate different steps in Drosophila tracheal tube fusion. Development *130*, 5989–5999.

Lee, M. and Vasioukhin, V. (2008). Cell polarity and cancer–cell and tissue polarity as a non-canonical tumor suppressor. J Cell Sci *121*, 1141–1150.

Leung, B., Hermann, G. J. and Priess, J. R. (1999). Organogenesis of the Caenorhabditis elegans intestine. Dev Biol *216*, 114–134.

Lin, R., Hill, R. J. and Priess, J. R. (1998). POP-1 and anterior-posterior fate decisions in C. elegans embryos. Cell *92*, 229–39.

Lin, R., Thompson, S. and Priess, J. R. (1995). pop-1 encodes an HMG box protein required for the specification of a mesoderm precursor in early C. elegans embryos. Cell *83*, 599–609.

Lubarsky, B. and Krasnow, M. A. (2003). Tube morphogenesis: making and shaping biological tubes. Cell *112*, 19–28.

Lundquist, E. A. (2006). Small GTPases. In Wormbook, (The C. elegans Research Community, ed.), pp. 1–18, `http://www.wormbook.org`.

Luschnig, S., Bätz, T., Armbruster, K. and Krasnow, M. A. (2006). serpentine and vermiform encode matrix proteins with chitin binding and deacetylation domains that limit tracheal tube length in Drosophila. Curr Biol *16*, 186–194.

Maduro, M. F., Broitman-Maduro, G., Mengarelli, I. and Rothman, J. H. (2007). Maternal deployment of the embryonic SKN-1→MED-1,2 cell specification pathway in C. elegans. Dev Biol *301*, 590–601.

Maduro, M. F., Meneghini, M. D., Bowerman, B., Broitman-Maduro, G. and Rothman, J. H. (2001). Restriction of mesendoderm to a single blastomere by the combined action of SKN-1 and a GSK-3beta homolog is mediated by MED-1 and -2 in C. elegans. Mol Cell *7*, 475–485.

Mango, S. (2009). The molecular basis of organ formation: insights from the C. elegans foregut. Annu Rev Cell Dev Biol *25*, 597–628.

Mango, S. E. (2007). The C. elegans pharynx: a model for organogenesis. In Wormbook, (The C. elegans Research Community, ed.), pp. 1–26, `http://www.wormbook.org`.

Mango, S. E., Lambie, E. J. and Kimble, J. (1994). The pha-4 gene is required to generate the pharyngeal primordium of Caenorhabditis elegans. Development *120*, 3019–31.

Mapes, C. J. (1965a). Structure and function in the nematode pharynx II. Pumping in Panagrellus, Aplectana and Rhabditis. Parasitology *55*, 583–94.

Mapes, C. J. (1965b). Structure and function in the nematode pharynx. I. The structure of the pharynges of Ascaris lumbricoides, Oxyuris equi, Aplectana brevicaudata and Panagrellus silusiae. Parasitology *55*, 269–284.

Marinkovich, M. P. (2007). Tumour microenvironment: laminin 332 in squamous-cell carcinoma. Nat Rev Cancer *7*, 370–380.

McMahon, L., Legouis, R., Vonesch, J. L. and Labouesse, M. (2001). Assembly of C. elegans apical junctions involves positioning and compaction by LET-413 and protein aggregation by the MAGUK protein DLG-1. J Cell Sci *114*, 2265–2277.

Mello, C. and Fire, A. (1995). DNA transformation. Methods Cell Biol *48*, 451–82.

Mello, C. C., Draper, B. W., Krause, M., Weintraub, H. and Priess, J. R. (1992). The pie-1 and mex-1 genes and maternal control of blastomere identity in early C. elegans embryos. Cell *70*, 163–76.

Mello, C. C., Kramer, J. M., Stinchcomb, D. and Ambros, V. (1991). Efficient gene transfer in C.elegans: extrachromosomal maintenance and integration of transforming sequences. EMBO J *10*, 3959–70.

Metzger, R. J., Klein, O. D., Martin, G. R. and Krasnow, M. A. (2008). The branching programme of mouse lung development. Nature *453*, 745–750.

Miner, J. H. and Yurchenco, P. D. (2004). Laminin functions in tissue morphogenesis. Annu Rev Cell Dev Biol *20*, 255–84.

Mohler, W. A., Shemer, G., del Campo, J. J., Valansi, C., Opoku-Serebuoh, E., Scranton, V., Assaf, N., White, J. G. and Podbilewicz, B. (2002). The type I membrane protein EFF-1 is essential for developmental cell fusion. Dev Cell *2*, 355–362.

Mohler, W. A., Simske, J. S., Williams-Masson, E. M., Hardin, J. D. and White, J. G. (1998). Dynamics and ultrastructure of developmental cell fusions in the Caenorhabditis elegans hypodermis. Curr Biol *8*, 1087–1090.

Mörck, C., Axäng, C. and Pilon, M. (2003). A genetic analysis of axon guidance in the C elegans pharynx. Dev Biol *260*, 158–175.

Moussian, B., Tång, E., Tonning, A., Helms, S., Schwarz, H., Nüsslein-Volhard, C. and Uv, A. E. (2006). Drosophila Knickkopf and Retroactive are needed for epithelial tube growth and cuticle differentiation through their specific requirement for chitin filament organization. Development *133*, 163–171.

Mullen, G., Rogalski, T., Bush, J., Gorji, P. and Moerman, D. (1999). Complex patterns of alternative splicing mediate the spatial and temporal distribution of perlecan/UNC-52 in Caenorhabditis elegans. Mol Biol Cell *10*, 3205–21.

Munro, E., Nance, J. and Priess, J. R. (2004). Cortical flows powered by asymmetrical contraction transport PAR proteins to establish and maintain anterior-posterior polarity in the early C. elegans embryo. Dev Cell *7*, 413–24.

Murray, J. I., Bao, Z., Boyle, T. J., Boeck, M. E., Mericle, B. L., Nicholas, T. J., Zhao, Z., Sandel, M. J. and Waterston, R. H. (2008). Automated analysis of embryonic gene expression with cellular resolution in C. elegans. Nat Methods *5*, 703–9.

Nance, J., Lee, J.-Y. and Goldstein, B. (2005). Gastrulation in C. elegans. In Wormbook, (The C. elegans Research Community, ed.), pp. 1–13, `http://www.wormbook.org`.

Nance, J., Munro, E. M. and Priess, J. R. (2003). C. elegans PAR-3 and PAR-6 are required for apicobasal asymmetries associated with cell adhesion and gastrulation. Development *130*, 5339–50.

Nance, J. and Priess, J. R. (2002). Cell polarity and gastrulation in C. elegans. Development *129*, 387–97.

Nance, J. and Zallen, J. A. (2011). Elaborating polarity: PAR proteins and the cytoskeleton. Development *138*, 799–809.

Neves, A., English, K. and Priess, J. R. (2007). Notch-GATA synergy promotes endoderm-specific expression of ref-1 in C. elegans. Development *134*, 4459–68.

Neves, A. and Priess, J. R. (2005). The REF-1 family of bHLH transcription factors pattern C. elegans embryos through Notch-dependent and Notch-independent pathways. Dev Cell *8*, 867–79.

Nishimura, T. and Takeichi, M. (2008). Shroom3-mediated recruitment of Rho kinases to the apical cell junctions regulates epithelial and neuroepithelial planar remodeling. Development *135*, 1493–502.

O'Brien, L. E., Jou, T. S., Pollack, A. L., Zhang, Q., Hansen, S. H., Yurchenco, P. and Mostov, K. E. (2001). Rac1 orientates epithelial apical polarity through effects on basolateral laminin assembly. Nat Cell Biol *3*, 831–838.

O'Brien, L. E., Zegers, M. M. P. and Mostov, K. E. (2002). Opinion: Building epithelial architecture: insights from three-dimensional culture models. Nat Rev Mol Cell Biol *3*, 531–537.

Oikonomou, G., Perens, E. A., Lu, Y., Watanabe, S., Jorgensen, E. M. and Shaham, S. (2011). Opposing activities of LIT-1/NLK and DAF-6/patched-related direct sensory compartment morphogenesis in C. elegans. PLoS Biol *9*, e1001121.

Okkema, P. G. and Fire, A. (1994). The Caenorhabditis elegans NK-2 class homeoprotein CEH-22 is involved in combinatorial activation of gene expression in pharyngeal muscle. Development *120*, 2175–2186.

Okkema, P. G., Ha, E., Haun, C., Chen, W. and Fire, A. (1997). The Caenorhabditis elegans NK-2 homeobox gene ceh-22 activates pharyngeal muscle gene expression in combination with pha-1 and is required for normal pharyngeal development. Development *124*, 3965–3973.

Oliphant, L. W. and Cloney, R. A. (1972). The ascidian myocardium: sarcoplasmic reticulum and excitation-contraction coupling. Z Zellforsch Mikrosk Anat *129*, 395–412.

Oren-Suissa, M., Hall, D. H., Treinin, M., Shemer, G. and Podbilewicz, B. (2010). The fusogen EFF-1 controls sculpting of mechanosensory dendrites. Science *328*, 1285–1288.

Perens, E. A. and Shaham, S. (2005). C. elegans daf-6 encodes a patched-related protein required for lumen formation. Dev Cell *8*, 893–906.

Petri, B. and Bixel, M. G. (2006). Molecular events during leukocyte diapedesis. FEBS J *273*, 4399–4407.

Podbilewicz, B. (2006). Cell fusion. In Wormbook, (The C. elegans Research Community, ed.), pp. 1–32, `http://www.wormbook.org`.

Podbilewicz, B., Leikina, E., Sapir, A., Valansi, C., Suissa, M., Shemer, G. and Chernomordik, L. V. (2006). The C. elegans developmental fusogen EFF-1 mediates homotypic fusion in heterologous cells and in vivo. Dev Cell *11*, 471–81.

Portereiko, M. F. and Mango, S. E. (2001). Early morphogenesis of the Caenorhabditis elegans pharynx. Dev Biol *233*, 482–94.

Portereiko, M. F., Saam, J. and Mango, S. E. (2004). ZEN-4/MKLP1 is required to polarize the foregut epithelium. Curr Biol *14*, 932–41.

Priess, J. R. (2005). Notch signaling in the C. elegans embryo. In Wormbook, (The C. elegans Research Community, ed.), pp. 1–16, `http://www.wormbook.org`.

Priess, J. R. and Hirsh, D. I. (1986). Caenorhabditis elegans morphogenesis: the role of the cytoskeleton in elongation of the embryo. Dev Biol *117*, 156–73.

Priess, J. R., Schnabel, H. and Schnabel, R. (1987). The glp-1 locus and cellular interactions in early C. elegans embryos. Cell *51*, 601–611.

Priess, J. R. and Thomson, J. N. (1987). Cellular interactions in early C. elegans embryos. Cell *48*, 241–50.

Pruss, R. M., Mirsky, R., Raff, M. C., Thorpe, R., Dowding, A. J. and Anderton, B. H. (1981). All classes of intermediate filaments share a common antigenic determinant defined by a monoclonal antibody. Cell *27*, 419–28.

Raharjo, I. and Gaudet, J. (2007). Gland-specific expression of C. elegans hlh-6 requires the combinatorial action of three distinct promoter elements. Dev Biol *302*, 295–308.

Raharjo, W. H., Ghai, V., Dineen, A., Bastiani, M. and Gaudet, J. (2011). Cell Architecture: Surrounding Muscle Cells Shape Gland Cell Morphology in the Caenorhabditis elegans Pharynx. Genetics *189*, 885–97.

Randlett, O., Poggi, L., Zolessi, F. R. and Harris, W. A. (2011). The oriented emergence of axons from retinal ganglion cells is directed by laminin contact invivo. Neuron *70*, 266–280.

Rasmussen, J. P., English, K., Tenlen, J. R. and Priess, J. R. (2008). Notch signaling and morphogenesis of single-cell tubes in the C. elegans digestive tract. Dev Cell *14*, 559–569.

Raya-Rivera, A., Esquiliano, D. R., Yoo, J. J., Lopez-Bayghen, E., Soker, S. and Atala, A. (2011). Tissue-engineered autologous urethras for patients who need reconstruction: an observational study. Lancet *377*, 1175–1182.

Ribeiro, C., Neumann, M. and Affolter, M. (2004). Genetic control of cell intercalation during tracheal morphogenesis in Drosophila. Curr Biol *14*, 2197–207.

Rocheleau, C. E., Yasuda, J., Shin, T. H., Lin, R., Sawa, H., Okano, H., Priess, J. R., Davis, R. J. and Mello, C. C. (1999). WRM-1 activates the LIT-1 protein kinase to transduce anterior/posterior polarity signals in C. elegans. Cell *97*, 717–26.

Samakovlis, C., Hacohen, N., Manning, G., Sutherland, D. C., Guillemin, K. and Krasnow, M. A. (1996a). Development of the Drosophila tracheal system occurs by a series of morphologically distinct but genetically coupled branching events. Development *122*, 1395–407.

Samakovlis, C., Manning, G., Steneberg, P., Hacohen, N., Cantera, R. and Krasnow, M. A. (1996b). Genetic control of epithelial tube fusion during Drosophila tracheal development. Development *122*, 3531–6.

Santella, A., Du, Z., Nowotschin, S., Hadjantonakis, A.-K. and Bao, Z. (2010). A hybrid blob-slice model for accurate and efficient detection of fluorescence labeled nuclei in 3D. BMC Bioinformatics *11*, 580.

Sapir, A., Avinoam, O., Podbilewicz, B. and Chernomordik, L. V. (2008). Viral and developmental cell fusion mechanisms: conservation and divergence. Dev Cell *14*, 11–21.

Sapir, A., Choi, J., Leikina, E., Avinoam, O., Valansi, C., Chernomordik, L. V., Newman, A. P. and Podbilewicz, B. (2007). AFF-1, a FOS-1-regulated fusogen, mediates fusion of the anchor cell in C. elegans. Dev Cell *12*, 683–98.

Sawyer, J. M., Harrell, J. R., Shemer, G., Sullivan-Brown, J., Roh-Johnson, M. and Goldstein, B. (2010). Apical constriction: a cell shape change that can drive morphogenesis. Dev Biol *341*, 5–19.

Schonegg, S., Constantinescu, A. T., Hoege, C. and Hyman, A. A. (2007). The Rho GTPase-activating proteins RGA-3 and RGA-4 are required to set the initial size of PAR domains in Caenorhabditis elegans one-cell embryos. Proc Natl Acad Sci U S A *104*, 14976–14981.

Schreiber, A. M., Cai, L. and Brown, D. D. (2005). Remodeling of the intestine during metamorphosis of Xenopus laevis. Proc Natl Acad Sci U S A *102*, 3720–3725.

Sharma-Kishore, R., White, J. G., Southgate, E. and Podbilewicz, B. (1999). Formation of the vulva in Caenorhabditis elegans: a paradigm for organogenesis. Development *126*, 691–699.

Shaw, S. K., Bamba, P. S., Perkins, B. N. and Luscinskas, F. W. (2001). Real-time imaging of vascular endothelial-cadherin during leukocyte transmigration across endothelium. J Immunol *167*, 2323–2330.

Sherwood, D. R., Butler, J. A., Kramer, J. M. and Sternberg, P. W. (2005). FOS-1 promotes basement-membrane removal during anchor-cell invasion in C. elegans. Cell *121*, 951–962.

Smit, R. B., Schnabel, R. and Gaudet, J. (2008). The HLH-6 transcription factor regulates C. elegans pharyngeal gland development and function. PLoS Genet *4*, e1000222.

Stone, C., Hall, D. and Sundaram, M. (2009). Lipocalin signaling controls unicellular tube development in the Caenorhabditis elegans excretory system. Dev Biol *329*, 201–11.

Strilić, B., Eglinger, J., Krieg, M., Zeeb, M., Axnick, J., Babál, P., Müller, D. J. and Lammert, E. (2010). Electrostatic cell-surface repulsion initiates lumen formation in developing blood vessels. Curr Biol *20*, 2003–2009.

Strilić, B., Kucera, T., Eglinger, J., Hughes, M. R., McNagny, K. M., Tsukita, S., Dejana, E., Ferrara, N. and Lammert, E. (2009). The molecular basis of vascular lumen formation in the developing mouse aorta. Dev Cell *17*, 505–515.

Stroeher, V. L., Kennedy, B. P., Millen, K. J., Schroeder, D. F., Hawkins, M. G., Goszczynski, B. and McGhee, J. D. (1994). DNA-protein interactions in the Caenorhabditis elegans embryo: oocyte and embryonic factors that bind to the promoter of the gut-specific ges-1 gene. Dev Biol *163*, 367–80.

Sulston, J. E., Schierenberg, E., White, J. G. and Thomson, J. N. (1983). The embryonic cell lineage of the nematode Caenorhabditis elegans. Dev Biol *100*, 64–119.

Thiery, J. P. and Sleeman, J. P. (2006). Complex networks orchestrate epithelial-mesenchymal transitions. Nat Rev Mol Cell Biol *7*, 131–42.

Timmerman, L. A., Grego-Bessa, J., Raya, A., Bertran, E., Perez-Pomares, J. M., Diez, J., Aranda, S., Palomo, S., McCormick, F., Izpisua-Belmonte, J. C. and de la Pompa, J. L. (2004). Notch promotes epithelial-mesenchymal transition during cardiac development and oncogenic transformation. Genes Dev *18*, 99–115.

Tonning, A., Hemphälä, J., Tång, E., Nannmark, U., Samakovlis, C. and Uv, A. (2005). A transient luminal chitinous matrix is required to model epithelial tube diameter in the Drosophila trachea. Dev Cell *9*, 423–430.

Totong, R., Achilleos, A. and Nance, J. (2007). PAR-6 is required for junction formation but not apicobasal polarization in C. elegans embryonic epithelial cells. Development *134*, 1259–1268.

Urbano, J. M., Torgler, C. N., Molnar, C., Tepass, U., López-Varea, A., Brown, N. H., de Celis, J. F. and Martín-Bermudo, M. D. (2009). Drosophila laminins act as key regulators of basement membrane assembly and morphogenesis. Development *136*, 4165–4176.

Uv, A., Cantera, R. and Samakovlis, C. (2003). Drosophila tracheal morphogenesis: intricate cellular solutions to basic plumbing problems. Trends Cell Biol *13*, 301–9.

Wallenfang, M. R. and Seydoux, G. (2000). Polarization of the anterior-posterior axis of C. elegans is a microtubule-directed process. Nature *408*, 89–92.

Wang, A. Z., Ojakian, G. K. and Nelson, W. J. (1990). Steps in the morphogenesis of a polarized epithelium. I. Uncoupling the roles of cell-cell and cell-substratum contact in establishing plasma membrane polarity in multicellular epithelial (MDCK) cysts. J Cell Sci *95 (Pt 1)*, 137–151.

Wang, S., Jayaram, S. A., Hemphälä, J., Senti, K.-A., Tsarouhas, V., Jin, H. and Samakovlis, C. (2006). Septate-junction-dependent luminal deposition of chitin deacetylases restricts tube elongation in the Drosophila trachea. Curr Biol *16*, 180–185.

Wang, Y., Kaiser, M. S., Larson, J. D., Nasevicius, A., Clark, K. J., Wadman, S. A., Roberg-Perez, S. E., Ekker, S. C., Hackett, P. B., McGrail, M. and Essner, J. J. (2010). Moesin1 and Ve-cadherin are required in endothelial cells during in vivo tubulogenesis. Development *137*, 3119–28.

Williams, B. D. and Waterston, R. H. (1994). Genes critical for muscle development and function in Caenorhabditis elegans identified through lethal mutations. J Cell Biol *124*, 475–90.

Wong, L. L. and Adler, P. N. (1993). Tissue polarity genes of Drosophila regulate the subcellular location for prehair initiation in pupal wing cells. J Cell Biol *123*, 209–221.

Xu, K. and Cleaver, O. (2011). Tubulogenesis during blood vessel formation. Semin Cell Dev Biol *22*, 993–1004.

Yochem, J., Gu, T. and Han, M. (1998). A new marker for mosaic analysis in Caenorhabditis elegans indicates a fusion between hyp6 and hyp7, two major components of the hypodermis. Genetics *149*, 1323–34.

Yu, W., Datta, A., Leroy, P., O'Brien, L. E., Mak, G., Jou, T.-S., Matlin, K. S., Mostov, K. E. and Zegers, M. M. P. (2005). Beta1-integrin orients epithelial polarity via Rac1 and laminin. Mol Biol Cell *16*, 433–445.

Yu, W., Shewan, A. M., Brakeman, P., Eastburn, D. J., Datta, A., Bryant, D. M., Fan, Q.-W., Weiss, W. A., Zegers, M. M. P. and Mostov, K. E. (2008). Involvement of RhoA, ROCK I and myosin II in inverted orientation of epithelial polarity. EMBO Rep *9*, 923–929.

Yuen, P. H. (1968). Electron microscopical studies on Ditylenchus dipsaci II. Oesophagus. Nematologica *14*, 385–94.

Zhong, M., Niu, W., Lu, Z. J., Sarov, M., Murray, J. I., Janette, J., Raha, D., Sheaffer, K. L., Lam, H. Y. K., Preston, E., Slightham, C., Hillier, L. W., Brock, T., Agarwal, A., Auerbach, R., Hyman, A. A., Gerstein, M., Mango, S. E., Kim, S. K., Waterston, R. H., Reinke, V. and Snyder, M. (2010). Genome-wide identification of binding sites defines distinct functions for Caenorhabditis elegans PHA-4/FOXA in development and environmental response. PLoS Genet *6*, e1000848.

Ziel, J., Hagedorn, E., Audhya, A. and Sherwood, D. (2009). UNC-6 (netrin) orients the invasive membrane of the anchor cell in C. elegans. Nat Cell Biol *11*, 183–9.

Zimber-Strobl, U., Strobl, L. J., Meitinger, C., Hinrichs, R., Sakai, T., Furukawa, T., Honjo, T. and Bornkamm, G. W. (1994). Epstein-Barr virus nuclear antigen 2 exerts its transactivating function through interaction with recombination signal

binding protein RBP-J kappa, the homologue of Drosophila Suppressor of Hairless. Embo J *13*, 4973–82.

Zovein, A. C., Luque, A., Turlo, K. A., Hofmann, J. J., Yee, K. M., Becker, M. S., Fassler, R., Mellman, I., Lane, T. F. and Iruela-Arispe, M. L. (2010). Beta1 integrin establishes endothelial cell polarity and arteriolar lumen formation via a Par3-dependent mechanism. Dev Cell *18*, 39–51.

<div align="center">

CURRICULUM VITAE

</div>

Jeffrey Philip Rasmussen

Education

2005–2011   Ph.D. in Molecular and Cellular Biology
Fred Hutchinson Cancer Research Center and
University of Washington
Seattle, WA
Advisor: Professor James R. Priess

1998–2002   B.S. with honors in Computational Biology
Brown University
Providence, RI

Employment

2002–2005   Research Consultant, Department of Immunology
University of Washington
Seattle, WA
Advisor: Professor Alexander Y. Rudensky

Teaching Experience

2006   Graduate Teaching Assistant, Biol 402, Cell Biology Lab, University of Washington

2006   Graduate Teaching Assistant, Biol 355, Foundations in Molecular and Cellular Biology, University of Washington

1999–2001   Undergraduate Teaching Assistant, CS 15, Introduction to Object-Oriented Programming and Computer Science, Brown University

1999   Undergraduate Teaching Assistant, CS 4, Introduction to Scientific Computing and Problem Solving, Brown University

Awards/Fellowships

2007–2010   Predoctoral Trainee, NIH Training Grant in Developmental Biology, University of Washington

2005–2008   Achievement Rewards for College Scientists (ARCS) Foundation Scholarship, University of Washington

2006   Honorable Mention, NSF Predoctoral Fellowship

2002   Magna cum laude and Sigma Xi, Brown University

Publications

Rasmussen, J. P., English, K., Tenlen, J. R. and Priess, J. R. (2008). Notch signaling and morphogenesis of single-cell tubes in the C. elegans digestive tract. Dev Cell *14*, 559–569.

Rubtsov, Y. P., **Rasmussen, J. P.**, Chi, E. Y., Fontenot, J., Castelli, L., Ye, X., Treuting, P., Siewe, L., Roers, A., Henderson, Jr, W. R., Muller, W. and Rudensky, A. Y. (2008). Regulatory T cell-derived interleukin-10 limits inflammation at environmental interfaces. Immunity *28*, 546–558.

Chong, M. M. W., **Rasmussen, J. P.**, Rudensky, A. Y., Rundensky, A. Y. and Littman, D. R. (2008). The RNAseIII enzyme Drosha is critical in T cells for preventing lethal inflammatory disease. J Exp Med *205*, 2005–2017.

Liston, A., Nutsch, K. M., Farr, A. G., Lund, J. M., **Rasmussen, J. P.**, Koni, P. A. and Rudensky, A. Y. (2008). Differentiation of regulatory Foxp3+ T cells in the thymic cortex. Proc Natl Acad Sci U S A *105*, 11903–11908.

Lu, L.-F., Gavin, M. A., **Rasmussen, J. P.** and Rudensky, A. Y. (2007). G protein-coupled receptor 83 is dispensable for the development and function of regulatory T cells. Mol Cell Biol *27*, 8065–8072.

Denning, T. L., Granger, S. W., Granger, S., Mucida, D., Graddy, R., Leclercq, G., Zhang, W., Honey, K., **Rasmussen, J. P.**, Cheroutre, H., Rudensky, A. Y. and Kronenberg, M. (2007). Mouse TCRalphabeta+CD8alphaalpha intraepithelial lymphocytes express genes that down-regulate their antigen reactivity and suppress immune responses. J Immunol *178*, 4230–4239.

Gavin, M. A., **Rasmussen, J. P.**, Fontenot, J. D., Vasta, V., Manganiello, V. C., Beavo, J. A. and Rudensky, A. Y. (2007). Foxp3-dependent programme of regulatory T-cell differentiation. Nature *445*, 771–775.

Kim, J. M., **Rasmussen, J. P.** and Rudensky, A. Y. (2007). Regulatory T cells prevent catastrophic autoimmunity throughout the lifespan of mice. Nat Immunol *8*, 191–197.

Fontenot, J. D., **Rasmussen, J. P.**, Gavin, M. A. and Rudensky, A. Y. (2005). A function for interleukin 2 in Foxp3-expressing regulatory T cells. Nat Immunol *6*, 1142–1151.

Fontenot, J. D., **Rasmussen, J. P.**, Williams, L. M., Dooley, J. L., Farr, A. G. and Rudensky, A. Y. (2005). Regulatory T cell lineage specification by the forkhead transcription factor foxp3. Immunity *22*, 329–341.

Vienne, A., **Rasmussen, J.**, Abi-Rached, L., Pontarotti, P. and Gilles, A. (2003). Systematic phylogenomic evidence of en bloc duplication of the ancestral 8p11.21-8p21.3-like region. Mol Biol Evol *20*, 1290–1298.

Presentations

Northwest Society for Developmental Biology (SDB) Regional Meeting, Friday Harbor, WA, March 2011 (Talk)

C. elegans: Development and Gene Expression, EMBL Heidelberg, Germany, June 2010 (Poster)

Northwest SDB Regional Meeting, Friday Harbor, WA, March 2010 (Poster; Award for Best Student Poster)

17th International *C. elegans* Meeting, University of California, Los Angeles, CA, June 2009 (Plenary talk)

Annual Developmental Biology Training Grant Retreat, University of Washington, WA, April 2007, 2008, 2009, 2010 (Talk)

Northwest SDB Regional Meeting, Friday Harbor, WA, March 2009 (Talk)

Tubes, Branches and Pumps in Development, University of Minnesota, September 2008 (Poster; Award for Best Poster)

67th Annual SDB Meeting, Philadelphia, PA, July 2008 (Poster)

Northwest SDB Regional Meeting, Friday Harbor, WA, March 2008 (Talk; Award for Best Student Oral Presentation)

9th Annual Seattle Developmental Biology Winter Meeting, Seattle, WA, December 2007 (Talk)